

Behavior of Composite Columns Subjected to Lateral Cyclic Loading

Mazen AL-Bdoor

Submitted to the
Institute of Graduate Studies and Research
in partial fulfillment of the requirements for the Degree of

Master of Science
in
Civil Engineering

Eastern Mediterranean University
July 2013
Gazimağusa, North Cyprus

Approval of the Institute of Graduate Studies and Research

Prof. Dr. Elvan Yılmaz
Director

I certify that this thesis satisfies the requirements as a thesis for the degree of Master of Science in Civil Engineering.

Asst. Prof. Dr. Murude Çelikağ
Chair, Department of Civil Engineering

We certify that we have read this thesis and that in our opinion it is fully adequate in scope and quality as a thesis for the degree of Master of Science in Civil Engineering.

Asst. Prof. Dr. Serhan Şensoy
Supervisor

Examining Committee

1. Asst. Prof. Dr. Giray Ozay

2. Asst. Prof. Dr. Erding Soyler

3. Asst. Prof. Dr. Serhan Şensoy

ABSTRACT

Nonlinear 3-D finite element models were developed to investigate the cumulative damage of composite columns subjected to cyclic loading by comparing the effects of different levels of axial loads on the cyclic capacity of steel, reinforced concrete, and composite beam-columns. The beam-column specimens were modeled as fixed cantilever beam-columns with an axial load level of 10%, 15%, and 20% of their axial load capacity as well as cyclic loading similar to that suggested by Applied Technology Council (ATC) guidelines (ATC 1992 - ATC 24).

The FEM output was then examined to determine the effect of different levels of axial loads on behavior of beam-columns under cyclic loading. Assessing whether the prototype elastic stiffness had changed, identifying the high stress and strain zones, and evaluating the effects of the level of axial load on stiffness, strength, and ductility of beam-column prototypes were facilitated.

The finite element analysis results demonstrate that the encased composite beam-columns reached the highest ductility among beam-columns specimens due to confinement effect of concrete. The results indicate that local buckling plays a crucial role in curvature ductility for the cyclic beam columns whereas extensive local buckling of steel section leads to significant reduction in stiffness and strength (softening damage). Moreover, the elastic flexural stiffness as well as ductility decreases significantly with an increase in the axial loads level.

Keywords: Cyclic Capacity, Confinement Effect, Finite Element Method, Local Buckling, Ductility

ÖZ

Doğrusal olmayan üç boyutlu kompozit kolon modelleri sonlu elemanlar yöntemi oluşturularak döngüsel yükler ve farklı eksenel yükler altında analiz edilmiş ve sonuçlar çelik ve betonarme kolon modelleri ile karşılaştırılmıştır. Kiriş-kolon modeli bir ucu tam ankastre diğer ucu serbest olacak şekilde modellenmiş (konsol kolon) ve ATC24 raporunda belirtildiği şekilde eksenel yük kapasitelerinin %10, %15 ve %20 değerlerine tekabül eden düşey yük ve döngüsel yatay yük uygulanarak çözümlenmiştir.

Döngüsel yük uygulanan Kiriş-kolon sonlu elemanlar modellerinden elde edilen sonuçlar, eksenel yük oranı da dikkate alınarak incelenmiş ve farklı eksenel yük oranlarının döngüsel yatay yük kapasitesine olan etkisi değerlendirilmiştir. Bu çalışmada modellerin farklı eksenel yükler altında elastik rigidlik, yüksek gerilme ve yüksek birim şekil değiştirme bölgeleri, dayanım ve süneklik düzeyleri incelenmiş ve sonuçlar sunulmuştur.

Sonlu elemanlar yöntemi uygulanarak elde edilen sonuçlardan kompozit kiriş-kolonun, betonun çelik profil etrafında oluşturduğu sargı etkisi nedeniyle, sünekliğinin diğerlerine göre daha yüksek olduğu görülmüştür. Ayrıca sonuçlar göstermiştir ki döngüsel yüklerden dolayı oluşan bölgesel burkulma sünekliği etkilediği, bu bağlamda çelik kiriş-kolonda görülen bölgesel burkulma nedeniyle bu elemanda ciddi bir rigidlik kaybına neden olmuştur. Buna paralel olarak tüm modellerde eğilme rigidliğinde ve süneklikte eksenel yük artışı ile düşüş görülmüştür.

Anahtar Kelimeler: Döngüsel yük kapasitesi, Sargı etkisi, Sonlu Elemanlar Yöntemi, Bölgesel Burkulma, Süneklik

ACKNOWLEDGMENTS

I would like to thank first of all almighty Allah who granted me the strength, patience, power and knowledge after all to fulfill the requirements for the Master's degree.

I would like to express my gratitude to my supervisor Dr. Serhan Şensoy for the useful comments, remarks, understanding and engagement through the learning process of this master thesis.

It is really my pleasure to extend my gratitude to my best friend Eng. Hashem AL Hendi for his assistance and guidance in getting my graduate career, for his support and helping me through all the period of working on my thesis and for his great friendship.

I wish to thank my parents, my brothers, my sisters and my lovely wife for their love and encouragement often provided the most needed motivation to go through the hard times. Throughout my study period, they have always been my foundation and unwavering in their belief of what I am capable.

I gratefully acknowledge Eng. Ahmed Al Yousif who always kindly granted his time and friendship. I must acknowledge my best friend, Eng. Moad Bani Yaseen (Al-haji), for his great support, encouragement and friendship. I would like to thank all my friends who supported me through my study period.

This dissertation is dedicated to my lovely family and to all my friends who supported me especially Eng. Hashem AL Hindi with thanks and appreciation.

TABLE OF CONTENTS

ABSTRACT	v
ÖZ	vii
ACKNOWLEDGMENTS	ix
TABLE OF CONTENTS	xi
LIST OF FIGURES	xiv
LIST OF TABLES	xviii
LIST OF SYMBOLS	xix
1 INTRODUCTION	1
1.1 General Introduction	1
1.2 Types of Composite Columns.....	2
1.2.1 Concrete-encased Composite Columns.....	3
1.2.2 Concrete -filled Composite Columns.....	3
1.3 Scope and Objectives of the Study	4
1.4 Outline.....	5
2 LITERATURE REVIEW.....	6
2.1 General Introduction	6
2.2 Composite Column Design via the Eurocode 4.....	10
2.2.1 Composite Section Design	11
2.2.2 Eurocode 4 Beam-Column Design.....	18
3 PRELIMINARY DESIGN AND FINITE ELEMENT MODELING	27
3.1 Preliminary Design	27
3.2 Finite Element Modeling	30

3.2.1 Introduction	30
3.2.2 Modeling Approach	32
3.2.3 Material Definition	32
3.2.3.1 Confined Concrete	33
3.2.3.2 Steel Section and Reinforcement Bars	40
3.2.4 Loading Definition	40
3.2.5 Finite Element Type and Mesh	45
3.2.6 Verification of FEM of the Encased Composite Beam-Columns	46
4 THE RESULTS AND DISCUSSION	48
4.1 General	48
4.2 Cyclic Behavior of Specimens	48
4.2.1 Encased Composite Beam-Columns	48
4.2.2 Reinforced Concrete Beam-Columns	51
4.2.3 Steel Beam-Columns	53
4.3 Strength	55
4.4 Ductility	66
4.5 Stiffness	71
5 CONCLUSIONS	73
5.1 Summary	73
5.2 Conclusions	74
5.3 Recommendation for Further Study	74
REFERENCES	76
APPENDICES	84
Appendix A: Design of Composite, Steel, and Reinforced Concrete Columns	85
Appendix B: The Calculation of Confined Concrete	110

Appendix C: PEEQ Contour Presentations, Ductility Calculations, and Stress

Contour at Failure 118

LIST OF FIGURES

Figure 1.1: Typical Cross-Section of Composite Columns with Fully or Partially Concrete-Encased H-Section	2
Figure 1.2: Typical Cross-Section of Composite Columns with Fully or Partially Concrete-Filled Hollow Sections	2
Figure 2.1: European Buckling Curves	18
Figure 2.2: Simplified Interaction Curve and Corresponding Stress Distributions ...	19
Figure 3.1: Suggested Frame with Conservative Loads.....	28
Figure 3.2: Maximum Bending Moment Values Resulting from Load Cases.....	29
Figure 3.3: Shear Force Values for Maximum Moment Load Case	29
Figure 3.4: Axial Force Values for Maximum Moment Load Case	29
Figure 3.5: Cross-Sections Resulting from Design.....	30
Figure 3.6: Modeling Parts that Used for Beam-Column Prototypes	32
Figure 3.7: Effectively Confined Core for Rectangular Cross-Section	33
Figure 3.8: Confinement Regions in a Concrete Encased Steel Composite Column	37
Figure 3.9: Stress-Strain Curves for Unconfiend and Confined Concrete in Reinforced Concrete Column.....	37
Figure 3.10: Stress-Strain Curves for Unconfiend, Partially, and Highly Confined Concrete in Encased Composite Column.....	38
Figure 3.11: Stress-Crack Width Curve Proposed by Li et al. (2002)	39
Figure 3.12: Undeformed and Deformed Fixed Cantilever Beam-Column.....	41
Figure 3.13: The Loading History of Elastic Cycles.....	42
Figure 3.14: The Loading History of Inelastic Cycles.....	43

Figure 3.15: The Load-Displacement Curve for Composite Beam-Columns; CC-10P, CC-15P, and CC-20P	44
Figure 3.16: Specimens Layout and Stress Contour at Failure for Specimen 1	47
Figure 4.1: Lateral Load-Displacement Response of CC-10P.....	49
Figure 4.2: Lateral Load-Displacement Response of CC-15P.....	50
Figure 4.3: Lateral Load-Displacement Response of CC-20P.....	50
Figure 4.4: Lateral Load-Displacement Response of RC-10P.....	52
Figure 4.5: Lateral Load-Displacement Response of RC-15P.....	52
Figure 4.6: Lateral Load-Displacement Response of RC-20P.....	53
Figure 4.7: Lateral Load-Displacement Response of SC-10P	54
Figure 4.8: Lateral Load-Displacement Response of SC-15P	54
Figure 4.9: Lateral Load-Displacement Response of SC-20P.....	55
Figure 4.10: Influence of Axial Load Level on The Moment Capacity.....	56
Figure 4.11: Stress Contour at Maximum Force Level (a, and b) and at Maximum Displacement Level (c, and d) of CC-10P	57
Figure 4.12: Stress Contour at Maximum Force Level (a, and b) and at Maximum Displacement Level (c, and d) of CC-15P	58
Figure 4.13: Stress Contour at Maximum Force Level (a, and b) and at Maximum Displacement Level (c, and d) of CC-20P	59
Figure 4.14: Stress Contour at Maximum Force Level (a, and b) and at Maximum Displacement Level (c, and d) of RC-10P	60
Figure 4.15: Stress Contour at Maximum Force Level (a, and b) and at Maximum Displacement Level (c, and d) of RC-15P	61
Figure 4.16: Stress Contour at Maximum Force Level (a, and b) and at Maximum Displacement Level (c, and d) of RC-20P	62

Figure 4.17: Stress Contour at Maximum Force Level (a, and b) and at Maximum Displacement Level (c, and d) of SC-10P.....	63
Figure 4.18: Stress Contour at Maximum Force Level (a, and b) and at Maximum Displacement Level (c, and d) of SC-15P.....	64
Figure 4.19: Stress Contour at Maximum Force Level (a, and b) and at Maximum Displacement Level (c, and d) of CC-20P	65
Figure 4.20: Envelopes of Cyclic $M-\phi$ for CC-10P, RC-10P, and SC-10P	68
Figure 4.21: Envelopes of Cyclic $M-\phi$ for CC-15P, RC-15P, and SC-15P	69
Figure 4.22: Envelopes of Cyclic $M-\phi$ for CC-20P, RC-20P, and SC-20P	69
Figure 4.23: Elastic Stiffness Degradation of Specimens due to Cyclic Loading	71
Figure A.1: Defining Earthquack Variabels in ETABS	85
Figure A.2: The Interaction Curve for Composite Column.....	89
Figure A.3: The Stress Distribution and Neutral Axis Location.....	95
Figure A.4: Examples of different buckling modes and corresponding effective lengths for isolated members	102
Figure C.1: PEEQ Contour at Maximum Force Level (a, and b) and at Maximum Displacement Level (c, and d) of CC-10P	118
Figure C.2: Stress Contour at Maximum Force Level (a, and b) and at Maximum Displacement Level (c, and d) of CC-15P	119
Figure C.3: Stress Contour at Maximum Force Level (a, and b) and at Maximum Displacement Level (c, and d) of CC-20P	120
Figure C.4: Stress Contour at Maximum Force Level (a, and b) and at Maximum Displacement Level (c, and d) of RC-10P	121
Figure C.5: Stress Contour at Maximum Force Level (a, and b) and at Maximum Displacement Level (c, and d) of RC-15P	122

Figure C.6: Stress Contour at Maximum Force Level (a, and b) and at Maximum Displacement Level (c, and d) of RC-20P 123

Figure C.7: Stress Contour at Maximum Force Level (a, and b) and at Maximum Displacement Level (c, and d) of SC-10P..... 124

Figure C.8: Stress Contour at Maximum Force Level (a, and b) and at Maximum Displacement Level (c, and d) of SC-15P..... 125

Figure C.9: Stress Contour at Maximum Force Level (a, and b) and at Maximum Displacement Level (c, and d) of CC-20P 126

Figure C.10: Stress Contour at Fracture Stage for CC-10P 129

Figure C.11: Stress Contour at Fracture Stage for CC-15P 129

Figure C.12: Stress Contour at Fracture Stage for CC-20P 130

Figure C.13: Stress Contour at Fracture Stage for RC-10P 130

Figure C.14: Stress Contour at Fracture Stage for RC-15P 131

Figure C.15: Stress Contour at Fracture Stage for RC-20P 131

Figure C.16: Stress Contour at Fracture Stage for SC-10P..... 132

Figure C.17: Stress Contour at Fracture Stage for SC-15P..... 132

Figure C.18: Stress Contour at Fracture Stage for SC-20P..... 133

LIST OF TABLES

Table 2.1: Buckling Curves and Member Imperfections for Composite Columns....	16
Table 2.2: Buckling Reduction Factor, χ	17
Table 2.3: Stress Distributions at each Point of Interaction Curve (Major Axis Bending).....	23
Table 2.4: Stress Distributions at each Point of Interaction Curve (Minor Axis Bending).....	26
Table 3.1: Load Combinations.....	28
Table 3.2: Detailed Cross-Sections and Materials Properties.....	30
Table 3.3: Mechanical Properties of the Steel Section and Reinforcement Bars.....	40
Table 3.4: Specimens Matrix with Axial Load Capacity.....	42
Table 3.5: The Lateral Load Capacity and the Yield Displacement of the Cyclic Beam-Column Specimens.....	45
Table 3.6: Various Elements Used in ABAQUS (ABAQUS inc, 2012).....	46
Table 3.7: Specimen Dimensions and Materials Properties (Ellobody & Young, 2011).....	47
Table 3.8: Comparison between Test, FE (Ellobody & Young, 2011), and Modeling Results.....	47
Table A.1: Imperfection Factors for Flexural Buckling Curves	92
Table A.2: Selection of Buckling Curve for a Cross-Section	93
Table C.1: The Curvature Ductilites Calculation.....	127
Table C.2: The Displacement Ductilites Calculation.....	128

LIST OF SYMBOLS

A	Cross-sectional area
A_a	Cross-sectional area of the structural steel section
A_c	Cross-sectional area of concrete, area of core of section enclosed by the center lines of the perimeter spiral or hoop
A_{cc}	The area of the confined concrete
A_e	Area of effectively confined concrete core
A_{eff}	Effective area of a cross-section
A_{rE}	Area of reinforcing steel within $2hE$ region
A_{ri}	Area of one reinforcing bar
A_m	Is the sum of reinforcement inside within the $2h_n$ region
A_s	Cross-sectional area of reinforcement
A_{sx}, A_{sy}	the total area of transverse bars running in the x and y directions
$A_{s,min}$	Minimum cross sectional area of reinforcement
b	Length of longer side of rectangular steel tube
b_c	Core dimensions to centerlines of perimeter hoop in x direction
b_f	Width of the flange of a steel section
C_{min}	The minimum concrete cover
$C_{min,b}$	Minimum cover due to bond requirement
$C_{min,dur}$	Minimum cover due to environmental conditions
C_{nom}	The nominal cover
d	Overall depth of the structural steel section, is the external diameter of the column
d_c	Core dimensions to centerlines of perimeter hoop in y direction

E_a	Modulus of elasticity of structural steel
E_c	Tangent modulus of elasticity of the concrete
E_{cm}	Secant modulus of elasticity of concrete
$(EI)_{eff}$	Effective flexural stiffness for calculation of relative slenderness
E_s	Design value of modulus of elasticity of reinforcing steel
E_{sec}	Secant modulus of the confined concrete at peak stress
e	Is the eccentricity of loading
e_i	Distance to the bending axis considered
f_c	The longitudinal compressive concrete stress
f_{cc}'	Compressive strength of the confined concrete
f_{cd}	Design value of the cylinder compressive strength of concrete
f_{ck}	Characteristic compressive cylinder strength of concrete at 28 days
f_{cm}	Mean value of the measured cylinder compressive strength of concrete at 28 days
f_{co}'	Compressive strength of the unconfined concrete
f_L	Lateral pressure from the transverse reinforcement
f_{lx}, f_{ly}	The lateral confining stress on the concrete in the x and y direction
f_L'	The effective lateral confining pressure
f_{rd}	Design value of the cylinder compressive strength of reinforcement
f_{sd}	Design value of the yield strength of reinforcing steel in composite columns
f_y	Nominal value of the yield strength of structural steel in composite columns, yield strength of reinforcement in RC columns
f_{yd}	Design value of the yield strength of structural steel in composite columns, Design yield strength of reinforcement in RC columns
h_E	Distance from centroidal axis to neutral axis for point E

h_n	Distance from centroidal axis to neutral axis
h_1, h_2	Dimension of the section
I_a	Second moments of area of the structural steel section
I_c	Second moments of area of the un-cracked concrete section
I_s	Second moment of area of the steel reinforcement
i	Is the radius of gyration of the uncracked concrete section
K_e	Correction factor, confinement effectiveness coefficient
L	Buckling length of the column (effective length)
l_o	Is the effective length
M_E	Moment capacity for neutral axis located h_E from centroid axis
M_{Ed}	Design bending moment
M_{ed}	Is the design value of the moment
$M_{eI,Rd}$	Design value of the elastic resistance moment of the steel section
M_{max}	The maximum internal moment
$M_{pI,Rd}$	Design value of the elastic resistance moment of the steel section with full shear connection
$N_{b,Rd}$	Is the design buckling resistance of the compression member
N_{cr}	Elastic critical force for the relevant buckling mode based on the gross sectional properties in steel columns, the elastic critical normal force in composite columns
$N_{c,Rd}$	Design resistance to normal forces of the cross-section for uniform compression
N_{Ed}	Design value of the applied axial force (tension or compression) in composite columns, design value of the compressive normal force in RC columns
N_{pm}	Axial force resistance of concrete portion of cross-section

$N_{p1,Rd}$	Design value of plastic resistance of the composite section to compressive normal force
$N_{pl,Rk}$	Is the characteristic value of the plastic resistance of the composite section to compressive normal strength
N_{Rd}	Design value of the resistance to normal forces
r	The corner radius in a rectangular tube
s	Vertical spacing between spiral from center to center
s'	Clear vertical spacing between spiral or hoop bars
t	Is the wall thickness of the steel tube
t_f	Thickness of a flange of the structural steel section
t_w	Thickness of a web of the structural steel section
W_i	Is the i_{th} clear distance between adjacent longitudinal bars
Z_c	Plastic modulus of overall concrete cross-section
Z_{cE}	Plastic section modulus of concrete within $2h_E$ region
Z_{cn}	Plastic section modulus of concrete within $2h_n$ region
Z_r	Plastic modulus of reinforcement
Z_{rE}	Plastic section modulus of reinforcing steel within $2h_E$ region
Z_{rn}	Plastic section modulus of reinforcing steel within $2h_n$ region
Z_s	Plastic modulus of steel cross-section
Z_{sE}	Plastic section modulus of steel section within $2h_E$ region
Z_{sn}	Plastic section modulus of steel section within $2h_n$ region
a	Is an imperfection factor
β	Correction factor for the lateral torsional buckling curves for rolled and welded sections
ε_c	longitudinal concrete strain

ε_{cc}	Strain at maximum confined concrete stress
ε_{co}	Strain at maximum unconfined concrete stress
ρ_{cc}	Ratio of area of longitudinal reinforcement to area of core of section
ϕ	Value to determine the reduction factor χ
γ_M	Partial factors
γ_{M0}	Partial factor for resistance of cross-section whatever the class is
γ_{M1}	Partial factor for resistance of members to instability
γ_{M2}	Partial factor for resistance of cross-sections in tension to fracture
η_a	Factor for increasing concrete compressive strength due to confinement
η_c	Reduction factor for steel yield stress due to confinement
η_{ao}, η_{co}	Intermediate values for confinement calculations
λ	Slenderness ratio
δ	Is steel contribution ratio
χ	Is the reduction factor for the relevant buckling mode
ΔM_E	Plastic moment of cross-section resulting from region 2hE

Chapter 1

INTRODUCTION

1.1 General Introduction

During the last few years, steel-concrete composite structures have become popular system in tall buildings construction due to their higher load-carrying capacity and stiffness which results from combining the rigidity of reinforced concrete with structural steel sections. The use of composite structures has become widespread in the Middle East, with Dubai today housing some of the highest buildings in the world, in Japan and China. Also, there are extensive interests of using composite systems for the seismic resistance design.

Comparing with steel structure or traditional concrete, composite steel-concrete construction has gained more advantages from being system with: high load carrying capacity, admirable structural integrity, and excellent structural and dimensional stability etc. (Kwan & Chung, 1996).

Most of composite structures consist of structural steel frame with steel-concrete composite columns to satisfy the requirements of strength and serviceability under all probable condition of loading. These composite columns provide the required stiffness to limit the total drift of the building to acceptable levels of the lateral displacement, resist the lateral seismic and wind loads very effectively, and speed up the construction process by advancing the erection of the structural steel formwork to

support several floors at time before casting the concrete column encasement which produce an economic structure.

1.2 Types of Composite Columns

Two basic types of composite columns are mostly used in buildings: those with the steel section encased in concrete and those with the steel section filled with concrete, examples of which are shown in Figures 1.1 and 1.2 respectively.

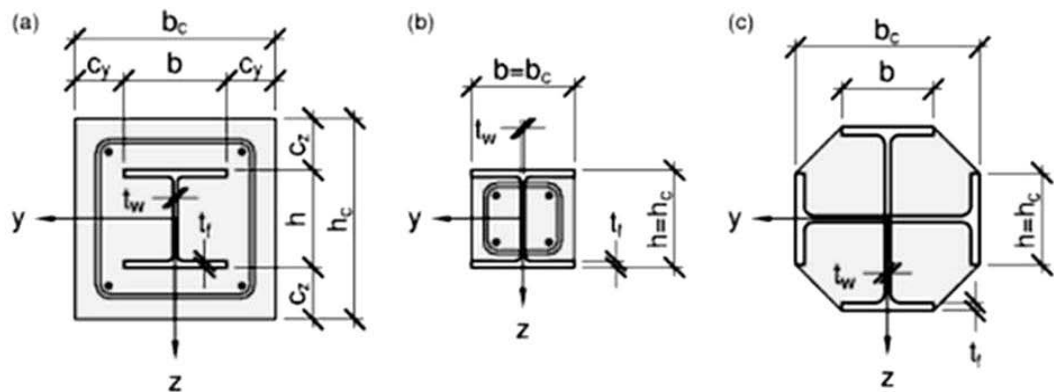


Figure 1.1: Typical Cross-Section of Composite Columns with Fully or Partially Concrete-Encased H-Section
(Source: Buick Davison, 2012)

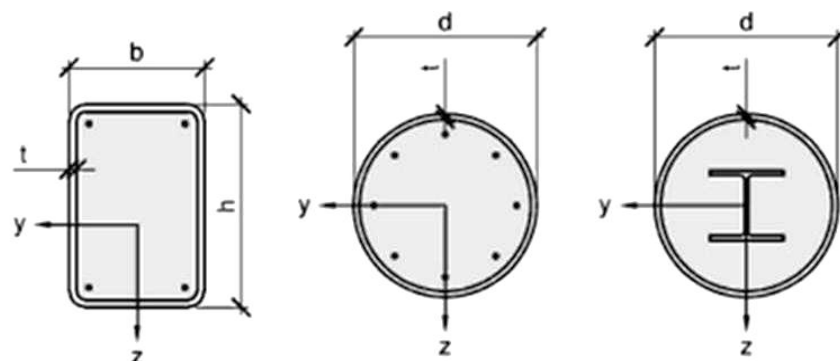


Figure 1.2: Typical Cross-Section of Composite Columns with Fully or Partially Concrete-Filled Hollow Sections
(Source: Buick Davison, 2012)

1.2.1 Concrete-encased Composite Columns

One of the common and popular columns is the encased steel profile (Figure.1.1) where a steel H-section is encased in concrete. Sometimes, structural pipe, tube, or built up section is placed instead of the H-section. In addition to upholding a proportion of the load acting on the column, the concrete encasement enhances the behavior of the structural steel core by and horizontal bar reinforcement, and so making it more effective against both local and overall buckling. The load-bearing concrete encasement performs the additional function of fireproofing the steel core. The cross sections, which normally are square or rectangular, must have one or extra longitudinal bars placed in every single corner and these have to be tied by lateral ties at regular vertical intervals in the manner of a reinforced concrete column. Ties are effective in rising column strength, confinement and ductility. Furthermore, they stop the longitudinal bars from being displaced during construction and they resist the tendency of these same bars to buckle outward under load, which would cause spalling of the outer concrete cover even at low load levels, remarkably in the case of eccentrically loaded columns. It will be noted that these ties will be open and U-shaped. Otherwise, they might not be installed, because the steel column shapes will have always been erected at an earlier time.

1.2.2 Concrete -filled Composite Columns

In this type of composite columns, a steel pipe, steel tubing, or built up section is filled with concrete (Figure.1.2). The most common steel sections used are the hollow rectangular and circular tubes. Filled composite columns may be the most efficient application of materials for column cross sections. It provides forms for the inexpensive concrete core and increases the strength and stiffness of the column. In addition, because of its relatively high stiffness and tensile resistance, the steel shell

provides transverse confinement to the concrete, making the filled composite column very ductile with remarkable toughness to survive local overloads.

1.3 Scope and Objectives of the Study

It is the purpose of this study to investigate the cumulative damage of composite columns subjected to cyclic loading by comparing the effects of different levels of axial loads on the cyclic capacity of steel, reinforced concrete, and composite beam-columns.

Version 6.12 of the finite element program ABAQUS (ABAQUS, 2012) was utilized to model the three prototype beam-columns; steel, reinforced concrete, and composite columns subjected to a cyclic loading similar to that suggested by Applied Technology Council (ATC) guidelines (ATC 1992- ATC 24). Each prototype beam-column was modeled under an axial load level of 10%, 15%, and 20% of their axial load capacity.

The objective of this study can be cast into the following points:

- 1) Determining the lateral load capacity of beam-column prototypes.
- 2) Determining the yield level lateral capacity by measure the elastic stiffness of each prototype.
- 3) Evaluating whether the prototype elastic stiffness had changed.
- 4) Identifying the high stress and strain zones.
- 5) Evaluating the effects of the level of axial load on stiffness, strength, and ductility of beam-column prototypes.

1.4 Outline

This thesis is structured as follows:

Chapter I is the general introduction to the concept of this research and the objectives that need to be achieved in the process of the study.

Chapter II presents a literature review on the behaviors of composite column under cyclic loading, as well as a detailed review of Eurocode (Eurocode 4. , 2004) for composite, Reinforced concrete, and steel beam-column design.

Chapter III presents an overview of preliminary design of beam-column prototypes, materials definition, and loading protocols. In this chapter also information and details on the finite element models and analysis procedures to evaluate the behavior of prototypes are provided, and verification of the finite element part of this research is presented.

Chapter IV summarizes the result of the finite element analysis of the three prototype beam-columns; steel, reinforced concrete, and composite, and comparison between the results in order to understand the behavior of the beam-columns under variation of axial load level.

In Chapter V presents summary and conclusions of this thesis for composite columns. This chapter is followed by references.

Chapter 2

LITERATURE REVIEW

2.1 General Introduction

As main components of the composite frame system, the beam-columns are commonly adopted as most important components which resist lateral seismic loads especially in the regions of high seismic ground motion. They are subjected to both axial compressive force and moment.

After extensive review in literature, the overall performance of such a system has been investigated by many studies; Mirza et al. (1996), El-Tawil & Deierlein (1999), Lee & Pan (2001), Chen et al. (2001), Chicoine et al. (2002), Chicoine et al. (2003), Spacone & El-Tawil (2004), Mirza & Lacroix (2004), Chen et al. (2005), Tikka & Mirza (2005), Chen & Lin (2006), Begum et al. (2006), Begum et al. (2006), Mirza S. A. (2006), Ellobody et al. (2010), Ellobody & Young (2010), Denavit et al. (2011), Shim, Chung, & Yoon (2011), Cho et al. (2012), etc.. Most of them have focused on the ultimate strength of composite columns under axial loads. Various analytical models and design formulas have been proposed to describe the overall response.

A lot of experiments have been carried out to investigate the parameters that affect the axial capacity of composite columns. It was found that there are various parameters, including shape of steel section, longitudinal steel reinforcement,

material properties of the concrete, the confinement effect of the concrete, slenderness ratio of the column, and concrete and steel strength. (Ellobody & Young, 2011).

Ellobody et al. (2010) studied the responses of concrete encased steel composite columns to eccentrically load acting along the major axis. Many variables that influence this response such as the concrete strength, the steel section yield stress, eccentricities, column dimensions, and structural steel sizes were investigated. A three-dimensional finite element analysis using ABAQUS has been developed and it has been validated against experimental result. Eccentric Load–concrete strength curves, axial load-moment curves, and ultimate capacity were obtained. The results showed that the increase in steel section yield stress has significant effect on the strength of eccentrically load composite column with small eccentricity with concrete lower than 70 MPa compressive strength. A conclusion was drawn after compared the results with Eurocode 4 (Eurocode 4. , 2004) that the eccentric load were predicted correctly but the moment values were overestimated.

On the other hand, Ellobody & Young (2010) investigated the effect of varied slenderness ratios, concrete strength and steel yield stress on strength and behavior of pin-ended axially loaded concrete encased steel composite columns. To establish this effect, the 3D nonlinear finite element analysis and their results have been validated against actual tests results. The results demonstrated that the effect of increase in steel yield stress on the composite strength for slender column is less pronounced because of the flexural buckling failure mode.

Considering the researchers that investigated the confinement effect of the concrete in composite columns, Chen & Lin (2006) developed analytical model for anticipating the force-deformation response. Three different shapes of the structural steel section were used; I-, H-, T- and cross-shaped sections. The analytical model took into account the relationships between variables for materials used such as structural steel section, confined and unconfined concrete, and longitudinal reinforcing bar. In their analytical model, they evaluated the confinement factor for confined areas and they concluded that the steel shapes, the diameter and spacing of the lateral and longitudinal reinforcement, as well as layout of section effect the confining stress which have high pronounced enhancement in the axial capacity and ultimate strength.

Furthermore, Dundu (2012) conducted an experimental study to investigate the behavior of concrete-filled steel tube (CFST) columns, which consisted of the test of 24 Specimens loaded concentrically in compression to failure. In this study, slenderness ratio and the strength of materials were considered as main variables. The results have shown that the columns having larger slenderness ratio failed by overall flexural buckling. Whereas the composite columns that have lower slenderness ratio failed by crushing of the concrete and yielding of the steel tube. Moreover, the test results compared with Eurocode 4 and the South African code, so the conclusion was drawn that the codes are conservative.

The overriding point that was noticed during the review in literature was the cyclic behavior of the composite beam-columns has not received the same level of attention as monotonic behavior, especially for concrete-encased steel composite columns. A limited number of studies have been made on this behavior because it is expensive

regarding the cost of research; preparing a full-scale testing is expensive and time consuming. However, a remarkable number of researchers tried to capture and monitor the composite columns seismic behavior by means of strength, stiffness, ductility, and energy dissipation. For instance, Varma et al. (2004) investigated the seismic behavior of square concrete-filled steel tube beam-columns. Cyclic load tests conducted on eight beam-column specimens having different width-to-thickness ratio, different yield stress of the steel tube, and different level of axial load. The results indicate that in the plastic hinge zone, where the stress concentrations highly increase, most of the flexural energy was dissipated. Moreover, it was shown that the increase in axial load level has inverse effect on the cyclic curvature ductility. Also at lower axial load levels, the ductility is reduced for beam-columns having higher width-to-thickness ratio or yield stress of the steel tube. On the other hand, Gajalakshmi & Helena (2012) tested sixteen specimens of concrete-filled steel circular columns, which consisted of two types of in-fills; plain cement concrete and steel fiber reinforced concrete. The influences of cross-section details; the diameter-to-thickness ratio, as well as the types of in-fills on the columns strength, stiffness, ductility, failure mode and energy absorption capacity were investigated. Their tests confirmed that the steel fiber reinforced concrete-filled steel columns provide increase in strength, ductility and energy dissipation capacity compared to plain cement concrete-filled columns which are required for use in seismic moment frames.

From the detailed literature mentioned above, it should be noted that there is necessity to direct an effort towards for gaining a better understanding of the cyclic behavior of concrete-encased steel composite beam-columns to be able to represent the behavior by analytical models.

2.2 Composite Column Design via the Eurocode 4

For satisfaction of the main aim of this study; investigate the cumulative damage of composite columns subjected to cyclic loading by comparing the effects of different levels of axial loads on the cyclic capacity of steel, reinforce concrete, and composite beam-columns, it is first necessary to review the design procedures that will be used for composite, steel, and reinforce concrete beam-columns to be able to used them in preliminary design.

In fact, Eurocode presents the most recent rules and comprehensive review among other design codes and specifications. As a result, Eurocode 2, 3, and 4 were chosen for design of reinforce concrete, steel, and composite beam-columns, respectively. This section elucidates on the design procedure of composite columns according to Eurocode 4 (EN 1994) to resist axial loads and moments. Whereas the design procedures of reinforce concrete and steel columns, which will be used for the comparison purposes, are summarized in appendix A.

To begin with, there are two design methods mentioned in Eurocode 4 for composite columns design; the general method which appropriate for non-symmetrical or non-uniform columns and the simple method for members of doubly symmetrical and uniform over the member length.

For the composite columns design, Eurocode has mentioned some limitations which shall satisfy; Slenderness parameter of the column should be less than 2%, the longitudinal reinforcement which can be used should be no more than 6% and not less than 0.3% of the concrete area, 0.2 and 0.5 are given as limits for the depth to width ratio of the composite cross-section.

2.2.1 Composite Section Design

In order to calculate the plastic resistance of composite columns, the plastic resistance of its components; the structural steel, the concrete and the reinforcement, should be adding. The plastic resistance equation for encased-composite column is:

$$N_{p1,rd} = A_a f_{yd} + 0.85 A_c f_{cd} + A_s f_{sd} \quad (2.1)$$

where

- A_a the cross-sectional area of the structural steel
- A_c the cross-sectional area of the concrete
- A_s the cross-sectional area of the reinforcement
- f_{cd} Design value of the cylinder compressive strength of concrete
- f_{sd} Design value of the yield strength of reinforcing steel
- f_{yd} Design value of the yield strength of structural steel

For filled-composite column, the coefficient 0.85 may be replaced by 1.0. The plastic resistance of circular cross-section equation is:

$$N_{P1,Rd} = \eta_a A_a f_{yd} + A_c f_{cd} \left[1 + \eta_c \frac{t}{d} \frac{f_y}{f_{cK}} \right] + A_s f_{sd} \quad (2.2)$$

where

- f_y Nominal value of the yield strength of structural steel
- f_{cK} Characteristic compressive cylinder strength of concrete at 28 days
- d Is the outside diameter of the steel tube
- t Is the wall thickness of the steel tube
- η_a, η_c Factors related to the confinement of concrete

When the eccentricity of loading, e , equal to 0, the values of $\eta_a = \eta_{a0}$ and $\eta_c = \eta_{c0}$ are given by the following expressions:

$$\eta_{a0} = 0.25(3 + 2\lambda) \quad \text{but } \leq 1 \quad (2.3)$$

$$\eta_{c0} = 4.9 - 18.5\lambda + 17\lambda^2 \quad \text{but } \geq 0 \quad (2.4)$$

where

η_{a0}, η_{c0} Factors related to the confinement of concrete

λ General slenderness parameter

When eccentricity to outside diameter ratio, e/d , falls between 0 and 0.1, the values η_a and η_c should be determined from (Equation 2.5) and (Equation 2.6);

$$\eta_a = \eta_{a0} + (1 - \eta_{a0}) \left(10 \frac{e}{d} \right) \quad (2.5)$$

$$\eta_c = \eta_{c0} \left(1 - 10 \frac{e}{d} \right) \quad (2.6)$$

For $e/d > 0.1$, $\eta_a = 1.0$ and $\eta_c = 0$.

The eccentricity of loading, e , is defined as

$$e = \frac{M_{Ed}}{N_{Ed}} \quad (2.7)$$

where

M_{Ed} Design bending moment

N_{Ed} Design value of the compressive normal force

The steel contribution ratio, δ , is defined as

$$\delta = \frac{A_a f_{yd}}{N_{pl,rd}} \quad (2.8)$$

The relative slenderness, λ , is defined by:

$$\lambda = \sqrt{\frac{N_{pl,Rk}}{N_{cr}}} \quad (2.9)$$

where

$N_{pl,Rk}$ the characteristic value of the plastic resistance to compression given by (Equation 2.1)

N_{cr} the elastic critical normal force for the relevant buckling mode, calculated with the effective flexural stiffness $(EI)_{eff}$

$$N_{cr} = \frac{(EI)_{eff} \pi^2}{(KL)^2} \quad (2.10)$$

where

L buckling length of the column (effective length)

$(EI)_{eff}$ Effective flexural stiffness given by (Equation 2.11)

$$(EI)_{eff} = E_a I_a + E_s I_s + K_e E_{cm} I_c \quad (2.11)$$

where

K_e correction factor that should be taken as 0.6

I_a the second moment of area of the structural steel section

I_c the second moment of area of the un-cracked concrete section

I_s the second moment of area of the reinforcing steel

- E_a Modulus of elasticity of structural steel
- E_{cm} The secant modulus of concrete, (Equation 2.12)
- E_s Design value of modulus of elasticity of reinforcing steel

$$E_{cm} = 22 \left[\frac{f_{cm}}{10} \right]^{0.3} \quad (2.12)$$

$$f_{cm} = f_{ck} + 8 \quad (2.13)$$

For simplification for members in axial compression, the design value of the normal force N_{ed} ought to satisfy:

$$\frac{N_{Ed}}{\chi N_{pl,Rd}} \leq 1.0 \quad (2.14)$$

where

- $N_{pl,Rd}$ The plastic resistance of the composite section but with f_{yd} determined using the partial factor γ_{M1} which is equal 1 for buildings
- χ The reduction factor for column slenderness

$$\chi = \frac{1}{\phi + \sqrt{\phi^2 - \lambda^2}} \quad \chi \leq 1.0 \quad (2.15)$$

where

$$\phi = 0.5 \left[1 + \alpha(\lambda - 0.2) + \lambda^2 \right] \quad (2.16)$$

- α imperfection factor which can consider as 0.21 for concrete-filled circular and rectangular hollow sections, 0.34 for completely or partly concrete-encased I-section with bending about the major axis of the profile, and 0.49 for completely or partly concrete-encased I-section with bending about the minor axis of the profile

The relevant buckling curves for cross-sections of composite columns are given in Table 2.1, where ρ_s is the reinforcement ratio, A_s / A_c .

In order to find the value of the reduction factor, χ , the relative slenderness, λ , should be calculated first according to (Equation 2.9) then Figure 2.1, or Table 2.2 can be used.

Table 2.1: Buckling Curves and Member Imperfections for Composite Columns
(Source: Eurocode 4, 2004)

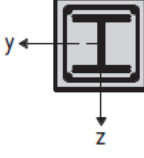
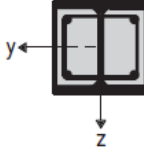
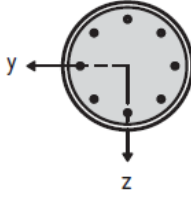
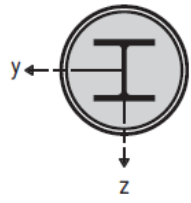
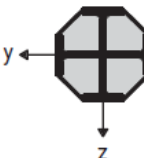
Cross-section	Limits	Axis of buckling	Buckling curve	Member imperfection
concrete encased section 		y-y	b	$L/200$
		z-z	c	$L/150$
partially concrete encased section 		y-y	b	$L/200$
		z-z	c	$L/150$
circular and rectangular hollow steel section 	$\rho_s \leq 3\%$	any	a	$L/300$
	$3\% < \rho_s \leq 6\%$	any	b	$L/200$
circular hollow steel sections with additional I-section 		y-y	b	$L/200$
		z-z	b	$L/200$
partially concrete encased section with crossed I-sections 		any	b	$L/200$

Table 2.2: Buckling Reduction Factor, χ
(Source: Eurocode 4, 2004)

λ	Buckling curve			
	a	b	c	d
0.00	1.00	1.00	1.00	1.00
0.10	1.00	1.00	1.00	1.00
0.20	1.00	1.00	1.00	1.00
0.30	0.98	0.96	0.95	0.92
0.40	0.95	0.93	0.90	0.85
0.50	0.92	0.88	0.84	0.78
0.60	0.89	0.84	0.79	0.71
0.70	0.85	0.78	0.72	0.64
0.80	0.80	0.72	0.66	0.58
0.90	0.73	0.66	0.60	0.52
1.00	0.67	0.60	0.54	0.47
1.10	0.60	0.54	0.48	0.42
1.20	0.53	0.48	0.43	0.38
1.30	0.47	0.43	0.39	0.34
1.40	0.42	0.38	0.35	0.31
1.50	0.37	0.34	0.31	0.28
1.60	0.33	0.31	0.28	0.25
1.70	0.30	0.28	0.26	0.23
1.80	0.27	0.25	0.23	0.21
1.90	0.24	0.23	0.21	0.19
2.00	0.22	0.21	0.20	0.18
2.10	0.20	0.19	0.18	0.16
2.20	0.19	0.18	0.17	0.15
2.30	0.17	0.16	0.15	0.14
2.40	0.16	0.15	0.14	0.13
2.50	0.15	0.14	0.13	0.12
2.60	0.14	0.13	0.12	0.11
2.70	0.13	0.12	0.12	0.11
2.80	0.12	0.11	0.11	0.10
2.90	0.11	0.11	0.10	0.09
3.00	0.10	0.10	0.10	0.09

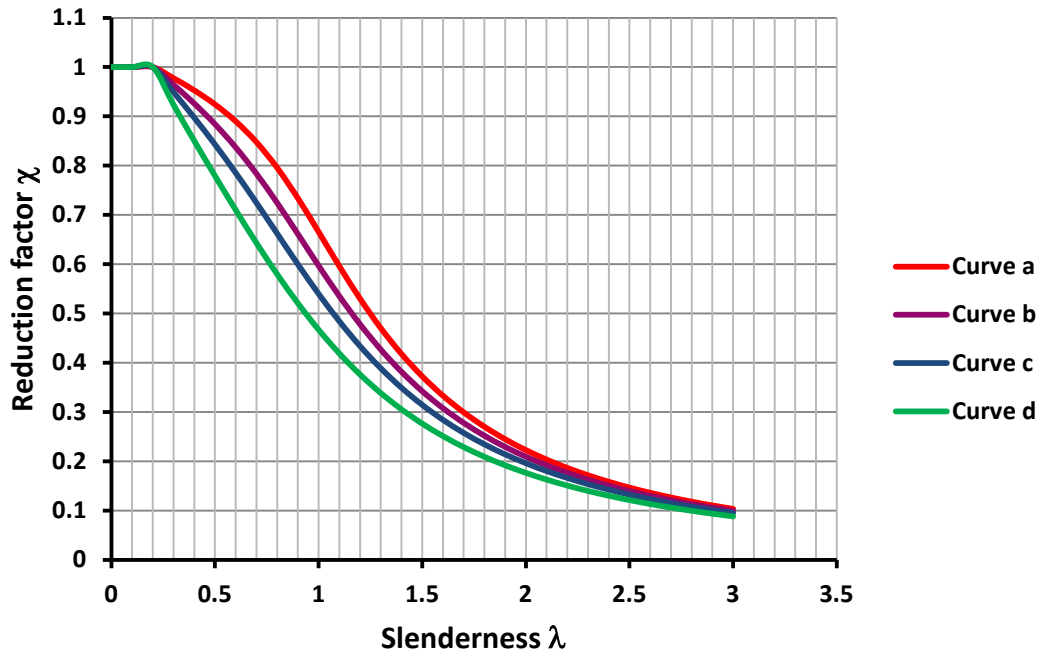


Figure 2.1: European Buckling Curves
(Source: Eurocode 3, 2005)

2.2.2 Eurocode 4 Beam-Column Design

The behavior of column subjected to axial load and bending moment can be given by interaction curve showing the reduction of ultimate load with increasing moment. An approximation to this curve can be obtained by considering fully plastic sections for different arbitrary positions of the neutral axis. The values of the moment and axial compression calculated from the stress block will give the points to construct the curve. Generally, the numbers of points required for drawing the interaction curve depend on moment application about which axis; if the end moment about major axis, four key points from A-D are required (see Figure 2.2). Otherwise, one additional key point is required at end of structural steel section if the end moment about minor axis; five key points from A-E.

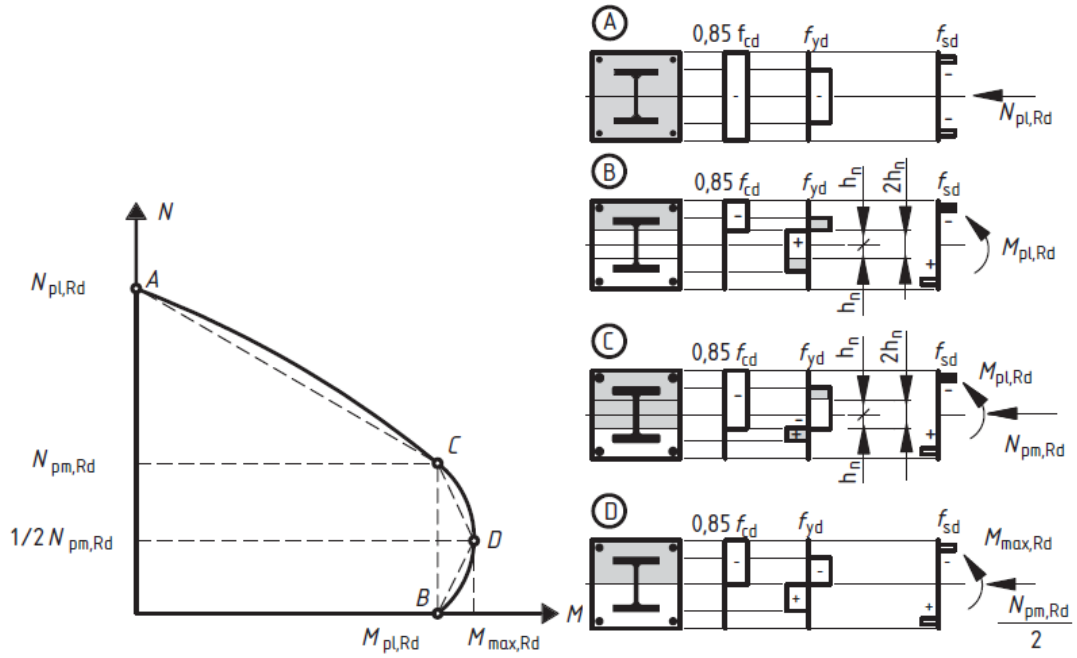


Figure 2.2: Simplified Interaction Curve and Corresponding Stress Distributions
(Source: Eurocode 4, 2004)

The maximum internal moment at point D is:

$$M_{\max} = Z_s f_{yd} + \frac{1}{2} Z_c f_{cd} + Z_r f_{sd} \quad (2.17)$$

where

Z_s plastic modulus of steel cross-section

Z_c plastic modulus of overall concrete cross-section.

Z_r plastic modulus of reinforcement

The plastic modulus of the reinforcement can be calculated as:

$$Z_r = \sum_{i=1}^n A_{ri} e_i \quad (2.18)$$

where

A_{ri} area of one reinforcing bar

e_i distance to the bending axis considered

For the region equal twice the distance between centroid axis and neutral axis, $2h_n$, the plastic moment can be calculated as:

$$M_{pn} = Z_{sn}f_{yd} + \frac{1}{2}Z_{cn}f_{cd} + Z_{rn}f_{sd} \quad (2.19)$$

where

Z_{sn} Plastic section modulus of steel section within $2h_n$ region

Z_{rn} Plastic section modulus of reinforcing steel within $2h_n$ region

Z_{cn} Plastic section modulus of concrete within $2h_n$ region

For concrete incased I- steel section, the plastic modulus about major axis can be taken from the design tables (Table 2.3), or the following equation can be used:

$$Z_s = \frac{(d - 2t_f)t_w^2}{4} + b_f t_f (d - t_f) \quad (2.20)$$

where

d Overall depth of the structural steel section

b_f Width of the flange of a steel section

t_f Thickness of a flange of the structural steel section

t_w Thickness of a web of the structural steel section

The plastic modulus of the concrete is:

$$Z_c = \frac{h_1 h_2}{4} - Z_s - Z_r \quad (2.21)$$

where

h_1, h_2 Dimension of the section

There are three possible zones to look into position of the neutral axis; neutral axis in the web ($h_n \leq d/2 - t_f$), neutral axis in the flange ($d/2 - t_f \leq h_n \leq d/2$), and Neutral Axis outside the steel section ($d/2 \leq h_n \leq h_2/2$). For finding the location of the neutral axis, assume h_n is located on a certain region, then use (Equations 2.22 to 2.26) to find new value for h_n . If the value of h_n is inside the supposed region, the assumption was correct. Otherwise, select another region and repeat the procedure.

The distance h_n and plastic modulus can be calculated according to possible position as follow:

a) Neutral Axis in the web ($h_n \leq d/2 - t_f$)

$$h_n = \frac{N_{pm} - A_{rn}(2f_{sd} - f_{cd})}{2h_1f_{cd} + 2t_w(2f_{yd} - f_{cd})} \quad (2.22)$$

$$Z_{sn} = t_w h_n^2 \quad (2.23)$$

where

A_{rn} Is the sum of reinforcement inside within the $2h_n$ region

N_{pm} Axial force resistance of concrete portion of cross-section

b) Neutral Axis in flange ($d/2 - t_f \leq h_n \leq d/2$)

$$h_n = \frac{N_{pm} - A_{rn}(2f_{sd} - f_{cd}) + (b_f - t_w)(d - 2t_f)(2f_{yd} - f_{cd})}{2h_1f_{cd} + 2b_f(2f_{yd} - f_{cd})} \quad (2.24)$$

$$Z_{sn} = b_f h_n^2 - \frac{(b_f - t_w)(d - 2t_f)^2}{4} \quad (2.25)$$

c) Neutral Axis outside the steel section ($d/2 \leq h_n \leq h_2/2$)

$$h_n = \frac{N_{pm} - A_m(2f_{sd} - f_{cd}) - A_s(2f_{yd} - f_{cd})}{2h_1 f_{cd}} \quad (2.26)$$

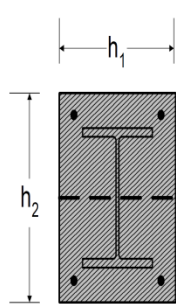
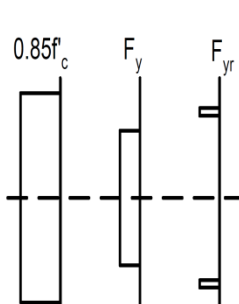
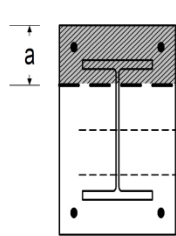
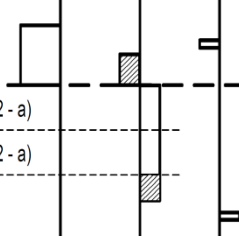
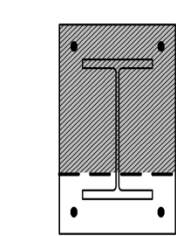
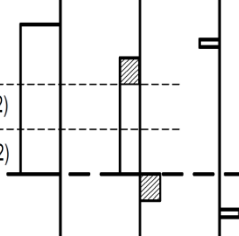
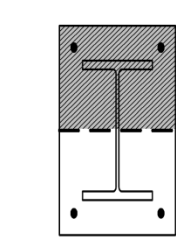
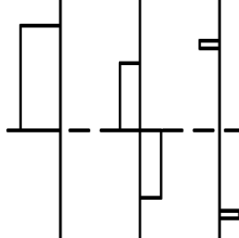
$$Z_{sn} = Z_s \quad (2.27)$$

The plastic modulus of the concrete in the region of $2h_n$ is given as

$$Z_{cn} = h_1 h_n^2 - Z_{sn} - Z_m \quad (2.28)$$

The following table (Table 2.3) demonstrates the previous procedure which leads to a better understanding.

Table 2.3: Stress Distributions at each Point of Interaction Curve (Major Axis Bending)
(Source: Kim, 2005)

	Section	Stress Distribution	Equation
A			$N = P_{pl} = A_c \cdot f_{cd} + A_s \cdot f_{yd} + A_r \cdot f_{rd}$ $f_{cd} = 0.85 \cdot f'_c / \gamma_c, f_{yd} = F_y / \gamma_s, f_{rd} = F_{yr} / \gamma_r$ <p>$\gamma_c, \gamma_s, \gamma_r$: partial safety factors</p> $A_c = h_1 \cdot h_2 - A_s - A_r$ $M = 0$
B			$N = 0$ $h_n \rightarrow h_1 \cdot a \cdot f_{cd} = (h_2 - 2a) \cdot t_w \cdot f_{yd}$ $M = M_{pn} = Z_{sn} \cdot f_{yd} + \frac{1}{2} \cdot Z_{cn} \cdot f_{cd} + Z_r \cdot f_{rd}$ $Z_{sn} = t_w \cdot h_n^2 ; Z_{cn} = h_1 \cdot h_n^2 - Z_{sn} - Z_r$
C			$N = N_{pm} = A_c \cdot f_{cd}$ $h_n \rightarrow h_1 \cdot a \cdot f_{cd} = (h_2 - 2a) \cdot t_w \cdot f_{yd}$ $M = M_{pn} = Z_{sn} \cdot f_{yd} + \frac{1}{2} \cdot Z_{cn} \cdot f_{cd} + Z_r \cdot f_{rd}$
D			$N = \frac{1}{2} \cdot N_{pm} = \frac{1}{2} \cdot A_c \cdot f_{cd}$ $M = M_{max} = Z_s \cdot f_{yd} + \frac{1}{2} \cdot Z_c \cdot f_{cd} + Z_r \cdot f_{rd}$ $Z_s = \frac{(d - 2 \cdot t_f) \cdot t_w^2}{4} + b_f \cdot t_f \cdot (d - t_f)$ $Z_c = \frac{h_1 \cdot h_2^2}{4} - Z_s - Z_r$

In case the end moment about minor axis, the plastic modulus can be taken from Table 2.4, or it calculates as:

$$Z_s = \frac{(d - 2t_f)t_w^2}{4} + \frac{2t_f b_f^2}{4} \quad (2.29)$$

For the concrete, the plastic modulus is obtained from:

$$Z_s = \frac{h_1 h_2}{4} - Z_s - Z_r \quad (2.30)$$

Here, for the location of the neutral axis, two regions need to be considered; neural axis in the flanges ($t_w/2 \leq h_n \leq b_f/2$), and neural axis in the flanges ($b_f/2 \leq h_n \leq h_2/2$). The same iterative procedure should be used. The following equations explain the way for finding the distance h_n and plastic modulus.

a) Neutral Axis in the web ($t_w/2 \leq h_n \leq b_f/2$)

$$h_n = \frac{N_{pm} - A_m(2f_{sd} - f_{cd}) - t_w(2t_f - d)(2f_{yd} - f_{cd})}{2h_1 f_{cd} + 4t_f(2f_{yd} - f_{cd})} \quad (2.31)$$

$$Z_{sn} = 2t_f h_n^2 + \frac{(d - 2t_f)t_w^2}{4} \quad (2.32)$$

b) Neutral Axis in the flanges ($b_f/2 \leq h_n \leq h_2/2$)

$$h_n = \frac{N_{pm} - A_m(2f_{sd} - f_{cd}) - A_s(2f_{yd} - f_{cd})}{2h_1 f_{cd}} \quad (2.33)$$

$$Z_{sn} = Z_s \quad (2.34)$$

The plastic modulus of the concrete in the region of $2h_n$ is given as

$$Z_{cn} = h_1 h_n^2 - Z_{sn} - Z_{rn} \quad (2.35)$$

The axial force at point E is given as

$$N_E = h_2 (h_E - h_n) f_{cd} + 2t_f (h_E - h_n) (2f_{yd} - f_{cd}) + A_{rE} (2f_{sd} - f_{cd}) + N_{pm} \quad (2.36)$$

where

A_{rE} reinforcement area within region between the distances h_n and h_E

h_E Distance from centroidal axis to neutral axis for point E

Finally, the moment M_E is obtained as

$$M_E = M_{\max} - \Delta M_E \quad (2.37)$$

where

$$\Delta M_E = Z_{sE} f_{yd} + \frac{1}{2} Z_{cE} f_{cd} + Z_{rE} F_{sd} \quad (2.38)$$

M_{\max} The maximum internal moment

Z_{cE} Plastic section modulus of concrete within $2h_E$ region

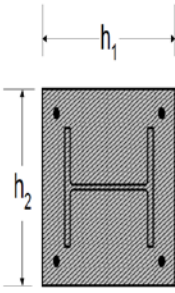
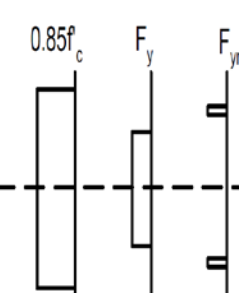
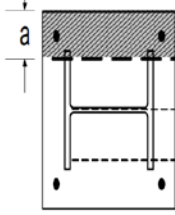
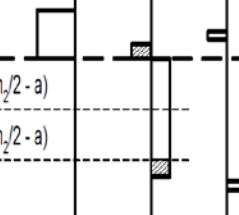
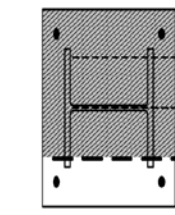
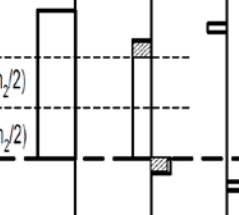
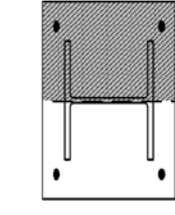
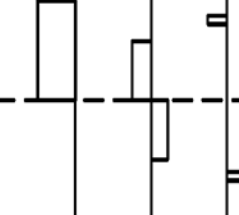
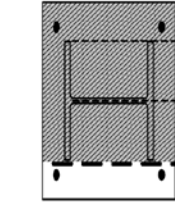
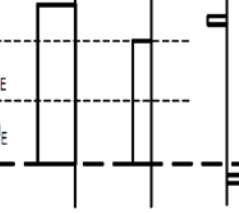
Z_{rE} Plastic section modulus of reinforcing steel within $2h_E$ region

Z_{sE} Plastic section modulus of steel section within $2h_E$ region

Which the terms Z_{sE} , Z_{cE} , and Z_{rE} can be calculated from the appropriate above equations by substituting h_E instead of h_n .

Table 2.4: Stress Distributions at each Point of Interaction Curve (Minor Axis Bending)

(Source: Kim, 2005)

	Section	Stress Distribution	Equation
A			$N = P_{pl} = A_c \cdot f_{cd} + A_s \cdot f_{yd} + A_r \cdot f_{rd}$ $A_c = h_1 \cdot h_2 - A_s - A_r$ $f_{cd} = 0.85 \cdot f'_c / \gamma_c, f_{yd} = F_y / \gamma_s, f_{rd} = F_{yr} / \gamma_r$ $M = 0$
B			$N = 0$ $h_n \rightarrow h_1 \cdot a \cdot f_{cd} = 2 \cdot (h_2 - 2a) \cdot t_f \cdot f_{yd} + (d - 2 \cdot t_f) \cdot t_w \cdot f_{yd}$ $M = M_{pn} = Z_{sn} \cdot f_{yd} + \frac{1}{2} \cdot Z_{cn} \cdot f_{cd} + Z_{rn} \cdot f_{rd}$ $Z_{sn} = 2 \cdot t_f \cdot h_n^2 + \frac{(d - 2 \cdot t_f) \cdot t_w^2}{4}$ $Z_{cn} = h_1 \cdot h_n^2 - Z_{sn} - Z_{rn}$
C			$N = N_{pm} = A_c \cdot f_{cd}$ $M = M_{pn} = Z_{sn} \cdot f_{yd} + \frac{1}{2} \cdot Z_{cn} \cdot f_{cd} + Z_r \cdot f_{rd}$
D			$N = \frac{1}{2} \cdot N_{pm} = \frac{1}{2} \cdot A_c \cdot f_{cd}$ $M = M_{max} = Z_s \cdot f_{yd} + \frac{1}{2} \cdot Z_c \cdot f_{cd} + Z_r \cdot f_{rd}$ $Z_s = \frac{(d - 2 \cdot t_f) \cdot t_w^2}{4} + \frac{1}{2} \cdot t_f \cdot b_f^2$ $Z_c = \frac{h_1 \cdot h_2^2}{4} - Z_s - Z_r$
E			$N = \frac{1}{2} \cdot (P_{pl} + N_{pm})$ $M = M_{max} - \Delta M_E, \Delta M_E = Z_{sE} \cdot f_{yd} + \frac{1}{2} \cdot Z_{cE} \cdot f_{cd} + Z_{rE} \cdot f_{rd}$ $Z_{sE} = 2 \cdot t_f \cdot h_E^2 + \frac{(d - 2 \cdot t_f) \cdot t_w^2}{4}$ $Z_{cE} = h_1 \cdot h_E^2 - Z_{sE} - Z_{rE}$

Chapter 3

PRELIMINARY DESIGN AND FINITE ELEMENT MODELING

3.1 Preliminary Design

Examining the cyclic behavior of concrete-encased steel composite beam-columns under different levels of axial loads will be carried out by performing a preliminary design of steel, reinforced concrete and composite beam-columns of a suggested frame, developing an efficient 3-D finite element model for each beam-columns prototype, and then comparing their behaviors.

In this study, the preliminary design was performed through the analysis of the suggested frame (Figure 3.1) subjected to conservative dead and live loads, as well as earthquake load. The earthquake parameters are set according to Eurocode 8 (Eurocode 8. , 2004). Thus the following parameters are set for the design as; Ground acceleration, $a_g = 0.4$, Soil Type A (rock and very stiff soil as classified by the code) and the behavior factor, $q=2$ (see also Figure A1 in Appendix A). The frame is designed according to Eurocode 2 for reinforced concrete column (Eurocode 2. , 2004), Eurocode 3 for steel column (Eurocode3, 2005), and Eurocode 4 for composite column (Eurocode 4. , 2004). For the comparison to be persuasive, the stress ratios resulted from loading were kept in range of 88% to 90%. The load cases that have been adopted in this study are given in Table 3.1. Throughout the analysis and design step ETABS (Non-Linear Version 9.7.2) is used. The maximum moment,

shear and axial values was obtained as shown in Figure 3.2-3.4, respectively.

Cross-sections resulting from design are shown in Figure 3.5 and detailed in Table 3.2. All detailed information, properties and governing parameters and equations are provided in Appendix A.

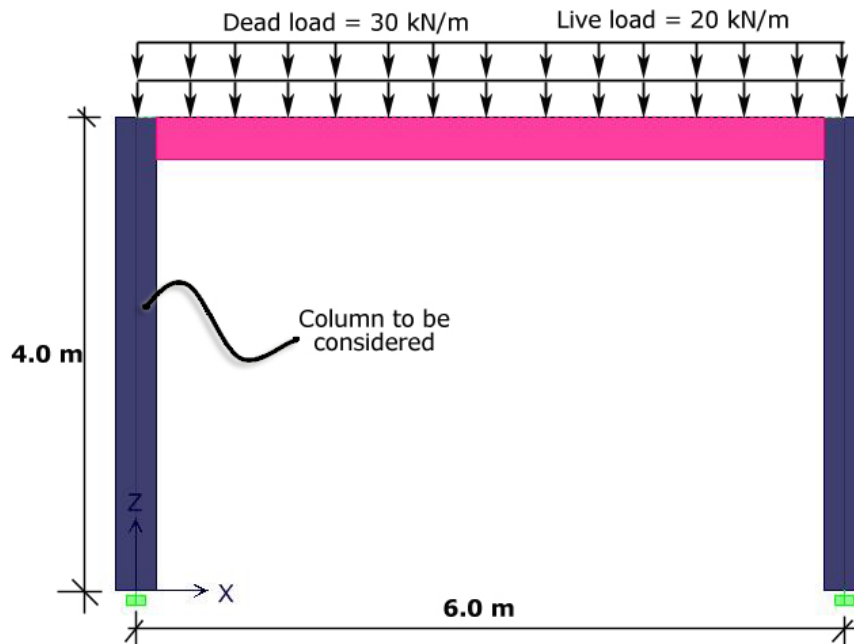


Figure 3.1: Suggested Frame with Conservative Loads

Table 3.1: Load Combinations

Combination	Factor
DSTLS1	1.35 DEAD
DSTLS2	1.35 DEAD+1.5 LIVE
DSTLS3	1 DEAD+0.3 LIVE+1 EQ
DSTLS4	1 DEAD+0.3 LIVE - 1 EQ
DSTLS5	1 DEAD+1 EQ
DSTLS6	1 DEAD - 1 EQ
DSTLD1	1 DEAD
DSTLD2	1 DEAD+1 LIVE

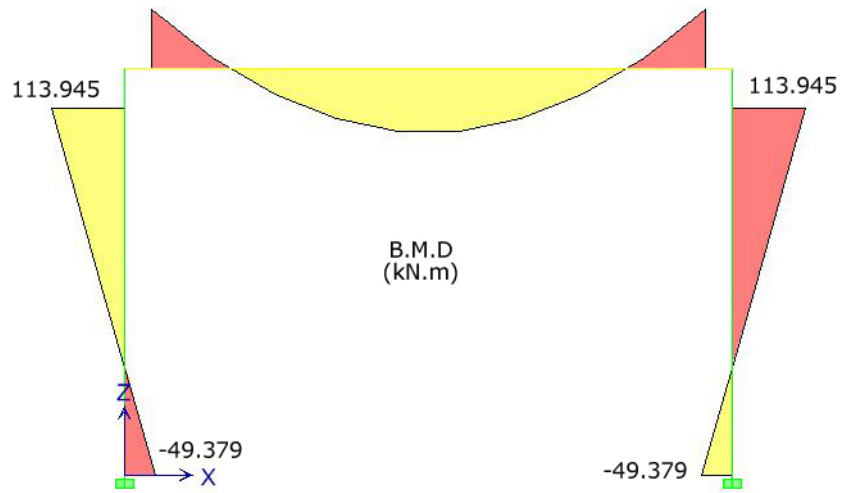


Figure 3.2: Maximum Bending Moment Values Resulting from Load Cases

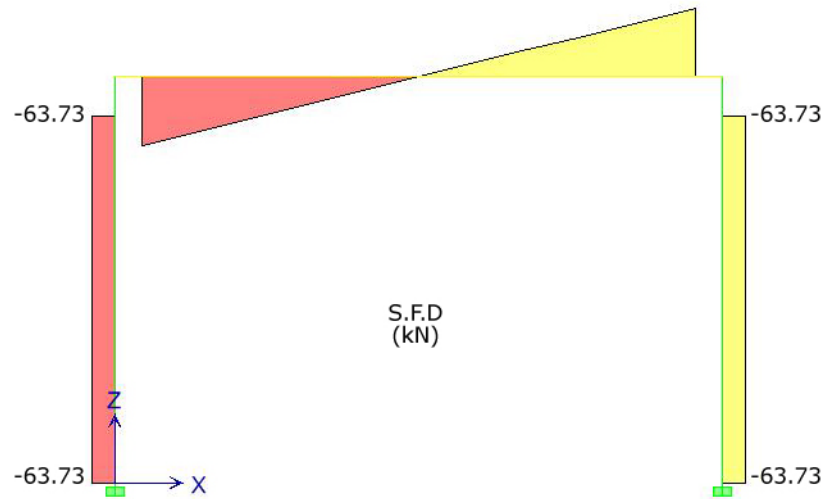


Figure 3.3: Shear Force Values for Maximum Moment Load Case

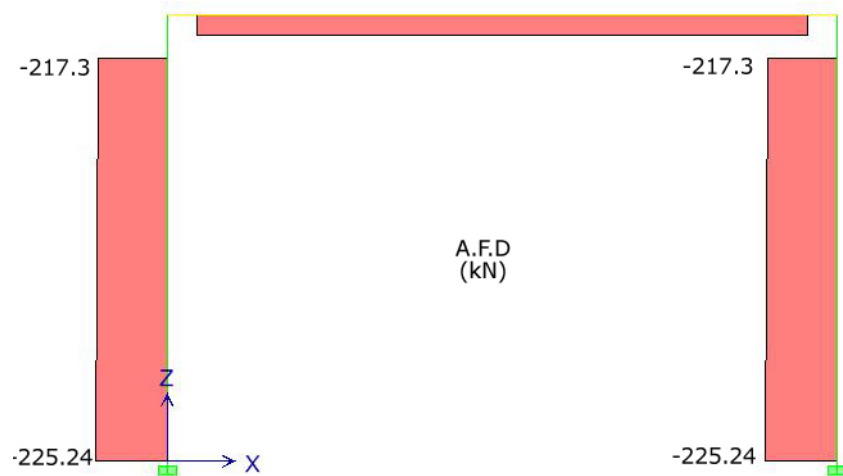


Figure 3.4: Axial Force Values for Maximum Moment Load Case

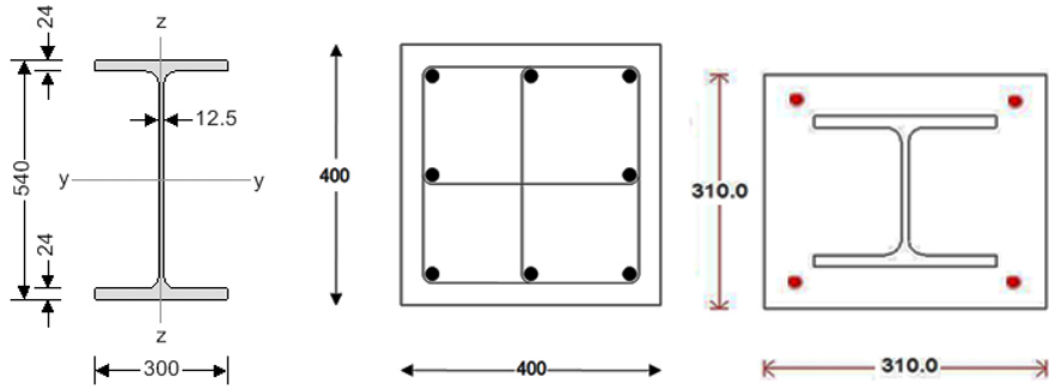


Figure 3.5: Cross-Sections Resulting from Design (all the unites in mm).

Table 3.2: Detailed Cross-Sections and Materials Properties

Beam-Column Type	Dimensions		Steel Section	Reinforcement Bars	stirrups	Material Properties	
	B (mm)	D (mm)				f_{ys}^*	f_{yr}^*
Steel	300	540	HE 550 A	-	-	275	-
Reinforced Concrete	400	400	-	4Ø20 and 4Ø16	Ø8@100mm	-	450
Encased Composite	310	310	HE200B	4Ø10	Ø8@100mm	275	450

*where f_{ys} and f_{yr} Design value of the yield strength of structural steel, Design yield strength of reinforcement bars respectively

3.2 Finite Element Modeling

3.2.1 Introduction

Finite Element Method (FEM) can provide significant perception into the likely behavior of columns under cyclic loading comparing with preparing full-scale testing which consider as expensive and time consuming alternative. Although finite element can reduce the cost of research, such analysis has significant limitation which can substantially impact on the main behavior. Some of these limitations can

be summarized as material imperfections and nonlinearity, residual stresses and strain especially for steel column, unilateral effect which related to concrete behavior under cyclic loading. Furthermore, the difficulties resulting from adopted a cyclic loading similar to that suggested by Applied Technology Council (ATC) guidelines (ATC 1992- ATC 24) which is really time consuming and computationally costly.

Version 6.12 of the finite element program ABAQUS (ABAQUS, 2012) was utilized to model the three prototype beam-columns as described in chapter 2; SC-(10P, 15P, and 20P), RC-(10P, 15P, and 20P), and CC-(10P, 15P, and 20P) where 10P for example represents 10% of axial load capacity. The main objectives here were to evaluate and compare the effects of different axial loads levels on the cyclic capacity of steel, reinforced concrete, and composite beam-columns. These main objectives were facilitated by

- 1) Determining the lateral load capacity of beam-column prototypes
- 2) Determining the yield level lateral capacity by measure the elastic stiffness of each prototype
- 3) Evaluating whether the prototype elastic stiffness had changed
- 4) Identifying the high stress and strain zones,
- 5) Evaluating the effects of the level of axial load on stiffness, strength, and ductility of beam-column prototypes.

This section elucidates on the materials definition and loading protocols as well as the details of the finite element models and analysis procedures.

3.2.2 Modeling Approach

The FEM of the concrete-encased steel composite beam-columns was carried out by modeling the reinforcement bars, stirrups and defining the companion interfaces. Then, the unconfined concrete which consists the concrete cover were modeled. After that, steel section and their companion interfaces, highly confined concrete and their companion interfaces, and partially confined concrete and their companion interfaces were defined, see Figure 3.6. (Ellobody & Young, 2011)

For steel and reinforced concrete beam-columns, the approach was similar as earlier approach but steps were less depending on the number of parts which include in modeling.

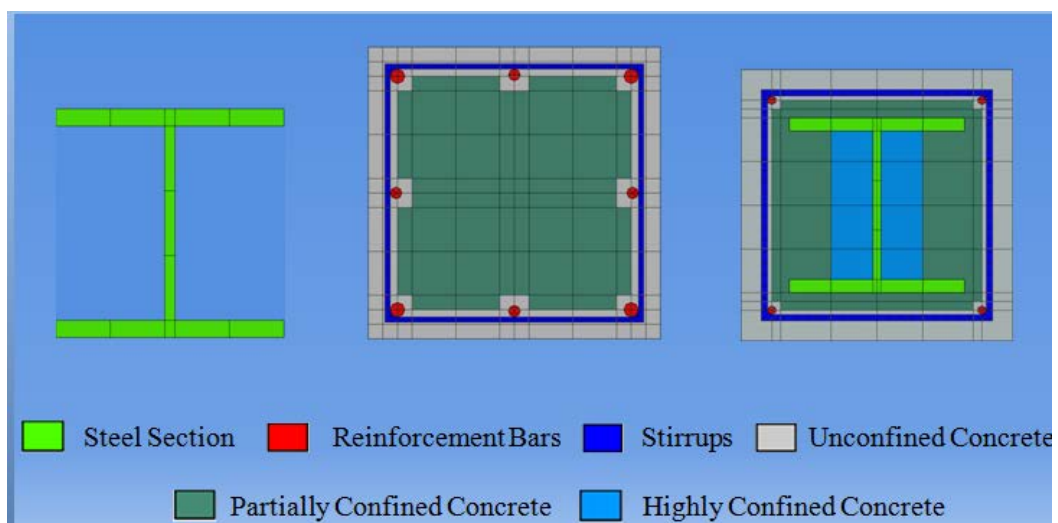


Figure 3.6: Modeling Parts that Used for Beam-Column Prototypes

3.2.3 Material Definition

The material definition is an important part of finite element analysis, and each component should be defined carefully and all parts should be defined with appropriate material parameters.

3.2.3.1 Confined Concrete

The confinement of the concrete by stirrups has been recognized in early research. This confinement can provide a confining pressure which leads in an enhancement in the strength and ductility of concrete (Chen & Lin, 2006). Moreover, Mander et al. (1988) have demonstrated that confinement is also affected by other factor, such as the spacing between the transverse reinforcement, existing of additional supplementary overlapping hoops or cross ties with several legs crossing the section, the distribution of longitudinal bars around the perimeter, the volume of transverse reinforcement to the volume of the concrete core or the yield strength of the transverse reinforcement, and loading type. Furthermore, they proposed a unified stress-strain approach for confined concrete applicable to different shape of cross-sections.

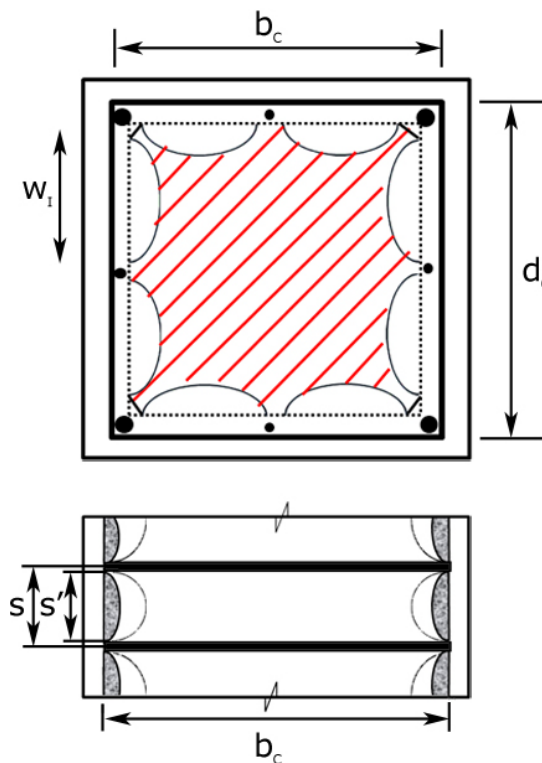


Figure 3.7: Effectively Confined Core for Rectangular Cross-Section
(Source: Mander et al., 1988)

As shown in Figure 3.7, the arching action occurs horizontally between longitudinal bars and vertically between the layers of the transverse reinforcement. This action assumed to act in the form of second-degree parabolas with an initial tangent slope of 45° (Mander et al., 1988).

The total plan area of unconfined concrete at the level of the stirrups when there are n longitudinal bars is

$$A_i = \sum_{i=1}^n \frac{(w_i)^2}{6} \quad (3.1)$$

where

w_i the clear distance between adjacent longitudinal bars (see Figure 3.7)

The confinement effectiveness coefficient, which is the ratio of area of effectively confined concrete core to the area of concrete core, can be expressed as

$$K_e = \frac{\left(1 - \sum_{i=1}^n \frac{(w_i)^2}{6b_c d_c}\right) \left(1 - \frac{S'}{2b_c}\right) \left(1 - \frac{S'}{2d_c}\right)}{1 - \rho_{cc}} \quad (3.2)$$

where

b_c is core dimensions to centerlines of perimeter hoop in x direction

d_c is core dimensions to centerlines of perimeter hoop in y direction

S' is clear vertical spacing between hoop bars

ρ_{cc} is ratio of area of longitudinal reinforcement to area of core of section

Ratio of the volume of transverse confining bars to the volume of confined core in the x and y directions may be expressed as

$$\rho_x = \frac{A_{sx}}{Sd_c} \quad \text{or} \quad \rho_y = \frac{A_{sy}}{Sb_c} \quad (3.3)$$

where

A_{sx}, A_{sy} the total area of transverse bars running in the x and y directions

S Vertical spacing between spirals from center to center

The lateral confining stress on the concrete (total transverse bar force divided by vertical area of confined concrete) is given in the x direction and in the y direction as

$$f_{Lx} = \rho_x f_{yh} \quad \text{or} \quad f_{Ly} = \rho_y f_{yh} \quad (3.4)$$

The effective lateral confining is

$$f'_L = f_L K_e \quad (3.5)$$

The compressive strength of confined concrete equation is

$$f'_{cc} = f'_{co} \left(-1.254 + 2.254 \sqrt{1 + \frac{7.94 f'_L}{f'_{co}}} - 2 \frac{f'_L}{f'_{co}} \right) \quad (3.6)$$

where

f'_{co} is unconfined concrete compressive strength

The longitudinal compressive concrete stress f_c is given by

$$f_c = \frac{f'_{cc} \chi^r}{r - 1 + \chi^r} \quad (3.7)$$

where

f'_{cc} is compressive strength of confined concrete (will be defined later)

$$\chi = \frac{\varepsilon_c}{\varepsilon_{cc}} \quad (3.8)$$

where

ε_c is the longitudinal compressive concrete strain, and

$$\varepsilon_{cc} = \varepsilon_{co} \left[1 + 5 \left(\frac{f'_{cc}}{f'_{co}} - 1 \right) \right] \quad (3.9)$$

where

f'_{co} is the unconfined concrete strength

ε_{co} is the strain corresponding to unconfined concrete ($\varepsilon_{co} = 0.002$)

$$r = \frac{E_c}{E_c - E_{sec}} \quad (3.10)$$

where

$$E_c = 5000 \sqrt{f'_{co}} \text{ MPa} \quad (3.11)$$

$$E_{sec} = \frac{f'_{cc}}{\varepsilon_{cc}} \quad (3.12)$$

For encased composite beam-columns, the amount of the confining pressure depends on the steel section shape and its yield strength in addition to the factors that mentioned earlier. As a result, a highly confined zone occurs resulting from arching action formed by steel section (Figure 3.8).

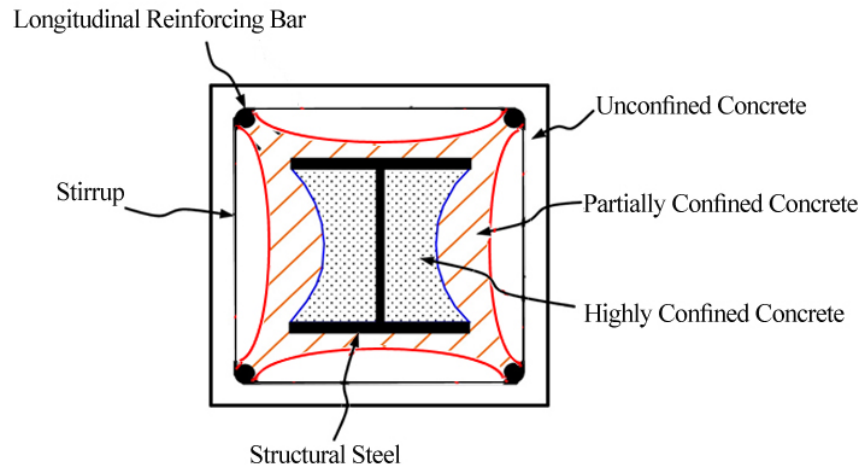


Figure 3.8: Confinement Regions in a Concrete Encased Steel Composite Column (Source: Chen & Lin, 2006)

Stress-strain curves for reinforced concrete column and encased composite column are shown in Figure 3.9 and Figure 3.10 respectively. All detailed information and calculations are provided in Appendix B as well.

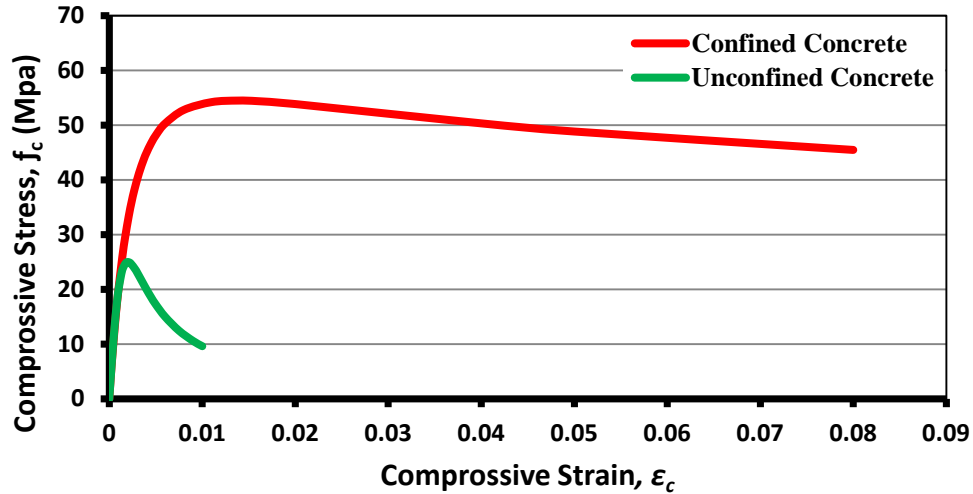


Figure 3.9: Stress-Strain Curves for Unconfined and Confined Concrete in Reinforced Concrete Column

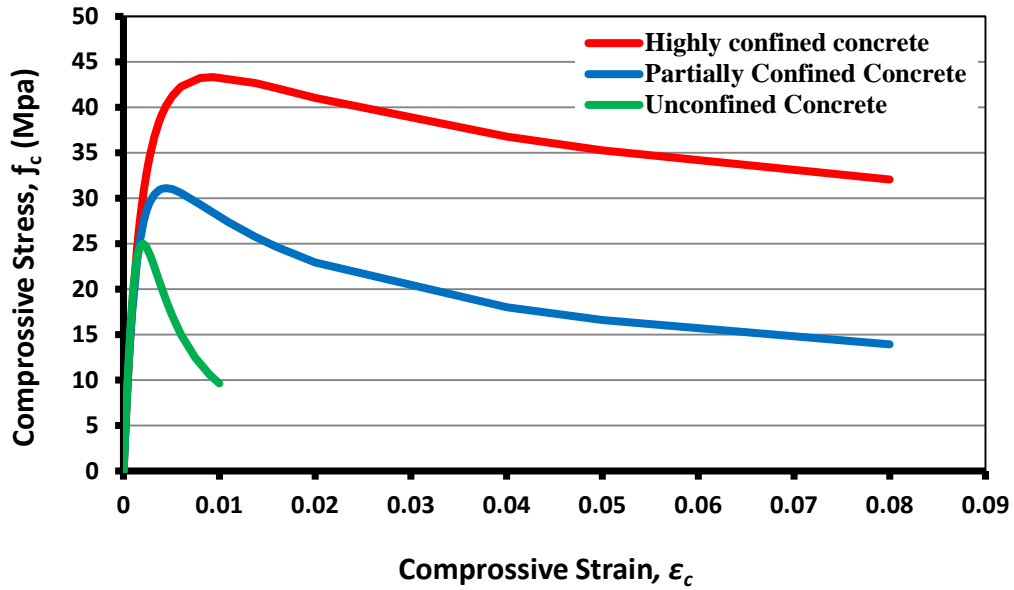


Figure 3.10: Stress-Strain Curves for Unconfined, Partially, and Highly Confined Concrete in Encased Composite Column

The concrete damaged plasticity model, which implemented in ABAQUS (ABAQUS, 2012), was used to simulate the inelastic behavior of concrete. This model is based on the assumption of scalar (isotropic) damage and it has capability for modeling plain and reinforced concrete which is subjected to all types of loading conditions under low confining pressures. The model accounts the degradation of the elastic stiffness and stiffness recovery effects under cyclic loading induced (ABAQUS, 2012). In addition to initial yield surface and hardening rule, the model has a flow rule which describe the plastic strain increments.

The definition of concrete damaged plasticity model was started by defined the dilation angle of concrete which assumed to be 15° (Begum et al., 2006). Then, the uniaxial compressive stress-strain of concrete curve (Figure 3.9 or Figure 3.10) was assigned in term of the true plastic strain. After that, the uniaxial tensile strength of concrete model proposed by Li et al. (2002), which represents the post-peak response as an exponential function of the ratio of crack width (Equation 3.13), was used to

define the uniaxial tensile response (Figure 3.11) which is set at 10% of the uniaxial compressive strength. Finally, the damage variables d_t and d_c , which characterize the degradation of the elastic stiffness, were defined as functions of the plastic strains. For more details see (ABAQUS, 2012).

The damage variables can take values from zero, representing the undamaged material, to one, which represents total loss of strength (ABAQUS, 2012).

$$\sigma = f_t' \left\{ 1 - \exp \left[- \left(\frac{0.5/w}{w_f} \right)^{1.3} \right] \right\} \quad (3.13)$$

where

f_t' the tensile strength of concrete

w the crack width in (mm)

w_f the final crack width in (mm)

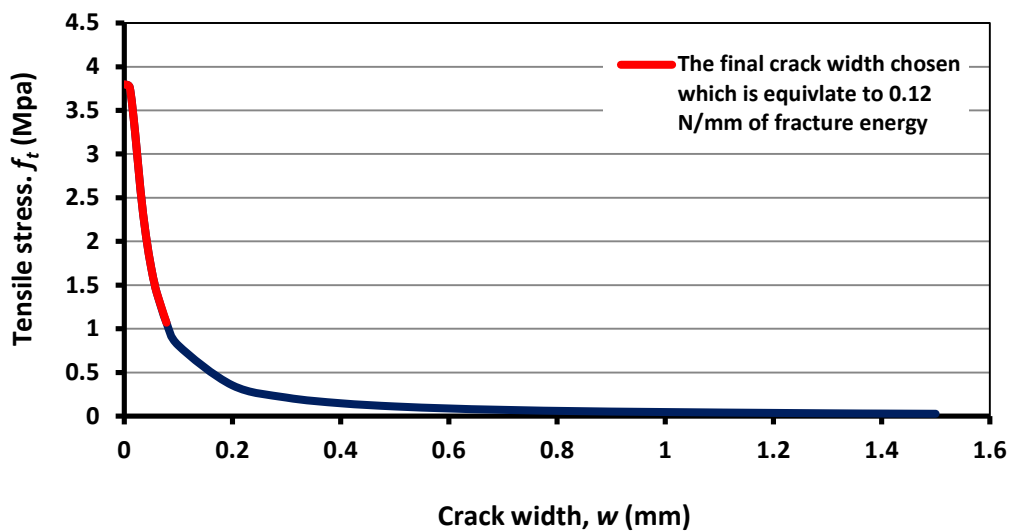


Figure 3.11: Stress-Crack Width Curve Proposed by Li et al. (2002)

3.2.3.2 Steel Section and Reinforcement Bars

The structural steel section and the reinforcement bars are modeled as an elastic–plastic material in both tension and compression as given in (Eurocode 3, 2005) and (Eurocode 2, 2004). The stress–strain responses in compression and tension are assumed to be the same. This response exhibits a linear elastic portion followed strain hardening stage until reach the ultimate stress. The metal plasticity model in ABAQUS was used to define the non-linear behavior of materials. The “ELASTIC” option was used to assign the value of 2.09×10^5 N/mm² for the Young’s modulus and 0.3 for the Poisson’s ratio. The “PLASTIC” option also used to define the plastic part of the stress–strain curve. According to ABAQUS manual (ABAQUS, 2012), true stress and true strain should be used to define the non-linear behavior of material properties. So, the true stresses were assigned in ABAQUS as a function of the true plastic strain.

Mechanical properties for the steel section and reinforcement bars that are used in these simulations are given in Table 3.3.

Table 3.3: Mechanical Properties of the Steel Section and Reinforcement Bars

Part	Yield stress (N/mm ²)	Ultimate stress (N/mm ²)	Density (Kg/m ³)	Young’s modulus (KN/mm ²)	Poisson ratio
Steel section	275	430	7850	209	0.3
Reinforcement bars	450	560	7850	200	0.3

3.2.4 Loading Definition

The specimens were modeled as fixed cantilever beam-columns (Figure 3.12) with an axial load level of 10%, 15%, and 20% of their axial load capacity, Table 3.4 summarizes the axial load capacity for each specimen with flexure stiffness in x and

y direction. A horizontal load was cyclically applied to the free end of the specimen with increasing amplitudes.

The cyclic loading history was applied in accordance with the ATC 24 guidelines for cyclic seismic testing of components of steel structures (ATC 24, 1992). The loading history consisted of elastic cycles (under load control) and inelastic cycles (under displacement control) as shown in Figure 3.13 and 3.14, respectively (Varma et al., 2004).

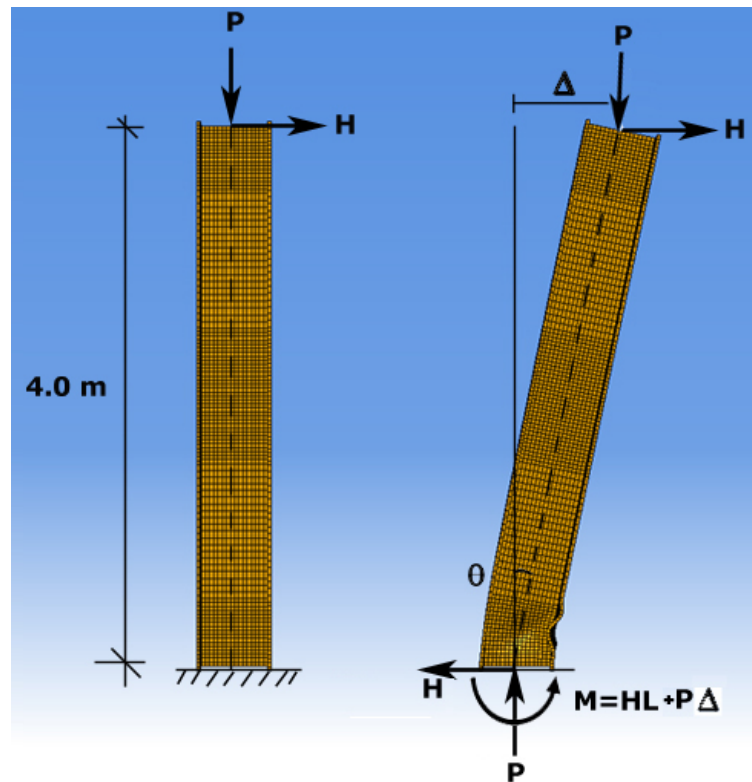


Figure 3.12: Undeformed and Deformed Fixed Cantilever Beam-Column
(Source: Varma, et al.2004)

Table 3.4: Specimens Matrix with Axial Load Capacity

Specimens (#)	Test length (mm)	Capacity (kN)	Axial load (kN)	P/P_o	EI_x	EI_y
SC-10P	4000	5823	582.3	0.10	2.35E+14	2.27E+13
SC-15P	4000		873.45	0.15		
SC-20P	4000		1164.6	0.20		
RC-10P	4000	2964.04	296.404	0.10	8.01E+12	8.01E+12
RC-15P	4000		444.606	0.15		
RC-20P	4000		592.808	0.20		
CC-10P	4000	3321.31	332.131	0.10	2.59E+13	1.88E+13
CC-15P	4000		498.1965	0.15		
CC-20P	4000		664.262	0.20		

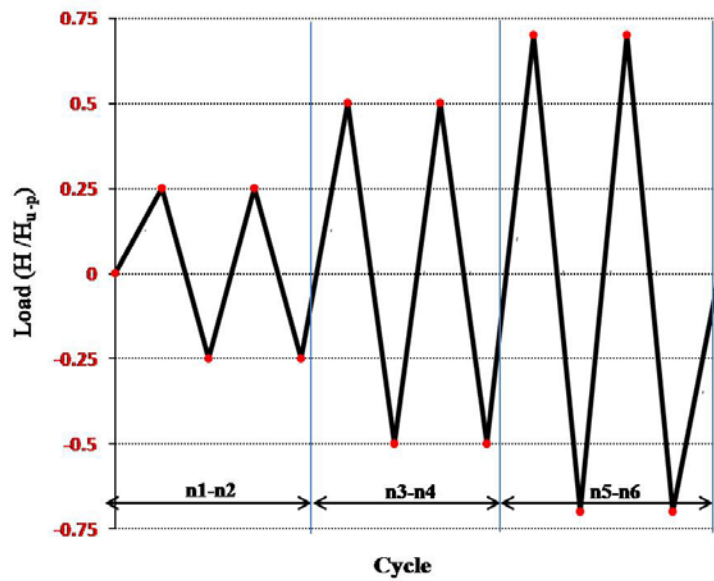


Figure 3.13: The Loading History of Elastic Cycles

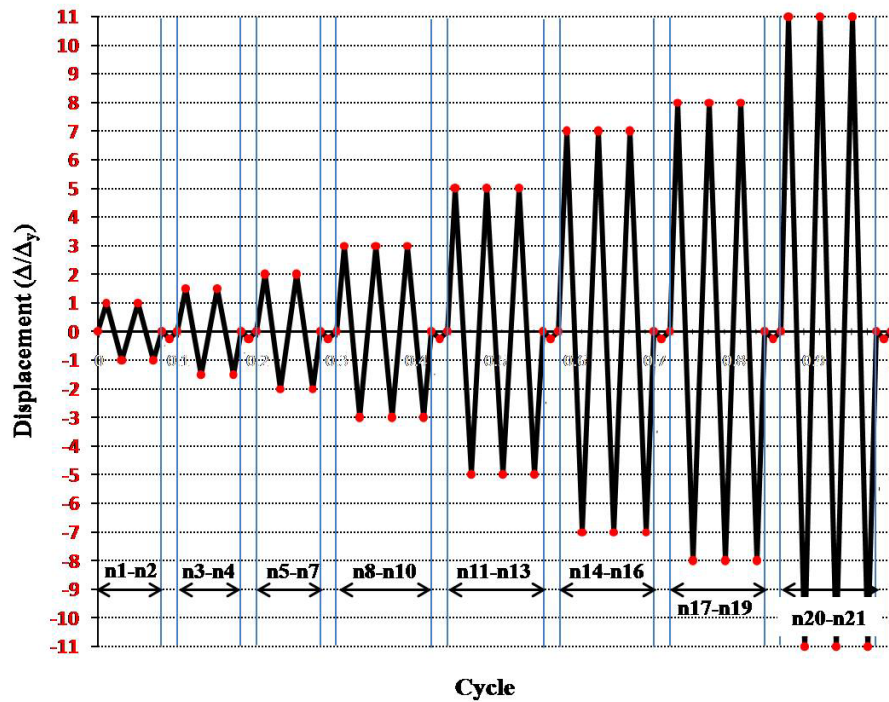


Figure 3.14: The Loading History of Inelastic Cycles

The first part of the analysis was performed to determine the lateral load capacity of the cyclic beam-column specimens, H_{u-p} . Risk Analysis in ABAQUS was used for this matter. It is generally used to predict buckling, or unstable post-buckling response of a structure. The load-displacement curve resulting from risk analysis for composite beam-columns; CC-10P, CC-15P, and CC-20P, is shown in Figure 3.15 which shows the lateral load capacity for each specimen. For steel and reinforced concrete beam-columns, the values of H_{u-p} are listed in Table 3.5.

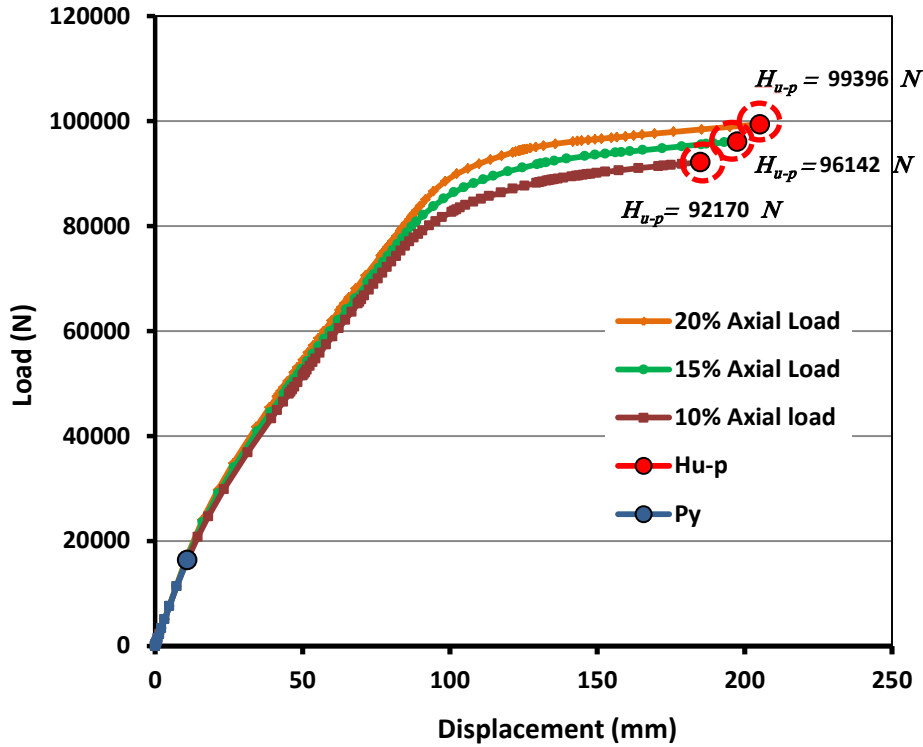


Figure 3.15: The Load-Displacement Curve for Composite Beam-Columns; CC-10P, CC-15P, and CC-20P

The second part of the analysis was performed to determine the yield displacement, Δ_y , based upon H_{u-p} . Two complete cycles (Figure 3.13) were completed at a peak lateral load of $0.25 H_{u-p}$, $0.50 H_{u-p}$, and $0.70 H_{u-p}$. The displacement Δ_y was computed using the recorded secant flexural stiffness from the first cycle at $0.70 H_{u-p}$ and pre-determined H_{u-p} . The values of Δ_y that are found are listed in Table 3.5.

Once Δ_y was determined, two complete inelastic cycles of $1.0 \Delta_y$, $1.5 \Delta_y$, and $2.0 \Delta_y$ were performed. Once these cycles were completed, three complete inelastic cycles of $3.0 \Delta_y$, $4.0 \Delta_y$, $5.0 \Delta_y$, and $6.0 \Delta_y$ were performed. At the end of each inelastic displacement level, a half-elastic cycle was performed (Figure 3.14). The specimen was cycled until the specimen capacity had dropped below 50% of its maximum value (Varma et al., 2004).

Table 3.5: The Lateral Load Capacity and the Yield Displacement of the Cyclic Beam-Column Specimens

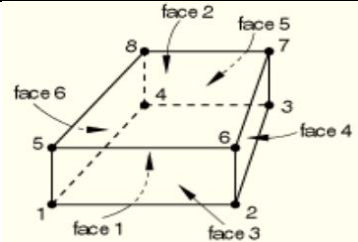

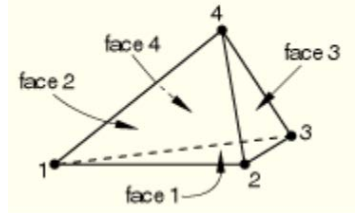
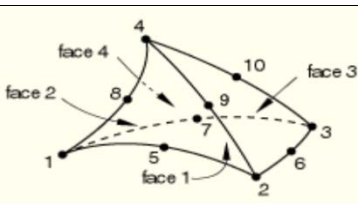
Specimens	P_y (N)	H_{u-p} (N)	K_{sec} (N/mm)	Δ_y (mm)
SC-10P	340090	390298	9721.0	40.15
SC-15P	351079	401287	9641.7	41.62
SC-20P	361722	411930	9562.0	43.08
RC-10P	21690.9	70231.8	3289.9	21.35
RC-15P	22130.7	75464.3	3284.0	22.98
RC-20P	22378	80913	3258.7	24.83
CC-10P	11346.4	92170.1	1418.6	64.97
CC-15P	17044.4	96141.5	1401.9	68.58
CC-20P	16999	99395.8	1343.8	73.97

3.2.5 Finite Element Type and Mesh

ABAQUS software contains a large variety of elements, but in finite element analysis the current ABAQUS library suggests a number of hexahedron elements. All the beam-columns components were modeled using the element C3D8 that is three dimensional 8-noded brick element (Table 3.6). The element has three degrees of freedom per node and suitable to all column components (Ellobody et al., 2011).

Since the stress distribution and plastic deformation are very important at plastic hinge zone, the model should have enough mesh density (ABAQUS, 2012). The critical zone is near the base of beam-columns. As a result, the mesh density increased in critical zones. It goes to reduce the analysis cost in this simulation.

Table 3.6: Various Elements Used in ABAQUS (ABAQUS inc, 2012)

Element	Description	D.O.F.	Element shape
C3D8	Hexagonal Element	24	
C3D20R	Hexagonal Element	60	
C3D4	Tetrahedral Element	12	
C3D10M	Tetrahedral Element	30	

3.2.6 Verification of FEM of the Encased Composite Beam-Columns

The finite element models of encased composite beam-columns developed in this study were verified against tests detailed in (Ellobody & Young, 2011). Three tests were used in this research to verify the finite element modeling approach. The details of the specimens, geometry and materials properties of encased composite beam-columns are shown in Table 3.7. Figure 3.16 shows the principal stress contour at failure.

Table 3.7: Specimen Dimensions and Materials Properties (Ellobody & Young, 2011)

Test	Dimensions			Steel section	Reinforcement		Material properties		
	B (mm)	D (mm)	Kl_e^* (mm)		Long.	Transverse	Concrete strength (MPa)	f_{ys} (MPa)	f_{yr} (MPa)
1	160	160	924	H 100×100×6×8	4Ø6	Ø4 @75 mm	18.5	306	376
2	160	160	2309	H 100×100×6×8	4Ø6	Ø4 @75 mm	21.4	298	376
3	160	160	3464	H 100×100×6×8	4Ø6	Ø4 @75 mm	22.5	304	376

*where k and l_e is effective length factor, effective length of column respectively

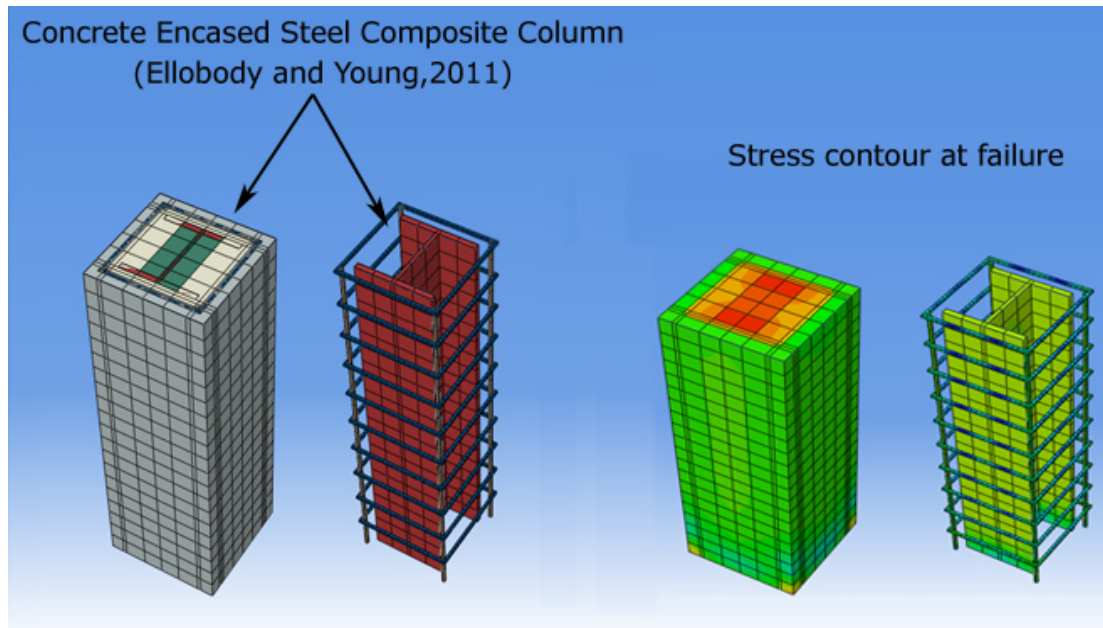


Figure 3.16: Specimens Layout and Stress Contour at Failure for Specimen 1

The ultimate axial capacity resulting from finite element model, P_{VE} , is compared with reference results (Ellobody & Young, 2011) in Table 3.8. It can be seen that there are good agreement between ultimate axial capacity from the test (P_{test}), FEM of (Ellobody & Young, 2011), and P_{VE} .

Table 3.8: Comparison between Test, FE (Ellobody & Young, 2011), and Modeling Results

Test	P_{VE}	P_{test}	P_{EC4}	P_{FE}	P_{VE}/P_{test}	P_{VE}/P_{FE}
1	1096	996	951	1009	1.1	1.08
2	892	974	759	868	0.91	1.02
3	792	874	567	800	0.90	0.99

Chapter 4

THE RESULTS AND DISCUSSION

4.1 General

The main purpose of this study was to determine the effects of different levels of axial loads on the cyclic capacity of steel, reinforced concrete, and composite beam-columns. To achieve this, a finite element analysis was conducted with all appropriate parameters considered and data was collected. This data was then analyzed to provide insights into encased composite columns behavior under cyclic loading. Factors explored included strength, ductility, and stiffness. Observations are made through the aid of plots of reduced data and photographs in developing relationships between parameters and behavior. Next sections provide a summary of key specimen results.

4.2 Cyclic Behavior of Specimens

4.2.1 Encased Composite Beam-Columns

Specimens CC-10P, CC-15P, and CC-20P were axially loaded of 332.13 kN, 498.19 kN, and 664.262 kN respectively. Then, they were cyclically loaded. Figure 4.1-4.3 are diagrams of the lateral load-displacement response of these specimens.

During cyclic loading of encased composite beam-column specimens, significant events were noticed which are as follow:

- 1) Unconfined concrete cracking was observed throughout the first cycle of $0.25 H_{u-p}$.
- 2) Unconfined concrete in compression zone was reached ultimate strain ($\epsilon_{cu} = 0.002$) at $0.5 H_{u-p}$ cycles.
- 3) Highly confined concrete in compression zone was reached ultimate strain ($\epsilon_{cu} = 0.0093$) during $0.7 H_{u-p}$ cycles.
- 4) Yielding of reinforcement bars was observed throughout the first cycle of $1.0 \Delta_y$.
- 5) Yielding of steel section was noticed during the first cycle of $1.5 \Delta_y$.
- 6) During $5.0 \Delta_y$ cycles, buckling of reinforcement bars was observed.
- 7) No local buckling of steel section was noticed during the cycle loading history.

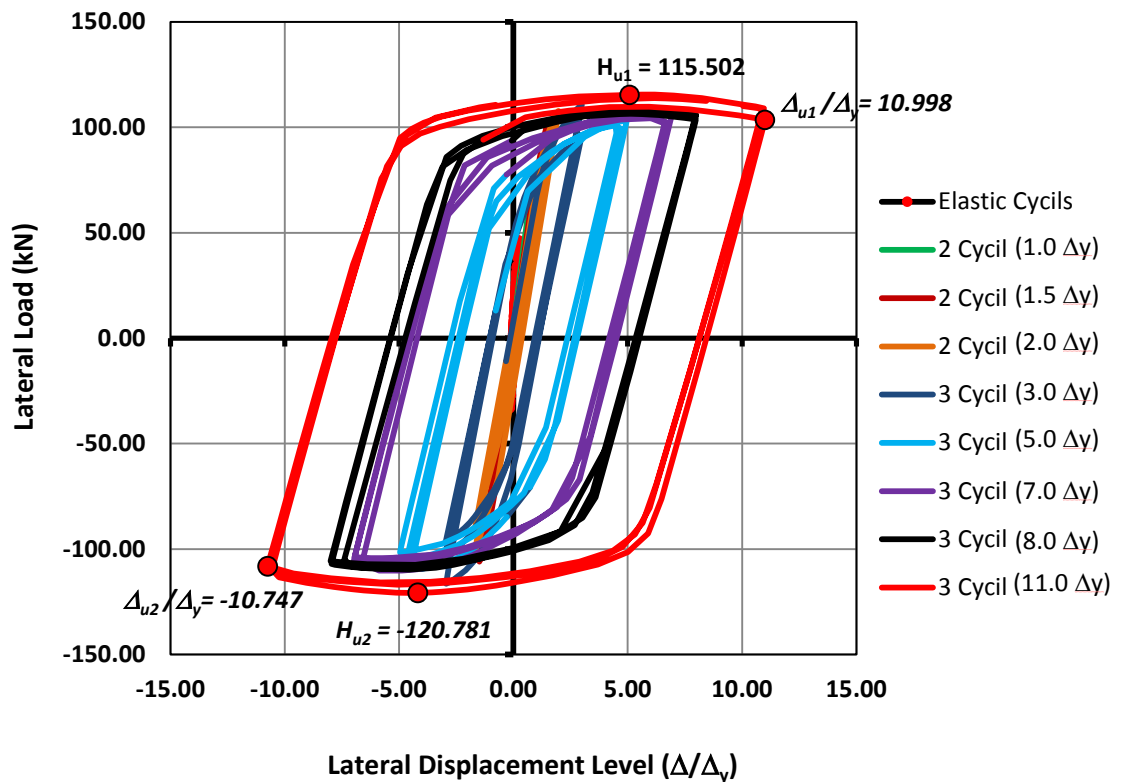


Figure 4.1: Lateral Load-Displacement Response of CC-10P

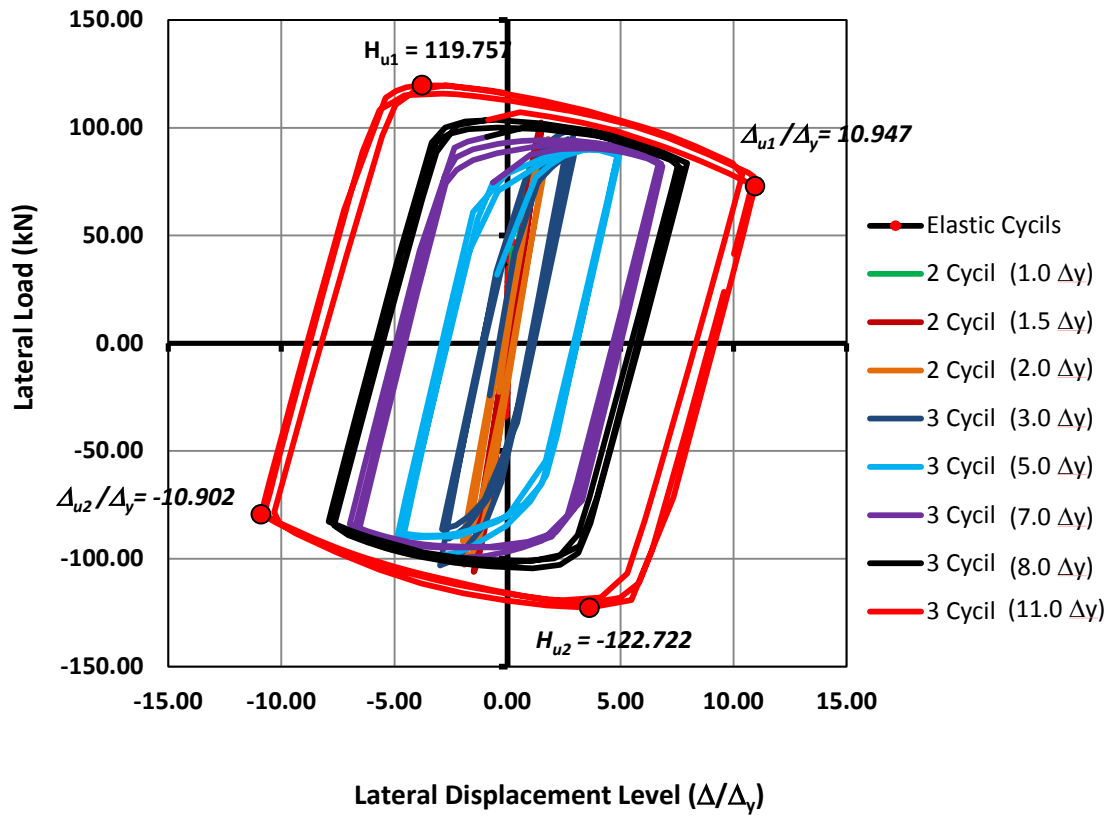


Figure 4.2: Lateral Load-Displacement Response of CC-15P

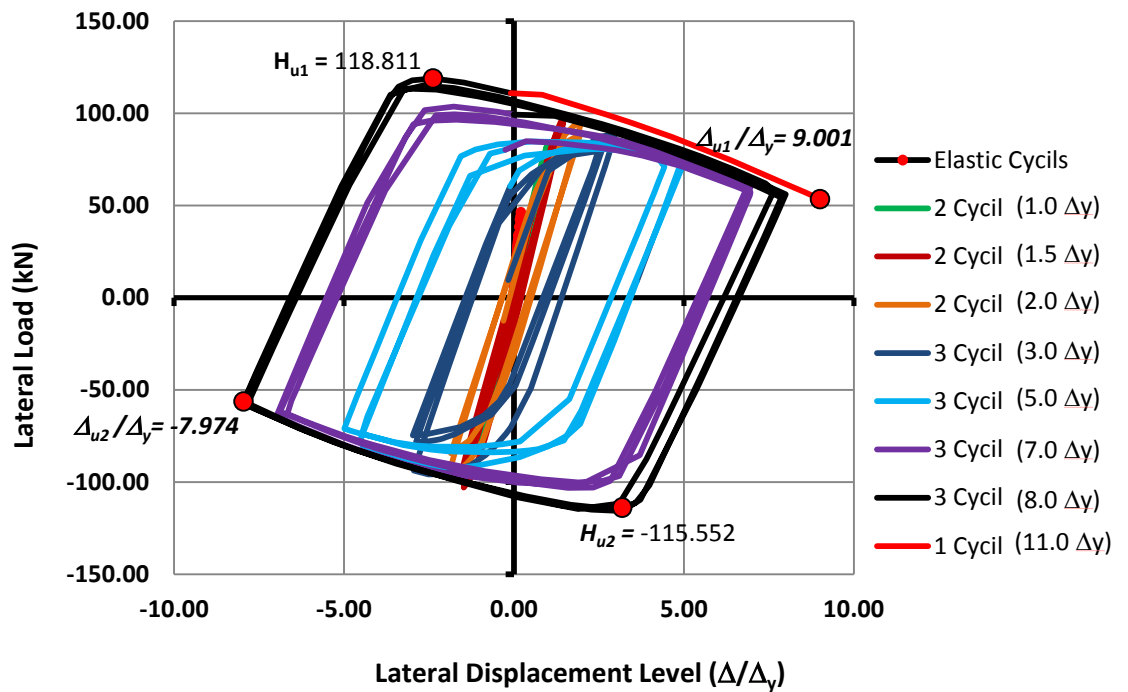


Figure 4.3: Lateral Load-Displacement Response of CC-20P

4.2.2 Reinforced Concrete Beam-Columns

Specimens RC-10P, RC-15P, and RC-20P were axially loaded of 296.4 kN, 444.61 kN, and 592.81 kN respectively. Then, they were cyclically loaded. Figure 4.4-4.6 are diagrams of the lateral load-displacement response of these specimens.

During cyclic loading of reinforced concrete beam-column specimens, significant events were noticed which are as follow:

- 1) Unconfined concrete cracking was observed throughout the first cycle of $0.25 H_{u-p}$.
- 2) Unconfined concrete in compression zone was reached ultimate strain ($\epsilon_{cu} = 0.002$) throughout the first cycle of $1.0 \Delta_y$.
- 3) Yielding of reinforcement bars was observed throughout the second cycle of $1.5 \Delta_y$.
- 4) Partially confined concrete in compression zone was reached ultimate strain ($\epsilon_{cu} = 0.0138$) during $0.7 H_{u-p}$ $2.0 \Delta_y$.
- 5) During first cycle of $11.0 \Delta_y$, buckling of reinforcement bars was observed.

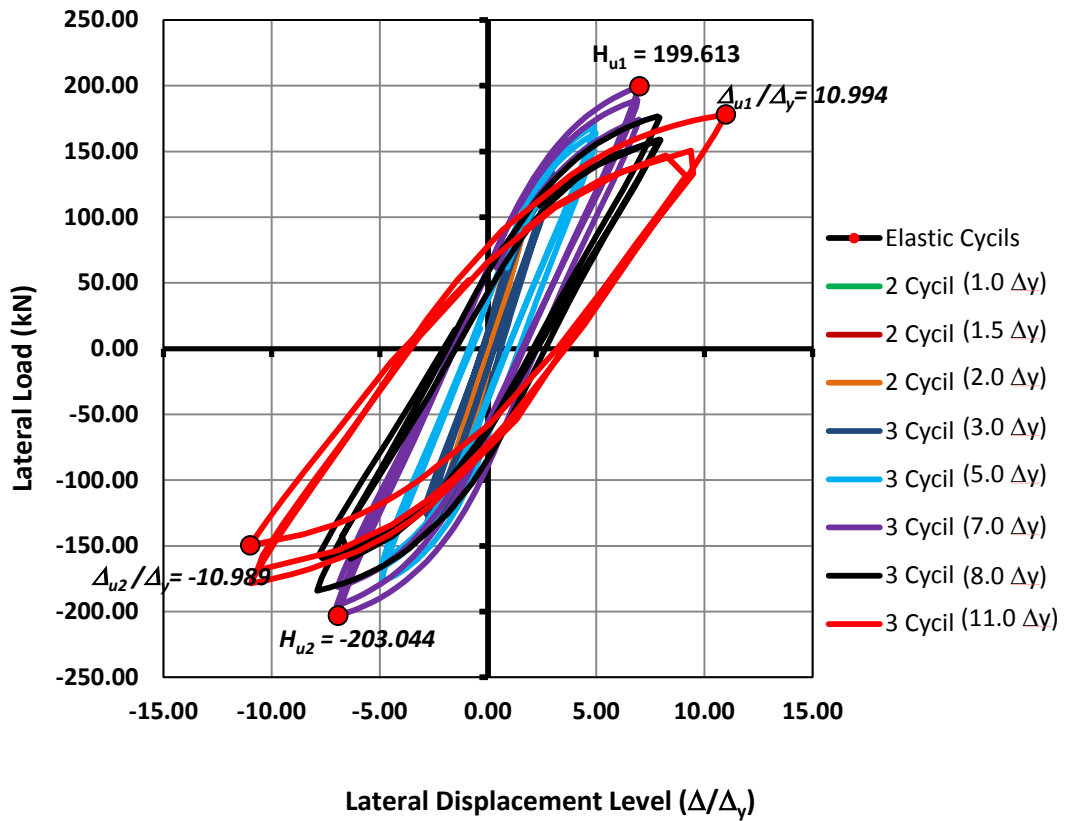


Figure 4.4: Lateral Load-Displacement Response of RC-10P

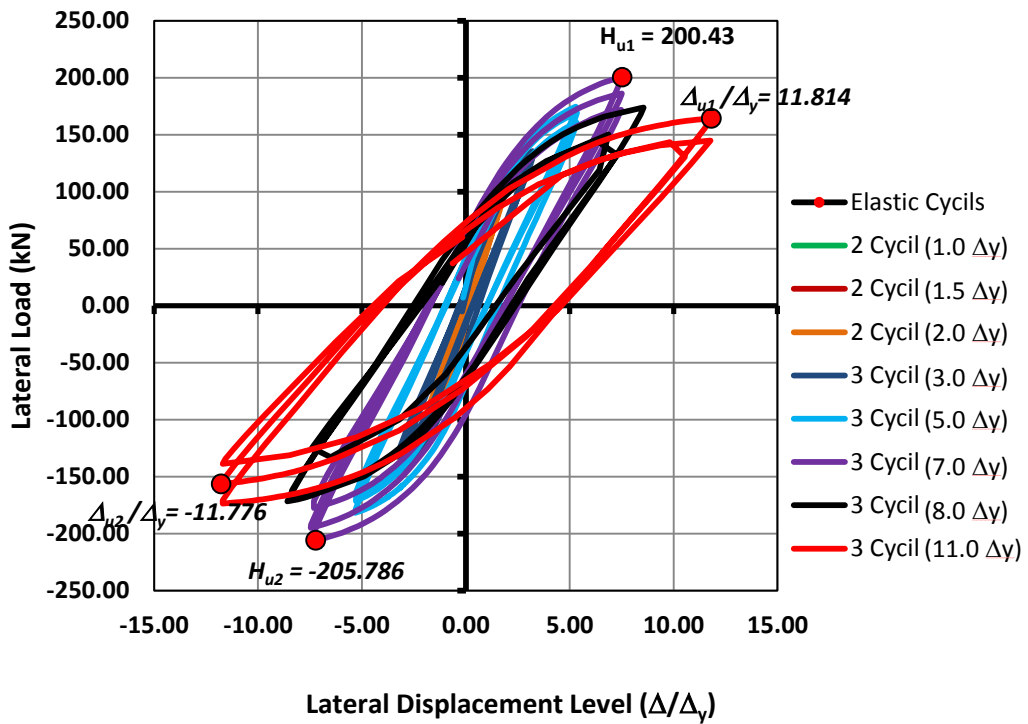


Figure 4.5: Lateral Load-Displacement Response of RC-15P

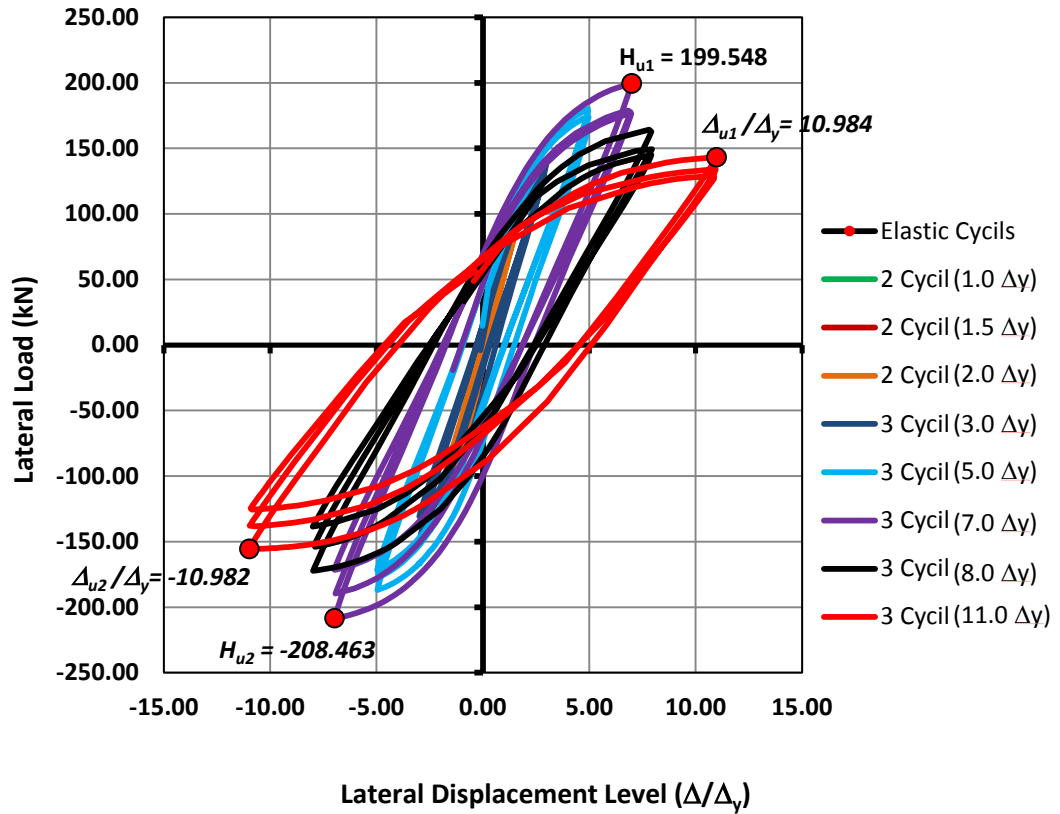


Figure 4.6: Lateral Load-Displacement Response of RC-20P

4.2.3 Steel Beam-Columns

Specimens SC-10P, SC-15P, and SC-20P were axially loaded of 582.3 kN, 873.45 kN, and 1164.6 kN respectively. Then, they were cyclically loaded. Figure 4.7-4.9 are diagrams of the lateral load-displacement response of these specimens.

During cyclic loading of steel concrete beam-column specimens, significant events were noticed which are as follow:

- 1) Yielding of steel section flanges and part of web were observed throughout the first cycle of $1.0 \Delta_y$.
- 2) Local buckling of steel section flange was noticed throughout the first cycle of $3.0 \Delta_y$.
- 3) Fracture of steel section was observed throughout the last cycle of $3.0 \Delta_y$.

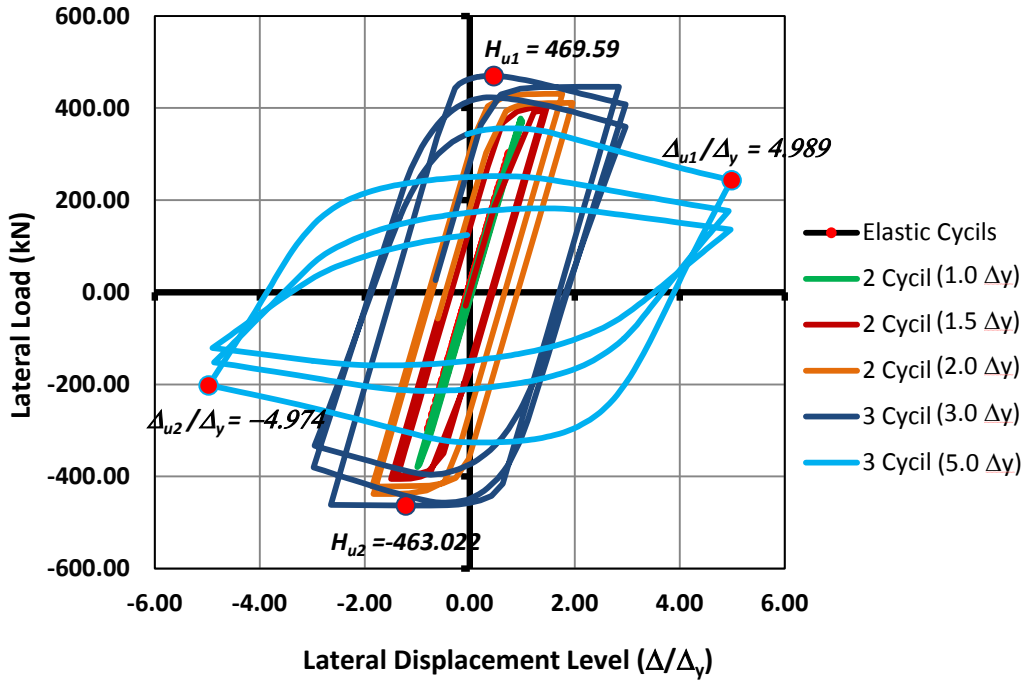


Figure 4.7: Lateral Load-Displacement Response of SC-10P

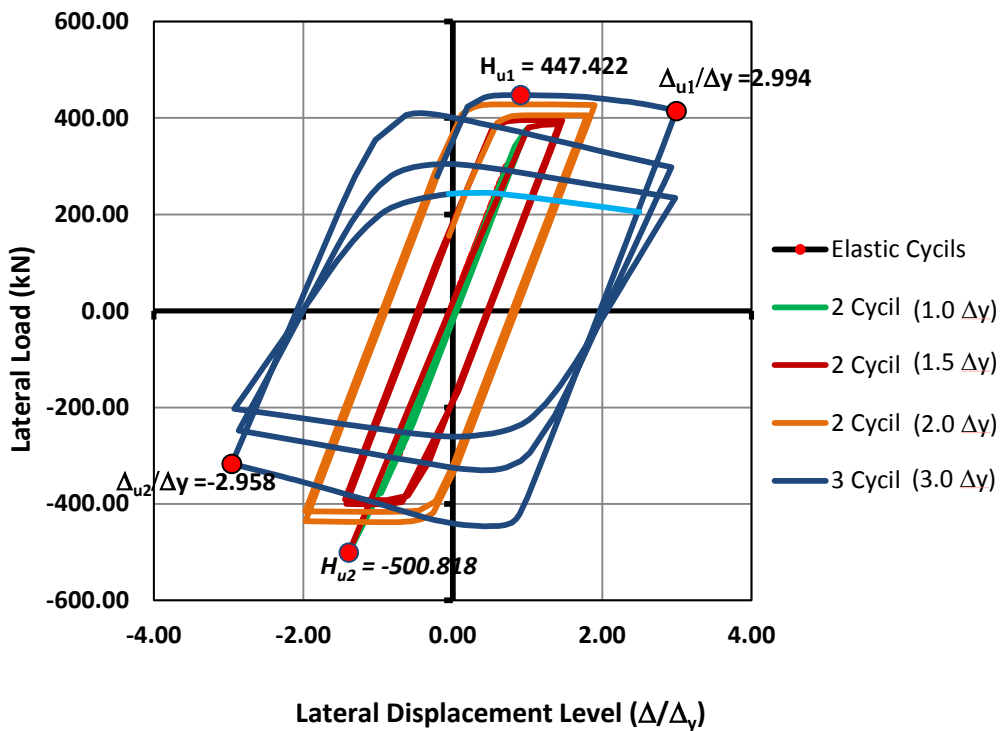


Figure 4.8: Lateral Load-Displacement Response of SC-15P

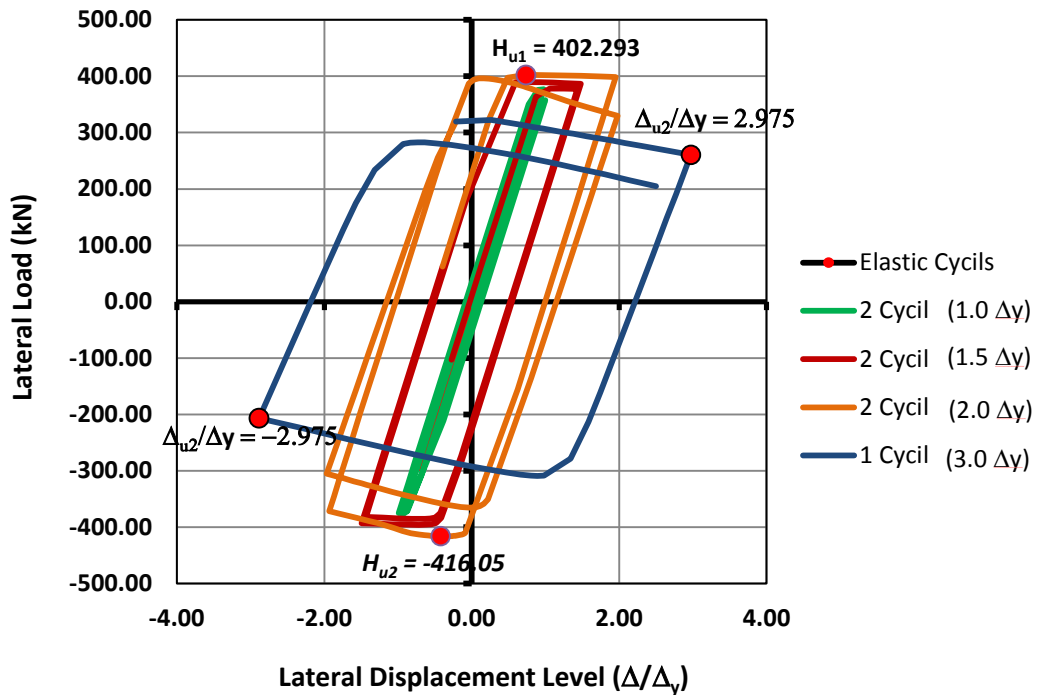


Figure 4.9: Lateral Load-Displacement Response of SC-20P

4.3 Strength

An important factor in member design is its strength. For evaluating the effects of cyclic loading on maximum beam-column specimen's capacity, the moment capacity, M_{u-c} , for specimens were plotted against axial load level (Figures 4.10). Moreover, stress contour at maximum force and displacement level were assessed (Figures 4.11-4.19). Conclusions drawn from the results plotted include:

- 1) As axial load in relation to capacity, P/P_o , increased, the ultimate moment capacity, M_{u-c} , reduced for the cyclic beam-column specimens.
- 2) Steel beam-column specimens had higher ultimate moment capacity comparing with the reinforced concrete and composite sections specimens. This due to having a higher stiffness.

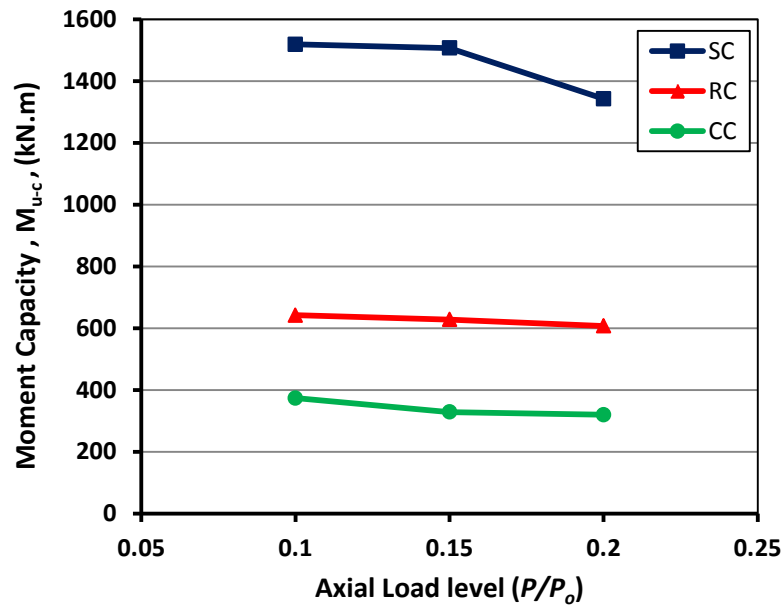


Figure 4.10: Influence of Axial Load Level on The Moment Capacity

- 3) The highly stressed regions are more evenly distributed over the lower portion of specimen, which termed as plastic hinge zone.
- 4) For the purpose of getting the plastic hinge length, the equivalent plastic strain contour, PEEQ, which is a measure of ductility at local level, were used (Appendix C, Figures C.1-C.9). The plastic hinge lengths which measured from the base are as follow: (210- 260 mm) for encased composite beam-columns, (260- 270 mm) for reinforced concrete beam-columns, and (410- 460 mm) for steel beam-columns. These discrepancies are attributable to the higher level of axial load. The specimens with higher axial load are subjected to more shortening and buckling.

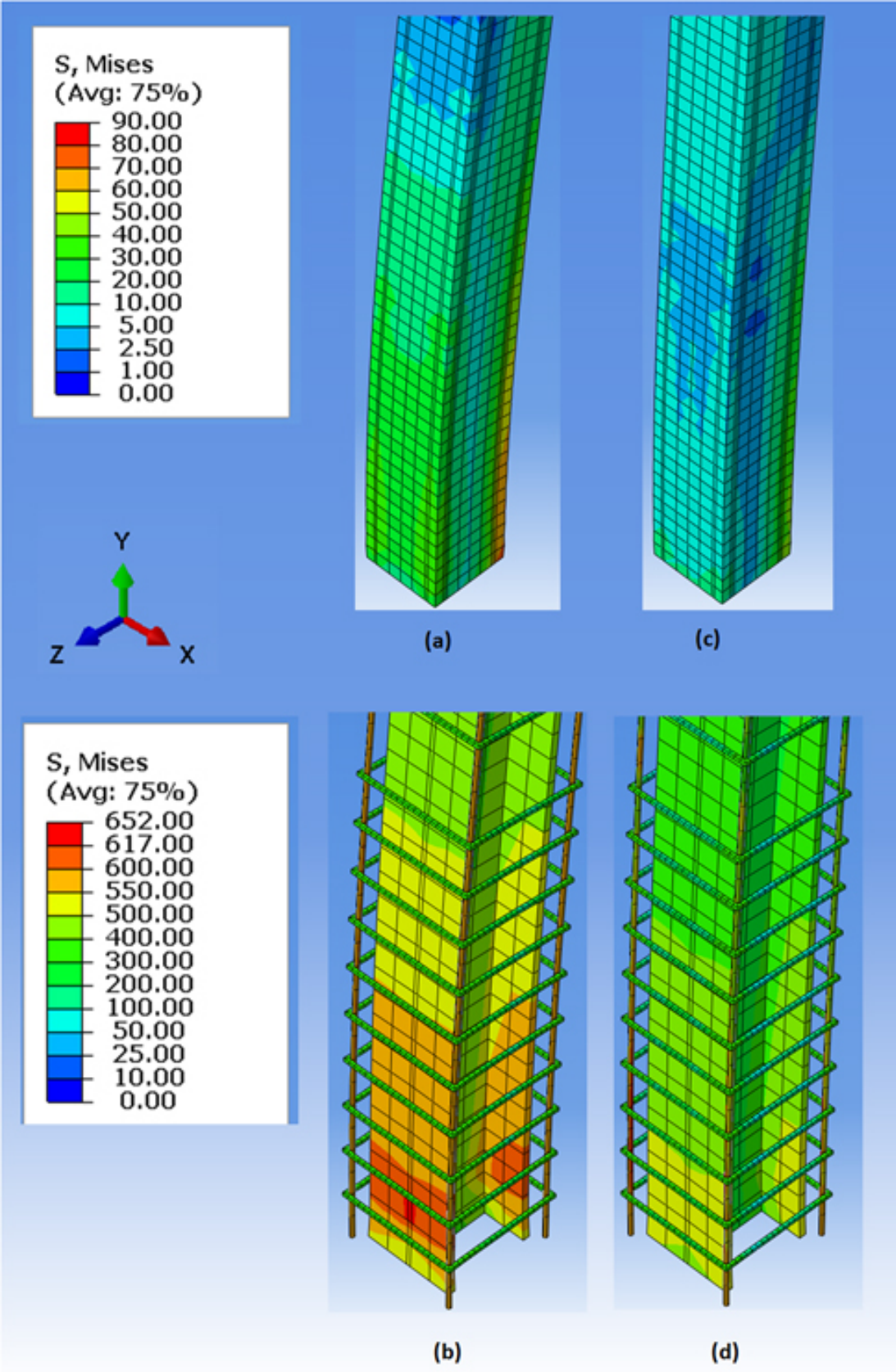


Figure 4.11: Stress Contour at Maximum Force Level (a, and b) and at Maximum Displacement Level (c, and d) of CC-10P

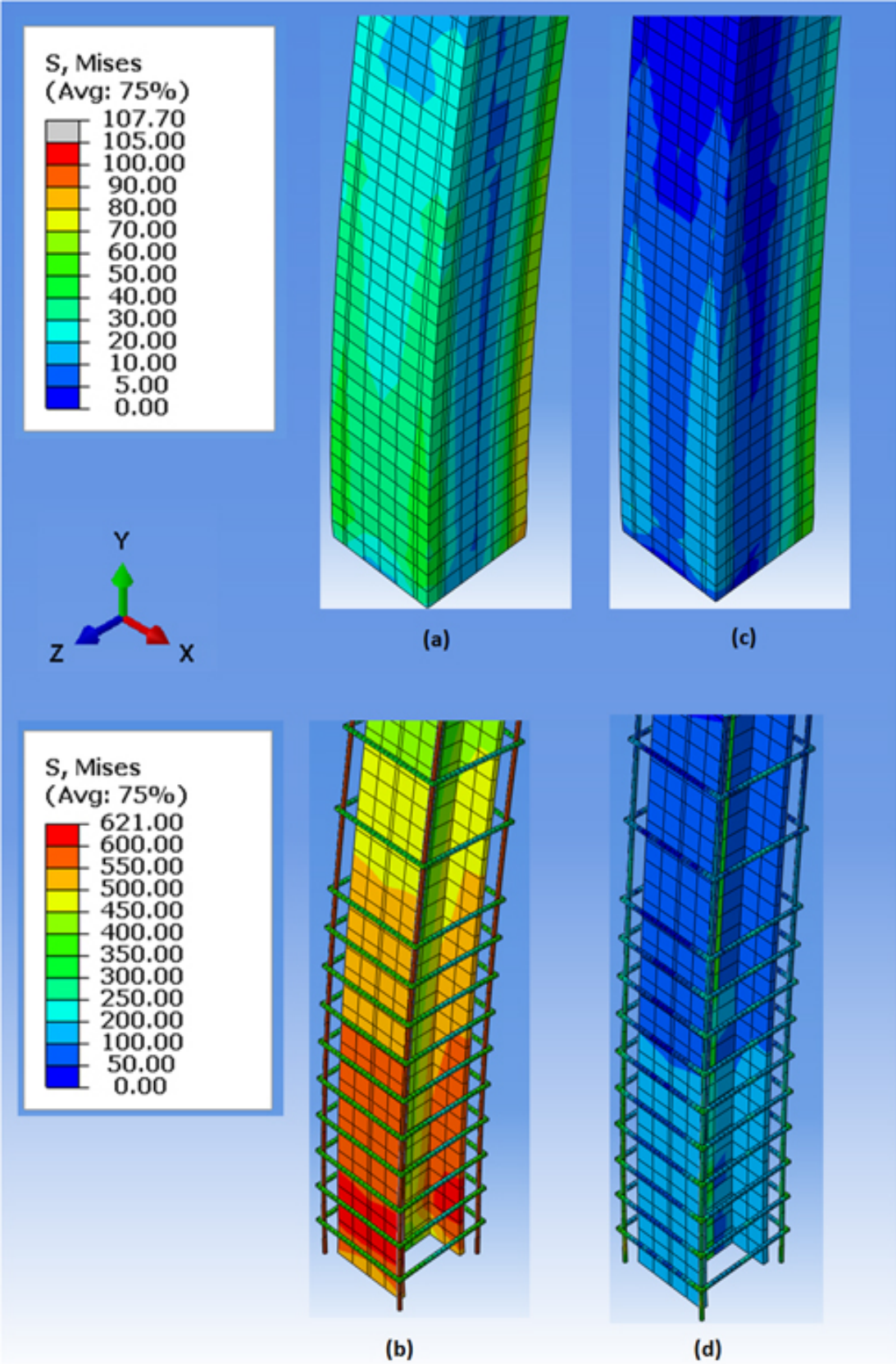


Figure 4.12: Stress Contour at Maximum Force Level (a, and b) and at Maximum Displacement Level (c, and d) of CC-15P

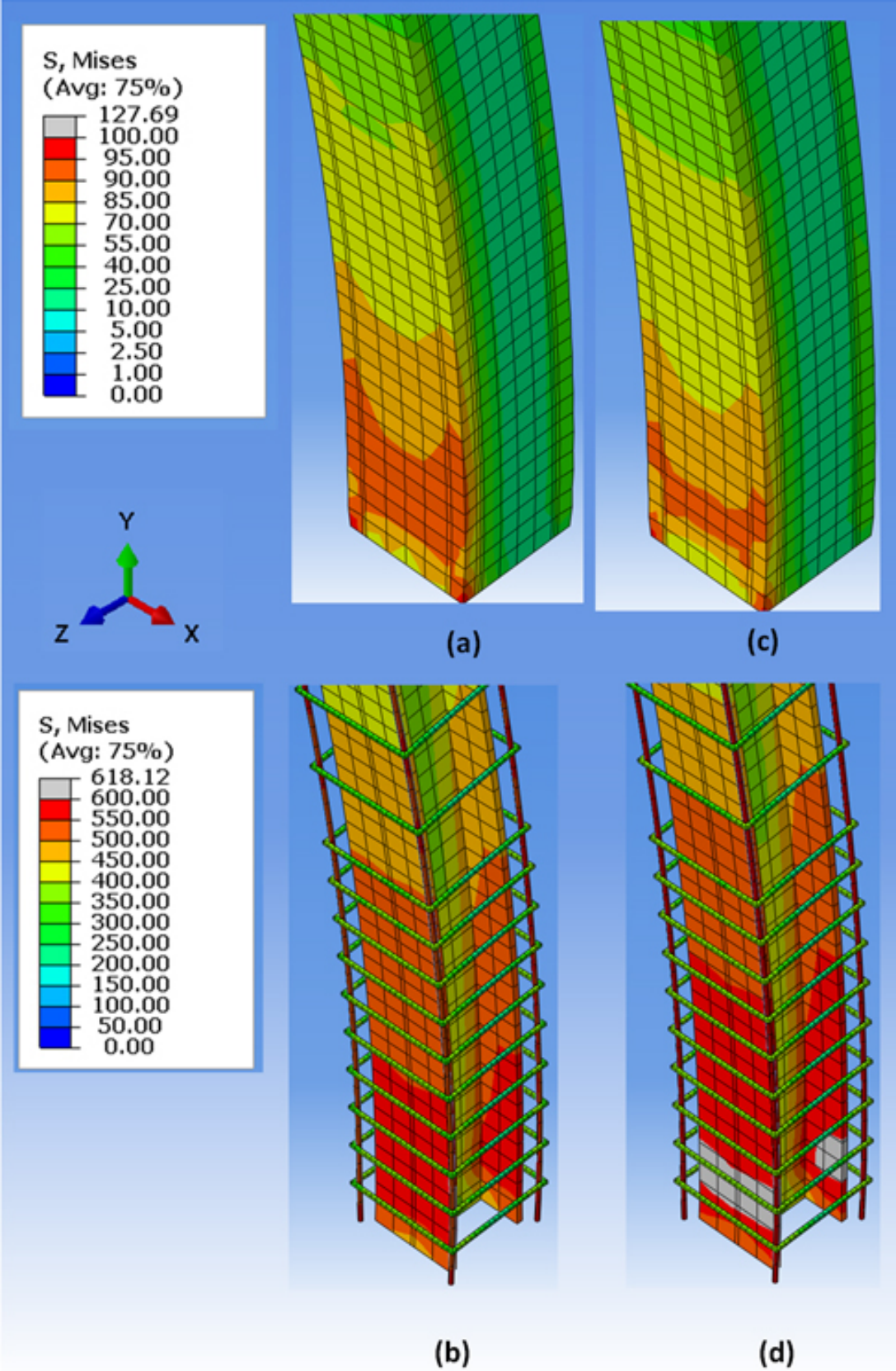


Figure 4.13: Stress Contour at Maximum Force Level (a, and b) and at Maximum Displacement Level (c, and d) of CC-20P

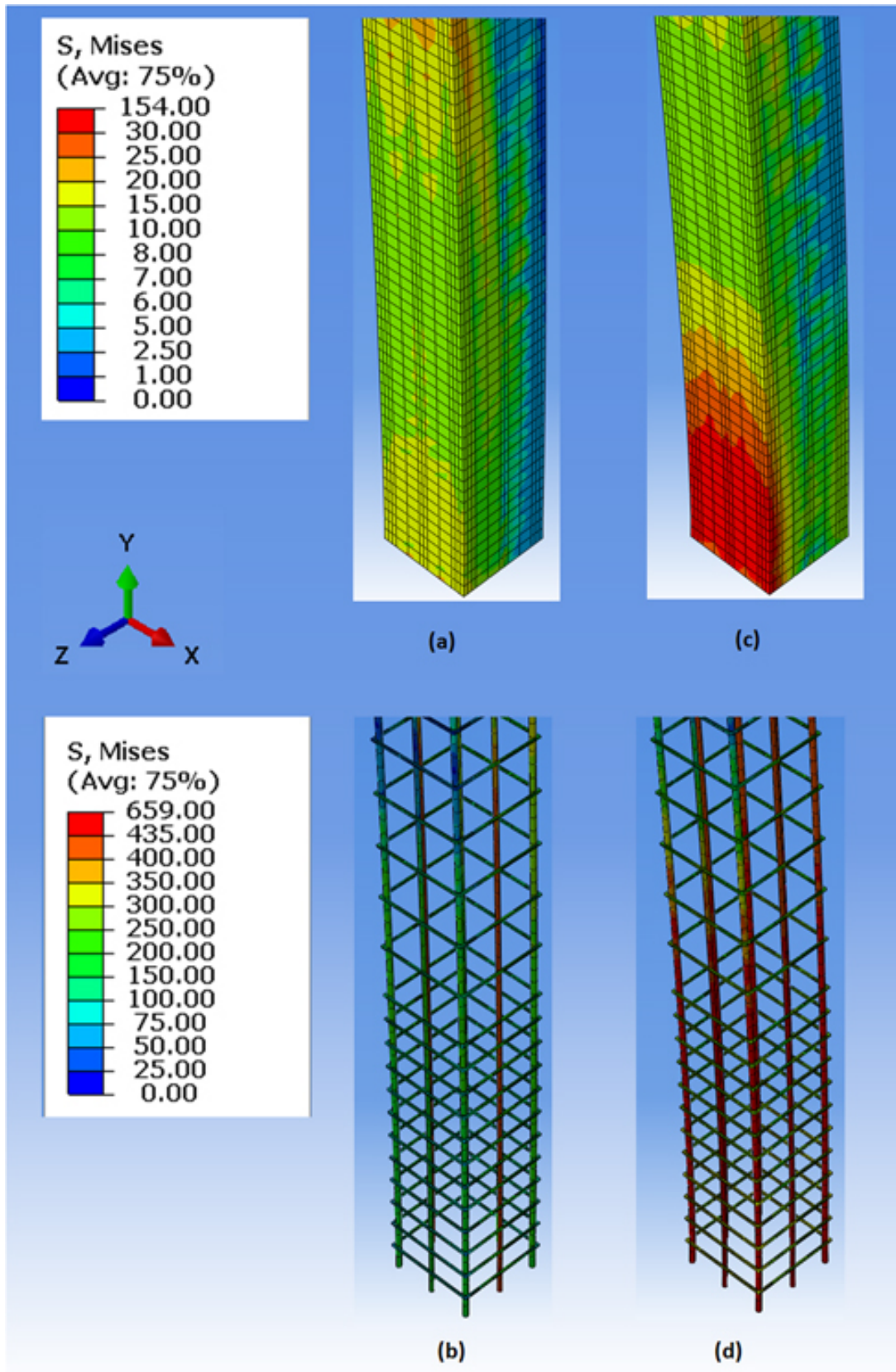


Figure 4.14: Stress Contour at Maximum Force Level (a, and b) and at Maximum Displacement Level (c, and d) of RC-10P

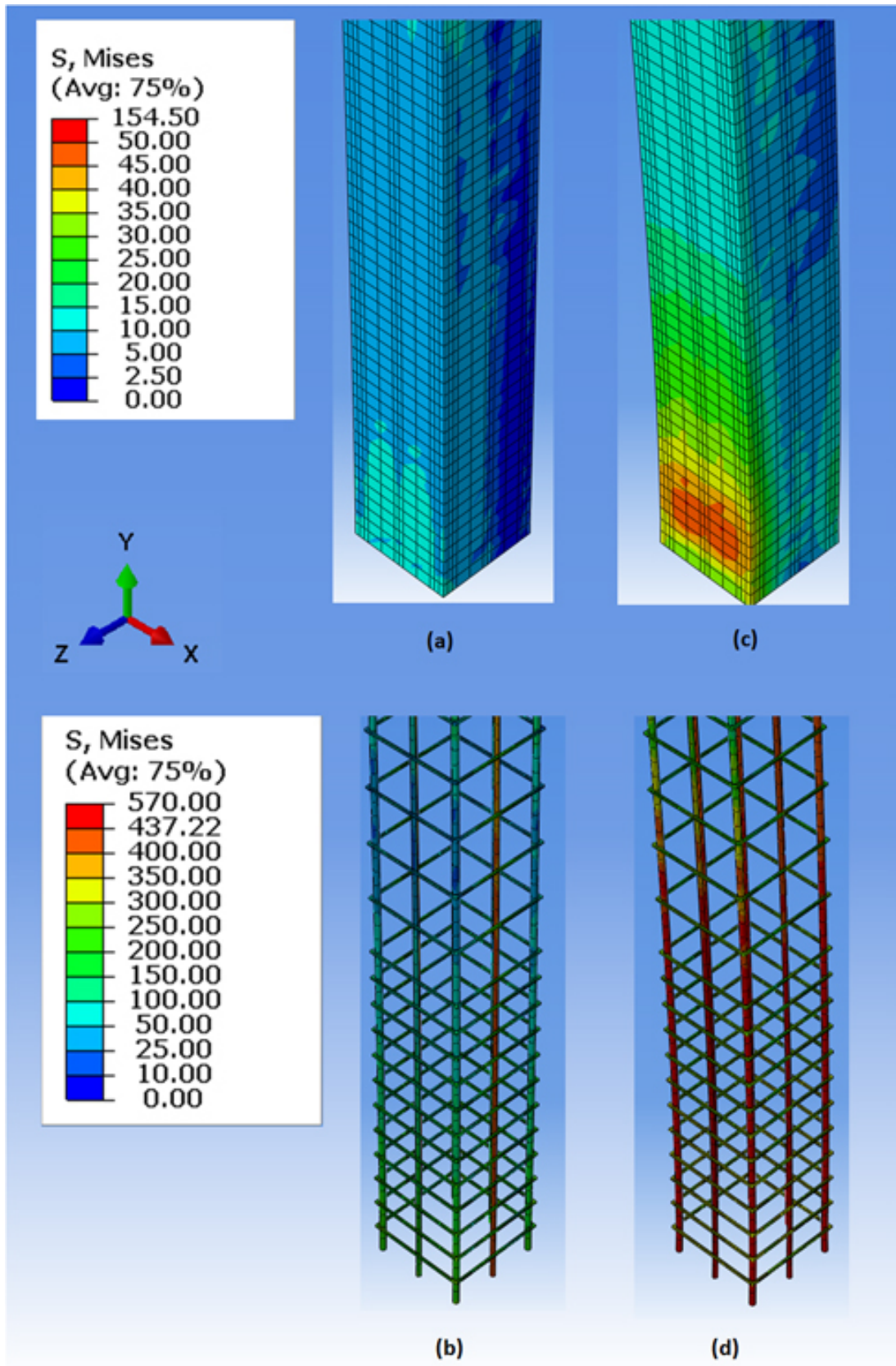


Figure 4.15: Stress Contour at Maximum Force Level (a, and b) and at Maximum Displacement Level (c, and d) of RC-15P

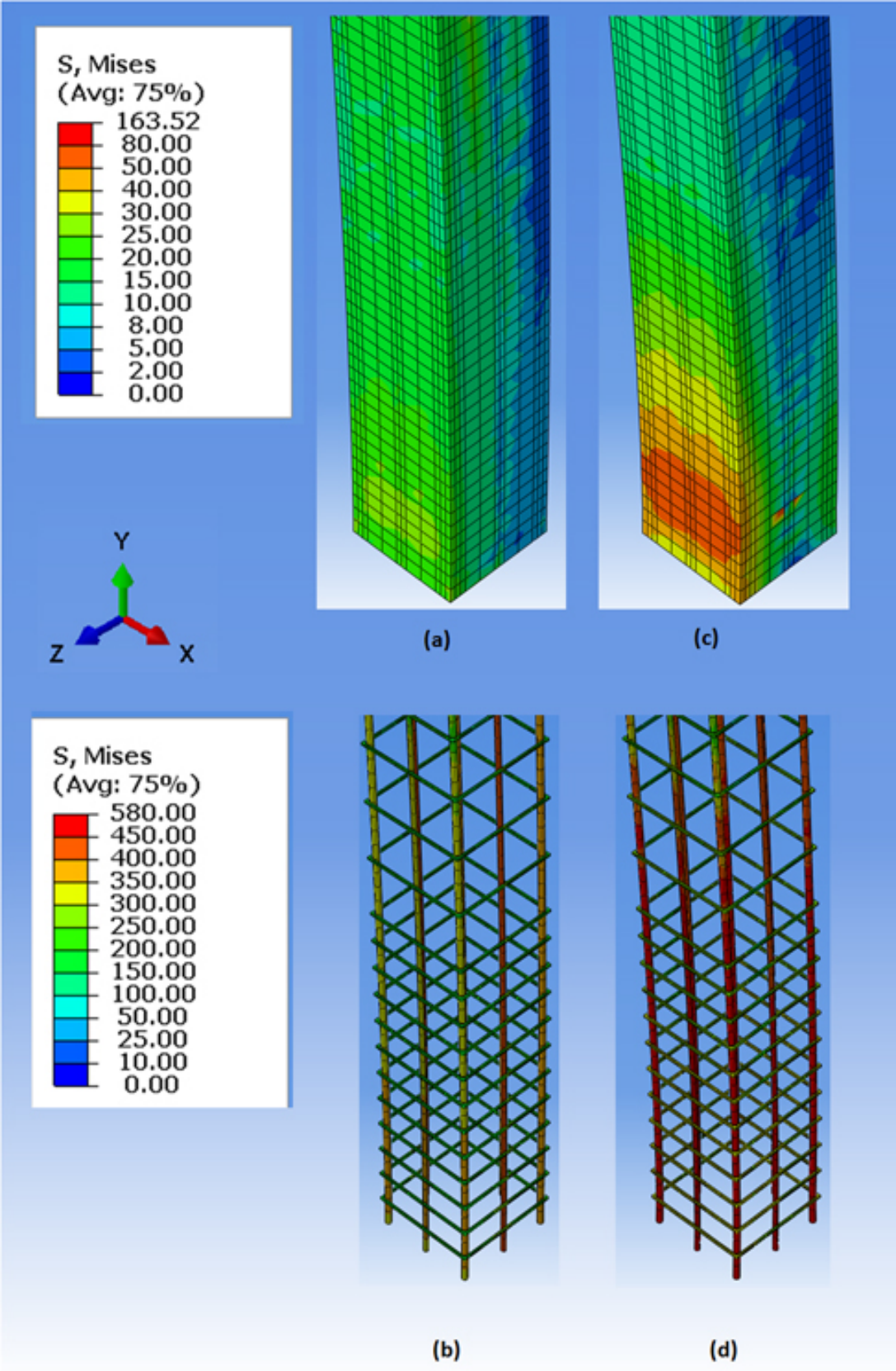


Figure 4.16: Stress Contour at Maximum Force Level (a, and b) and at Maximum Displacement Level (c, and d) of RC-20P

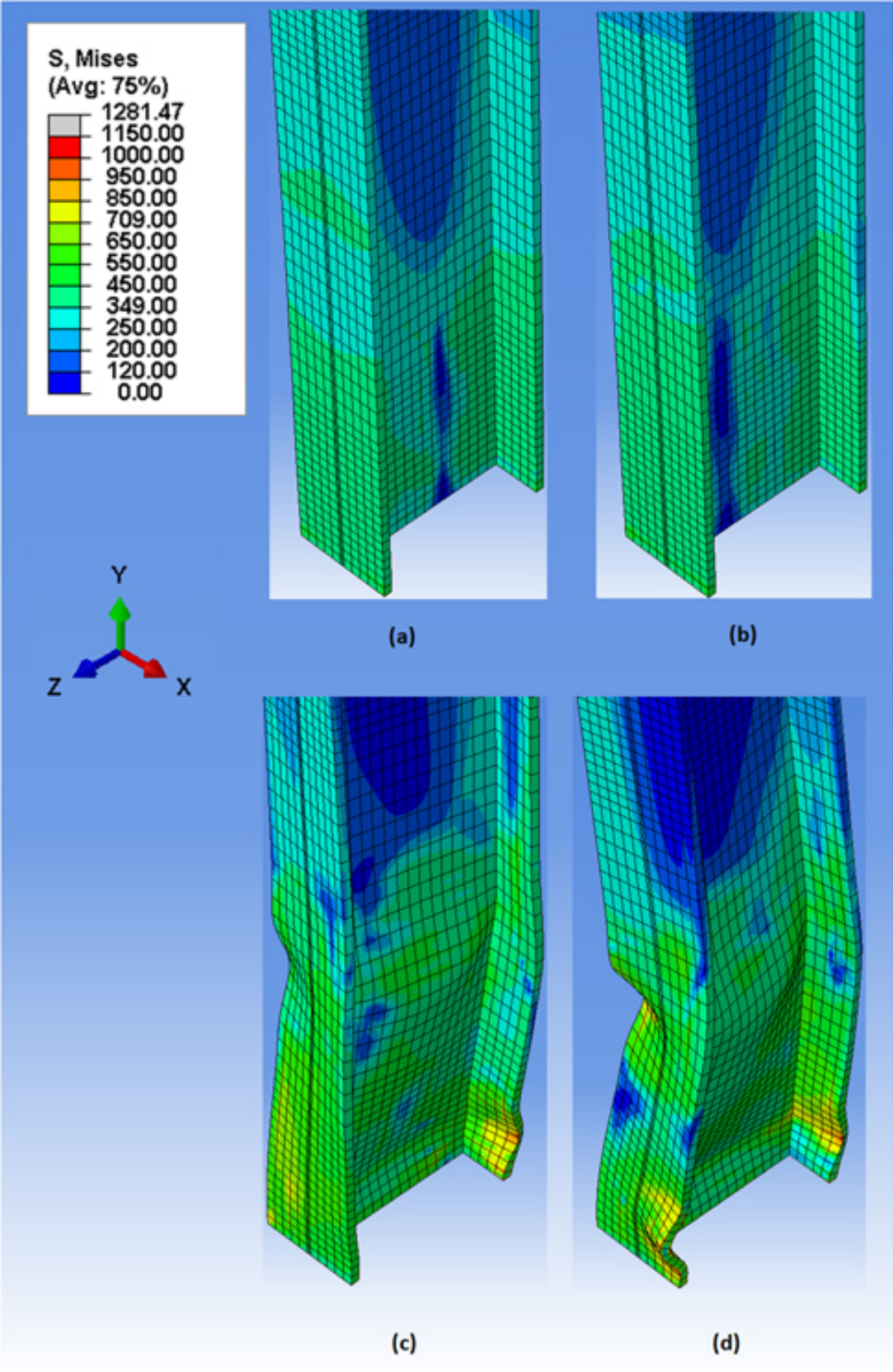


Figure 4.17: Stress Contour at Maximum Force Level (a, and b) and at Maximum Displacement Level (c, and d) of SC-10P

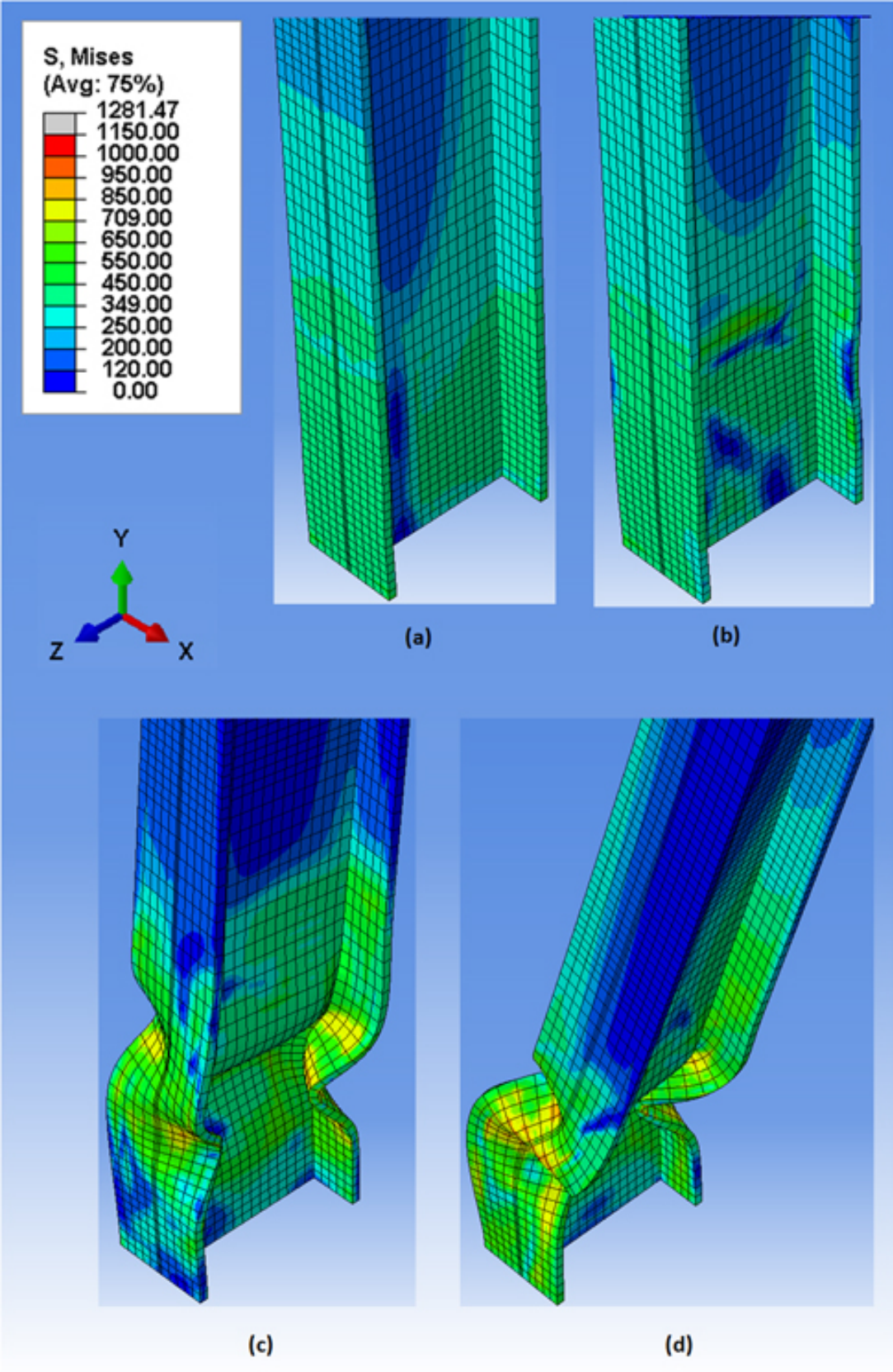


Figure 4.18: Stress Contour at Maximum Force Level (a, and b) and at Maximum Displacement Level (c, and d) of SC-15P

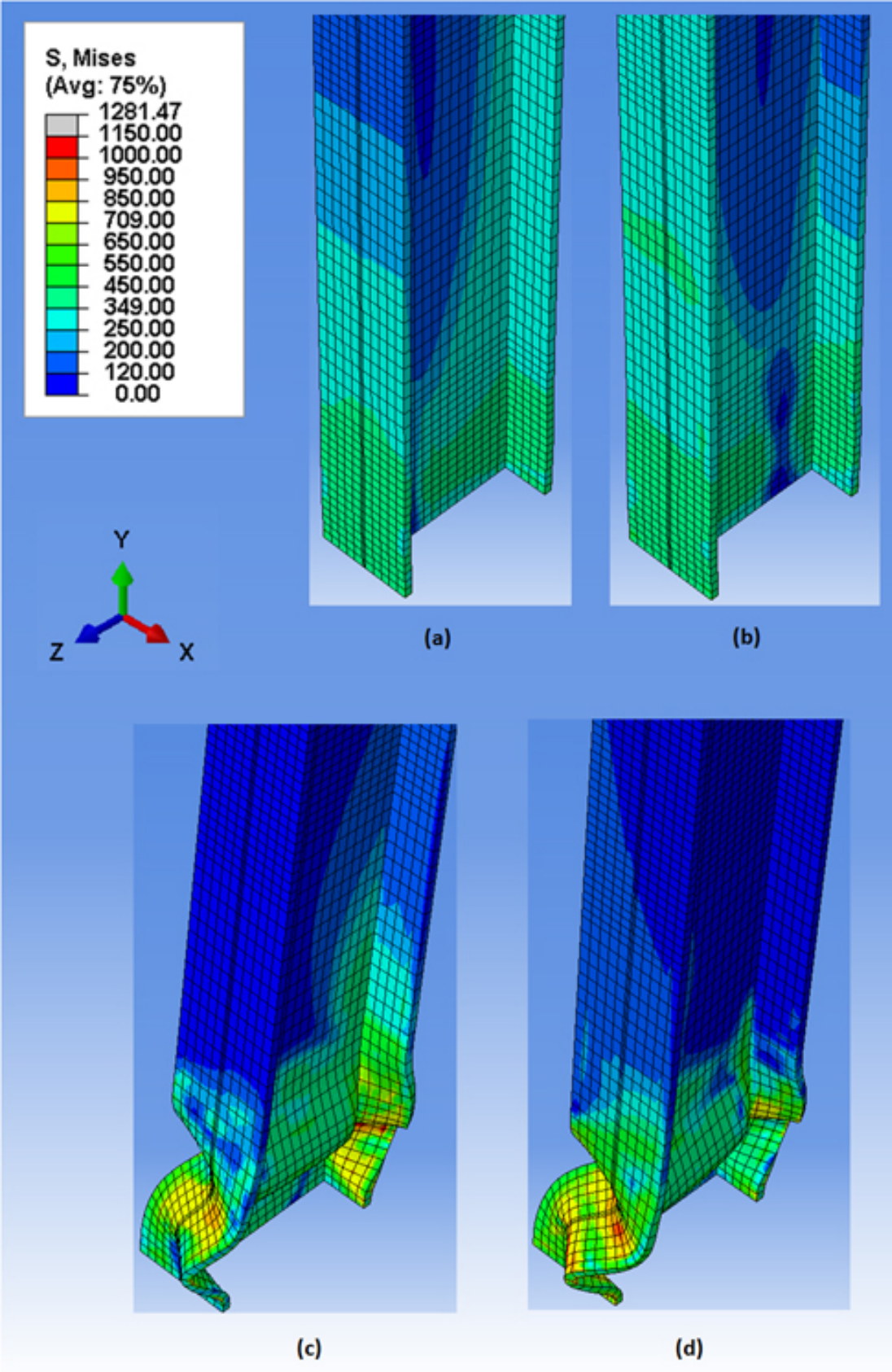


Figure 4.19: Stress Contour at Maximum Force Level (a, and b) and at Maximum Displacement Level (c, and d) of CC-20P

4.4 Ductility

Another important factor in member design is the ductility, especially the rotation capacity for earthquake loading. To explore the effects of axial load level on member ductility, the load-displacement and moment-curvature were computed and evaluated. Figures 4.20 through 4.22 are the moment curvature envelopes for all nine specimens. Each point on the envelope corresponds to the peak displacement of the last cycle for each displacement level.

The curvature, ϕ , was computed as the change in rotation over the segment height of the specimen:

$$\phi = \frac{\Delta\theta}{h} \quad (4.1)$$

Where: $\Delta\theta$ and h are the difference in rotation values at the ends of the segment and the height of the segment, respectively. The curvature was computed at failure segment (plastic hinge location) of the column, using the differential of rotation values at the base and at distance equal to two times the plastic hinge lengths above the base. The curvature was computed over this length since most of the inelastic deformation and concrete damage occurred.

The moment was computed at plastic hinge location according to Equation 4.2, which includes the bending moment caused by H and second order moment caused by axial load P (Figure 3.12).

$$M = H(h - L_p) + Pu \quad (4.2)$$

where

- H The lateral load
- h The length of column
- L_p The length of plastic hinge measured from base
- u In-plane displacement of plastic hinge location
- P The axial load

The curvature ductility, μ_ϕ , was defined as the ratio of the ultimate curvature, ϕ_u , to the yield curvature, ϕ_y , i.e.:

$$\mu_\phi = \frac{\phi_u}{\phi_y} \quad (4.3)$$

The yield curvature was defined as the point where the secant stiffness, $K_{0.6-S-C}$, taken though 60% of the ultimate moment capacity, M_{u-c} intersected the ultimate moment capacity (Varma et al., 2004). The ultimate moment capacity is considered to be the average in the two loading directions. The ultimate curvature, ϕ_u , is considered to be the point where the envelope ends and it is considered as the average value of the two loading directions. The curvature ductility calculations for all specimens are detailed in Appendix C.

As noted in Table C.1 in Appendix C, the curvature ductilities were 10.4, 11.8, 9.3, 3.4, 4.4, 4.3, 2.1, 2.2, and 1.7 for Specimens CC-10P, CC-15P, CC-20P, RC-10P, RC-15P, RC-20P, SC-10P, SC-15P, and SC-20P CBC, respectively. Comparisons of

the moment-curvature envelope plots between specimens that have same axial level are shown in Figures 4.20 through 4.22.

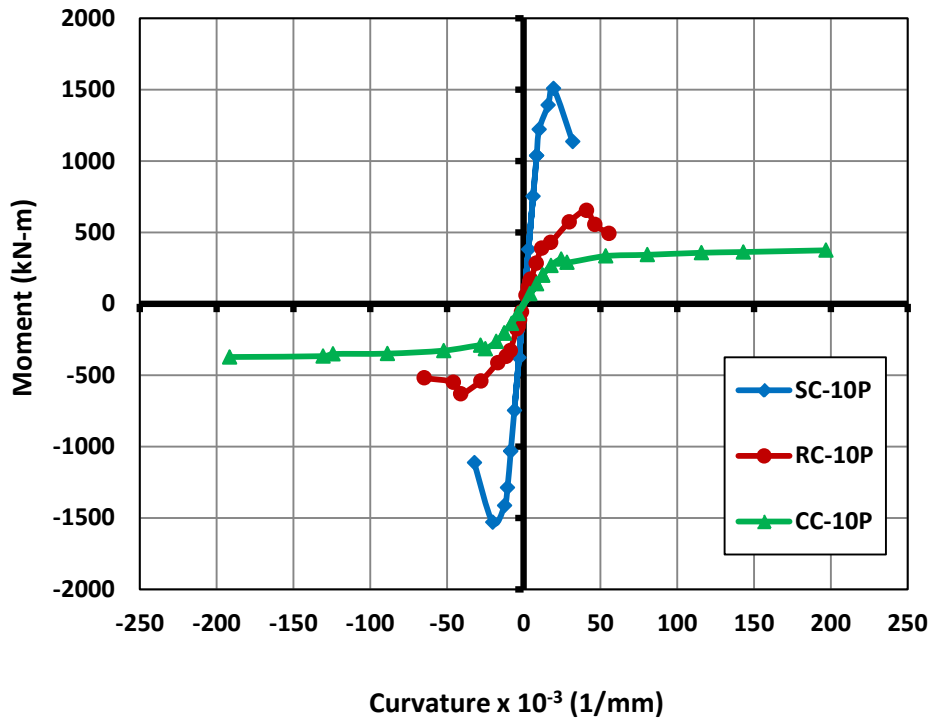


Figure 4.20: Envelopes of Cyclic $M-\phi$ for CC-10P, RC-10P, and SC-10P

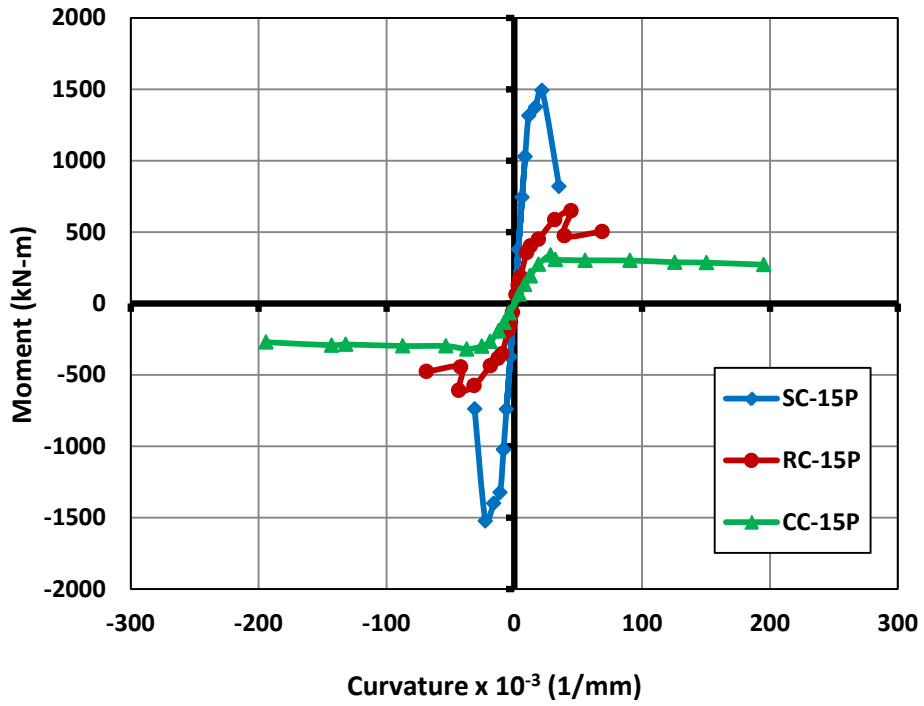


Figure 4.21: Envelopes of Cyclic $M-\phi$ for CC-15P, RC-15P, and SC-15P

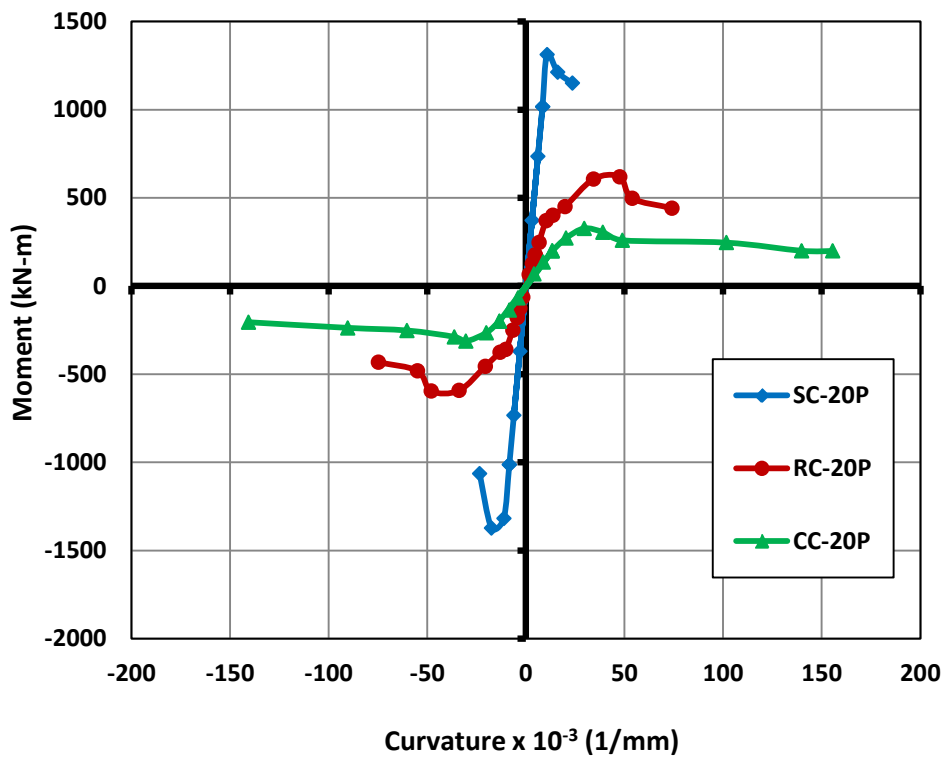


Figure 4.22: Envelopes of Cyclic $M-\phi$ for CC-20P, RC-20P, and SC-20P

Based on these results and comparisons, the following observations can be made:

- 1) The comparisons of μ_ϕ for steel specimens with RC and composite section specimens in Table C.1 indicate that the ladder have much less curvature ductility than the latter. In same while, they have a higher M_{u-c} . This is attributed to extensive local buckling of steel section which led to significant reduction in stiffness and strength (softening damage). In other words, losing stability during applying lateral load protocol.
- 2) It is quite clear that the curvature ductilities for encased composite beam-columns are 2.2-3 times higher than that of reinforced beam-columns and 5-5.5 times that of steel beam-columns. This shows that confinement effect of concrete provides enhancement of strength and ductility.
- 3) With an increase of P/P_o from 0.10 to 0.20 a significant drop in curvature ductility occurs.
- 4) It appears that the effect of confinement effect on curvature ductility is more pronounced for encased composite beam-columns compared to reinforced beam-columns tubes specimens.

Table C.2 in Appendix C displays the displacement ductilities calculations based on the envelopes of lateral load-displacement. Displacement ductility was computed in a similar manner as curvature ductility exchanging lateral load for moment and specimen top displacement for curvature. As summarized there, the specimens had displacement ductilities of 8.5, 8.7, 7.2, 3.8, 4.1, 4.4, 4.2, 2.5, and 3.0 for Specimens CC-10P, CC-15P, CC-20P, RC-10P, RC-15P, RC-20P, SC-

10P, SC-15P, and SC-20P CBC, respectively. Clearly, similar observations, which mentioned earlier, can be made.

4.5 Stiffness

Another important factor in member design is its stiffness. As mentioned earlier, in order to evaluate the change of the elastic stiffness of the specimen, half-elastic cycle was imposed after each set of inelastic cycles (Figure 3.14). The elastic stiffness degradation of specimens due to cyclic loading was illustrated clearly in Figure 4.23. Moreover, stresses contour at failure stage were also shown in Figure C.10 - C.18 in Appendix C. The following observations can be made according to this figure:

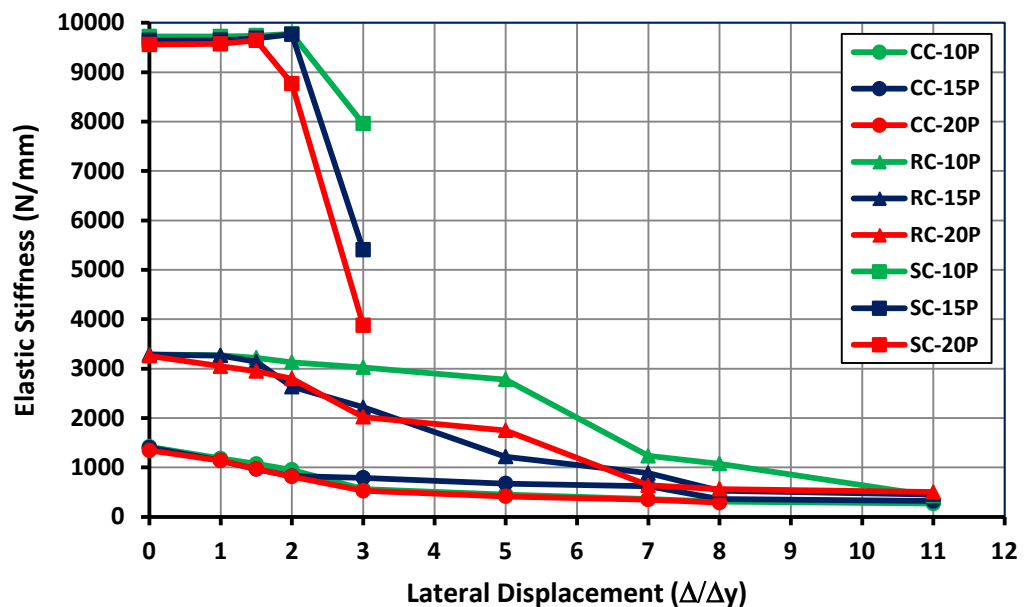


Figure 4.23: Elastic Stiffness Degradation of Specimens due to Cyclic Loading

- 1) Specimens with a P/P_o of 0.10 have higher initial stiffnesses than with a P/P_o of 0.15 or 0.20. There appears to be reduction in initial stiffness as long as there is increase of axial load level.
- 2) In general, it is clear that there are discrepancies in slopes especially for encased composite and reinforced concrete specimens. These discrepancies occur owing to stiffness recovery effect. In the cyclic experiments, direction and load was repeatedly alternated which involves opening and closing of micro cracks. For instance, when the load changes from tension to compression, tensile cracks force to close. As a result, there is some stiffness recovery effect.
- 3) It has been shown that concrete subjected to cyclic loading experiences a reduction in stiffness (Mander et al., 1988). This reduction in concrete cyclic stiffness and strength imposes a greater demand on the steel section to carry the load. When the concrete fails, this steel section has a large percentage of loads to bear. This explanation describes why encased composite specimens have not significant change in stiffness values during inelastic cycles.
- 4) For steel specimens, it should be noted that the stiffness values dramatically decrease during inelastic cycles of $3.0 \Delta_y$. This is attributed to extensive local buckling of steel section as discussed earlier.

Chapter 5

CONCLUSIONS

5.1 Summary

The purpose of this study was to investigate the cumulative damage of composite columns subjected to cyclic loading by comparing the effects of different levels of axial loads on the cyclic capacity of steel, reinforced concrete, and composite beam-columns. A nonlinear 3-D finite element models were developed to model the three prototype beam-columns; SC-(10P, 15P, and 20P), RC-(10P, 15P, and 20P), and CC-(10P, 15P, and 20P). These beam-column specimens were modeled as fixed cantilever beam-columns with an axial load level of 10%, 15%, and 20% of their axial load capacity. Then, they were analyzed under cyclic lateral load. The lateral loading was imposed under load control until 70% of the predetermined specimen capacity. The recorded secant flexural stiffness and predetermined axial capacity were used to determine the yield displacement. Loading then continued under displacement control, following a set displacement history until failure occurred.

The FEM output was then examined to determine the effect of different levels of axial loads on behavior under cyclic loading. Assessing whether the prototype elastic stiffness had changed, identifying the high stress and strain zones, and evaluating the effects of the level of axial load on stiffness, strength, and ductility of beam-column prototypes were facilitated.

5.2 Conclusions

On the basis of this study the following conclusions may be drawn:

1. It is apparent from results and comparisons that confinement effect of concrete provides enhancement of strength and ductility. Whereas, the encased composite beam-columns reach the highest ductility among beam-columns specimens.
2. Under cyclic loading, having a higher ultimate moment capacity does not mean that the specimen has the highest ductility. This represented in steel beam-column specimens which lost their stability because of extensive local buckling in steel section.
3. The elastic flexural stiffness as well as ductility decreases significantly with increases in the axial load level.
4. It is quite clear that the stiffness recovery effect, which resulting from opening and closing of micro cracks when direction and load alternated, gives the concrete amount of ductility before it fails.
5. It is proposed that local buckling plays a crucial role in curvature ductility for the cyclic beam columns because of concrete strength and stiffness degradation due to cyclic loading.
6. The finite element method is an effective and cheap way to predict the cyclic behavior of composite columns.

5.3 Recommendation for Further Study

1. The effects of shape of steel section, longitudinal steel reinforcement, material properties of the concrete, the confinement effect of the concrete, slenderness ratio of the column, and concrete and steel strength on the

behavior of encased composite beam-columns under cyclic loading should be investigated.

2. Finite element models should be developed to predict the behavior of encased composite beam-columns under various loading conditions.
3. A moment resisting frame with encased composite columns should be experimentally tested under cyclic loading to evaluate the effect of member proportioning on overall system behavior and the interaction with the various components of the system.
4. Results of the frame experiments should be combined with monotonic and cyclic beam-column experiments to develop seismic design guidelines for encased composite beam-columns.

REFERENCES

- ABAQUS, i. (2012). *ABAQUS analysis user's manual version 6.12*.
- Aboutaha, R. S., & Machado, R. I. (1999). Seismic Resistance of Steel-Tubed High-Strength Reinforced-Concrete Columns. *Journal of Structural Engineering*, 485–494.
- Begum, M., Driver, R. G., & Elwi, A. E. (2007). Finite-Element Modeling of Partially Encased Composite Columns Using the Dynamic Explicit Method. *Journal of Structural Engineering*, 326–334.
- Buick Davison, G. W. (2012). *Steel Designer's Manual*. Wiley- Blackwell.
- Chen, C.-C., & Lin, N.-J. (2006). Analytical model for predicting axial capacity and behavior of concrete encased steel composite stub columns. *Journal of Constructional Steel Research*, 424–433.
- Chen, C.-C., Li, J.-M., & Weng, C. (2005). Experimental behaviour and strength of concrete-encased composite beam–columns with T-shaped steel section under cyclic loading. *Journal of Constructional Steel Research*, 863–881.
- Chen, S. F., Teng, J. G., & Chan, S. L. (2001). Design of Biaxially Loaded Short Composite Columns of Arbitrary Section. *Journal of Structural Engineering*, 0678–0685.
- Chicoine, T., Massicotte, B., & Tremblay, R. (2003). Long-Term Behavior and Strength of Partially Encased Composite Columns Made with Built-Up Steel Shapes. *Journal of Structural Engineering*, 141–150.

- Chicoine, T., Tremblay, R., Massicotte, B., Ricles, J. M., & Lu, L.-W. (2002). Behavior and Strength of Partially Encased Composite Columns with Built-up Shapes. *Journal of Structural Engineering*, 279–288.
- Cho, C.-G., Kim, Y.-Y., Feo, L., & Hui, D. (2012). Cyclic responses of reinforced concrete composite columns strengthened in the plastic hinge region by HPFRC mortar. *Composite Structures*, 2246–2253.
- Corinaldesi, V., Letelier, V., & Mor, G. (2011). Behaviour of beam–column joints made of recycled-aggregate concrete under cyclic loading. *Construction and Building Materials*, 1877–1882.
- Denavit, M. D., Hajjar, J. F., & Leon, R. T. (2011). Seismic Behavior of Steel Reinforced Concrete Beam-Columns and Frames. *Structures Congress*, 2852-2861.
- Dundu, M. (2012). Compressive strength of circular concrete filled steel tube columns. *Elsevier, Thin-Walled Structures*, 62–70.
- Ellobody, E., & Young, B. (2006). Nonlinear analysis of concrete-filled steel SHS and RHS columns. *Thin-Walled Structures*, 919–930.
- Ellobody, E., & Young, B. (2011). Numerical simulation of concrete encased steel composite columns. *Journal of Constructional Steel Research*, 211–222.
- Ellobody, E., & Young, B. (2006). Design and behaviour of concrete-filled cold-formed stainless steel tube columns. *Engineering Structures*, 716–728.

- Ellobody, E., Young, B., & Lam, D. (2006). Behaviour of normal and high strength concrete-filled compact steel tube circular stub columns. *Journal of Constructional Steel Research*, 706–715.
- Ellobody, E., Young, B., & Lam, D. (2011). Eccentrically loaded concrete encased steel composite columns. *Thin-Walled Structures*, 53-65.
- El-Tawil, S., & Deierlein, G. G. (1999). Strength and Ductility of Concrete Encased Composite Columns. *Journal of Structural Engineering*, 1009–1019.
- Eurocode, 2. (2004). *EN 1992-1-1: Eurocode 2: Design of Concrete Structure- Part 1-1: General Rules and Rules for Buildings*. London: British Standard Institution.
- Eurocode, 4. (2004). *BS EN 1994-1-1, Eurocode 4: Design of Composite Steel and Concrete Structure Part 1-1: General Rules and Rules for Buildings*. London: British Standard Institution.
- Eurocode, 8. (2004). *BS EN 1998-1:2004 Design of structures for earthquake resistance Part 1 General rules, seismic actions and rules for buildings*. London: British Standard Institution.
- Eurocode3. (2005). *DD ENV 1993-1-1, Eurocode 3: Design of Steel Structures Part 1.1 General Rules and Rules for Buildings*. London: British Standards Institute.
- Fam, A., Qie, F. S., & Rizkalla, S. (2004). Concrete-Filled Steel Tubes Subjected to Axial Compression and Lateral Cyclic Loads. *Journal of Structural Engineering*, 631–640.

- Gajalakshmi, P., & Helena, H. J. (2012). Behaviour of concrete-filled steel columns subjected to lateral cyclic loading. *Journal of Constructional Steel Research*, 55-63.
- Galal, K. E., & Ghobarah, A. (2003). Flexural and shear hysteretic behaviour of reinforced concrete columns with variable axial load. *Engineering Structures*, 1353–1367.
- Gan, D., Guo, L., Liu, J., & Zhou, X. (2011). Seismic behavior and moment strength of tubed steel reinforced-concrete (SRC) beam-columns. *Journal of Constructional Steel Research*, 1516–1524.
- Han, L.-H., & Lin, X.-K. (2004). Tests on Cyclic Behavior of Concrete-Filled Hollow Structural Steel Columns after Exposure to the ISO-834 Standard Fire. *Journal of Structural Engineering*, 1807–1819.
- Hindi, R., & Turechek, W. (2008). Experimental behavior of circular concrete columns under reversed cyclic loading. *Construction and Building Materials*, 684–693.
- Kayal, S. (1984). Finite Element Analysis of RC Frames. *Journal of Structural Engineering*, 2891-2908.
- Kim, D. K. (2005). *A Database for Composite Columns*. Georgia: Georgia Institute of Technology.
- Kwak, H.-G., & Kim, J.-K. (2006). Implementation of bond-slip effect in analyses of RC frames under cyclic loads using layered section method. *Engineering Structures*, 1715–1727.

- Kwaka, H.-G., & Kim, J.-K. (2007). P-1 effect of slender RC columns under seismic load. *Engineering Structures*, 3121–3133.
- Kwan, A., & Chung, S. (1996). Load Transfer Mechanism and Cyclic Behaviour of Composite Concrete Filled H-Section Steel Columns. *Advance in steel structure*, 461-466.
- Lee, H.-S., Kage, T., Noguchi, T., & Tomosawa, F. (2003). An experimental study on the retrofitting effects of reinforced concrete columns damaged by rebar corrosion strengthened with carbon fiber sheets. *Cement and Concrete Research*, 563–570.
- Lee, T.-K., & Pan, A. D. (2001). Analysis of Composite Beam-Columns Under Lateral Cyclic Loading. *Journal of Structural Engineering*, 186-193.
- Li, Q., & Belarbi, A. (2011). Seismic Behavior of RC Columns with Interlocking Spirals under Combined Loadings Including Torsion. *Procedia Engineering*, 1281–1291.
- Li, Q., Duan, Y., & Wang, G. (2002). Behaviour of large concrete specimens in uniaxial tension. *Magazine of concrete research*, 385-391.
- Lu, Y., Vintzileou, E., Zhang, G. -F., & Tassios, T. P. (1999). Reinforced concrete scaled columns under cyclic actions. *Soil Dynamics and Earthquake Engineering*, 151-167.
- Ma, Y., Che, Y., & Gong, J. (2011). Behavior of corrosion damaged circular reinforced concrete columns under cyclic loading. *Construction and Building Materials*, 548–556.

- Mander, J. B., Priestley, M. J., Park, R., & Fellow. (1988). Theoretical Stress-Strain Model for Confined Concrete. *Journal of Structural Engineering*, 1804-1826.
- Mashaly, E., El-Heweity, M., Abou-Elfath, H., & Osman, M. (2011). Finite element analysis of beam-to-column joints in steel frames under cyclic loading. *Alexandria Engineering Journal*, 91–104.
- Mirza, S. A. (2006). Comparative strength analyses of structural concrete columns. *Can. J. Civ. Eng.*, 735–747.
- Mirza, S. A., Hyttinen, V., & Hyttinen, E. (1996). Physical Tests and Analysis of Composite Steel-Concrete Beam-Columns. *JourlUll of Structural Engineering*, 1317-1326.
- Mirza, S. A., & Lacroix, E. A. (2004). Comparative Strength Analyses of Concrete-Encased Steel Composite Columns. *Journal of Structural Engineering*, 1941–1953.
- Ozcana, O., Binicib, B., & Ozcebe, G. (2008). Improving seismic performance of deficient reinforced concrete columns using carbon fiber-reinforced polymers. *Engineering Structures*, 1632–1646.
- Pandeya, G. R., Mutsuyoshib, H., & Makib, T. (2008). Seismic performance of bond controlled RC columns. *Engineering Structures*, 2538–2547.
- Perea, T., & Leon, R. (2008). Behavior of Composite CFT Beam-Columns Based on Nonlinear Fiber Element Analysis. *Composite Construction in Steel and Concrete*, 237-251.

- Prakash, S., Belarbi, A., & You, Y.-M. (2009). Seismic performance of circular RC columns subjected to axial force, bending, and torsion with low and moderate shear. *Engineering Structures*, 46.
- REDDIAR, M. K. (2009). *Stress-Strain Model of Unconfined and Confined Concrete and Stress-Block Parameters*. Texas.
- Shahari, A. M. (2002). *Behavior of Lightweight Concrete-Encased Composite Columns*. Amman: University of Jordan.
- Shao, Y., & Mirmiran, A. (2005). Experimental Investigation of Cyclic Behavior of Concrete-Filled Fiber Reinforced Polymer Tubes. *Journal of Composites for Construction*, 263-273.
- Shi, G., Wanga, M., Bai, Y., Wang, F., Shi, Y., & Wang, Y. (2012). Experimental and modeling study of high-strength structural steel under cyclic loading. *Engineering Structures*, 1-13.
- Shim, C.-S., Chung, Y.-S., & Yoon, J.-Y. (2011). Cyclic behavior of prefabricated circular composite columns with low steel ratio. *Engineering Structures*, 2525–2534.
- Spacone, E., & El-Tawil, S. (2004). Nonlinear Analysis of Steel-Concrete Composite Structures:State of the Art. *Journal of Structural Engineering*, 159–168.
- Tikka, T. K., & Mirza, S. A. (2005). Equivalent Uniform Moment Diagram Factor for Composite Columns in Major Axis Bending. *Journal of Structural Engineering*, 569–581.

- Vandoros, K. G., & Dritsos, S. E. (2008). Concrete jacket construction detail effectiveness when strengthening RC columns. *Construction and Building Materials*, 264–276.
- Varma, A. H., Ricle, J. M., Sause, R., & Lu, L.-W. (2004). Seismic Behavior and Design of High Strength Square Concrete-Filled Steel Tube Beam-Columns. *Journal of Structural Engineering*, 169–179.
- Varma, A. H., Ricles, J. M., Sause, R., Ream, A., & Lu, L. W. (2004). Seismic Performance of High Strength CFT Beam-Columns. *Advanced Technology in Structural Engineering*, 1-8.
- Xiao, J., & Zhang, C. (2008). Seismic behavior of RC columns with circular, square and diamond sections. *Construction and Building Materials*, 801–810.
- Yaqub, M., & Bailey, C. G. (2012). Seismic performance of shear critical post-heated reinforced concrete square columns wrapped with FRP composites. *Construction and Building Materials*, 457–469.
- Zhang, S., & Liu, J. (2007). Seismic behavior and strength of square tube confined reinforced-concrete (STRC) columns. *Journal of Constructional Steel Research*, 1194–1207.
- Zhou, F., Mosalam, K. M., & Nakashima, M. (2007). Finite-Element Analysis of a Composite Frame under large Lateral Cyclic Loading. *Journal of Structure Engineering*, 1018–1026.
- Zhou, T., Chen, Z., & Liu, H. (2012). Seismic behavior of special shaped column composed of concrete filled steel tubes. *Journal of Constructional Steel Research*, 131–141.

APPENDICES

Appendix A: Design of Composite, Steel, and Reinforced Concrete Columns

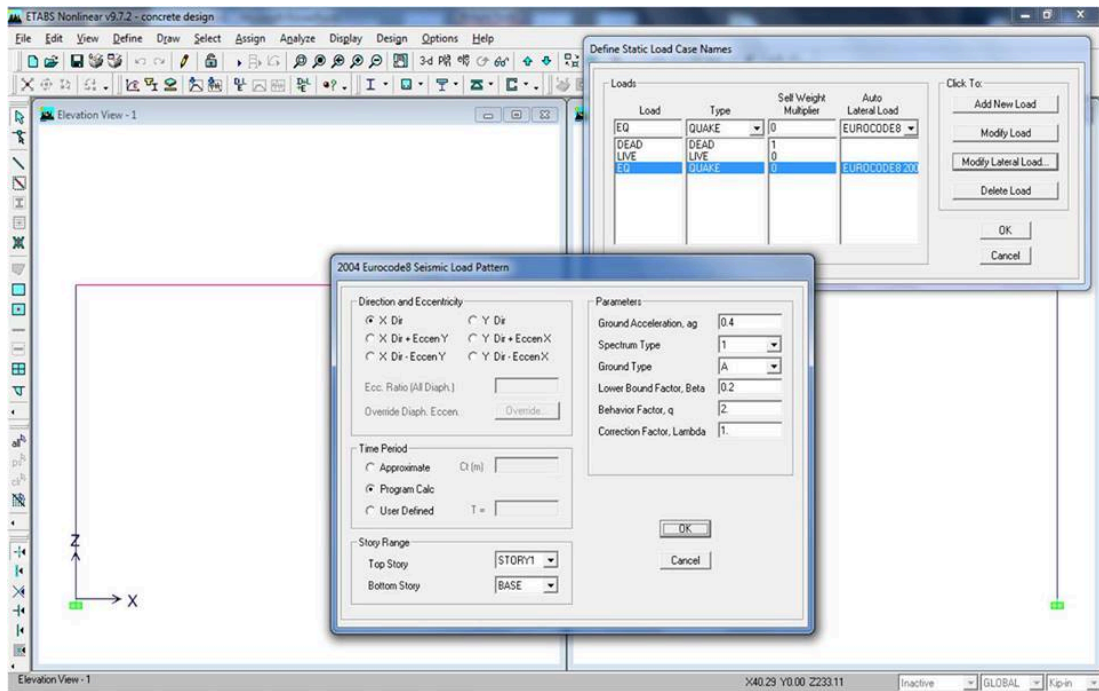


Figure A.1: Defining Earthquake Variables in ETABS

Composite column design sheet

Section Geometry			
Hight	(h1) =	310	mm
Width	(h2) =	310	mm
Concrete cover	(Cr) =	35	mm
Column Length	(L) =	4000	mm
Steel Section			
Section used		HE200B	
Yield Strength of Shape F_{yd} =		250	Mpa
Area of Steel Section A_a =		7810	mm ²
Elastic modulus of steel shape=		210000	MPa
Section Geometric Properties:			
d =	200	mm	b_f = 200 mm
tw =	9	mm	t_f = 15 mm
I_x =	5.70E+07	mm ⁴	I_y = 2.00E+07 mm ⁴
Z_x =	6.43E+05	mm ³	Z_y = 3.06E+05 mm ³
Reinforcing Steel			
Yield Strength of bars F_{yr} =		391.30435	Mpa
Elastic modulus of reinforcing steel =		210000	Mpa
Area of Longitudinal Reinforced bar A_b =		78.54	mm ²
No. of Longitudinal Reinforced bars n =		4	
area of reinforcing steel A_r =		314.16	mm ²
Moment of inertial of reinforcing steel I_r =		4523904	mm ⁴
Concrete:			
concrete strength f'_{cube} =		30.86	Mpa
cylinder strength $f'_{cylinder}$ =		16.66666667	Mpa
F_{cm}		24.66666667	
E_{cm} =		30500	Mpa
area of concrete A_c =		87975.84	mm ²
I_{cx} =		7.08E+08	mm ⁴
I_{cy} =		745046929.3	mm ⁴

THE PROCEDURE FOR DESIGN

1- Plastic resistance of the section:

$$N_{pl,Rd} = A_a f_{yd} + 0,85 A_c f_{cd} + A_s f_{sd} \quad 3321756.574 \text{ Mpa}$$

2- Effective elastic flexural stiffness of the section

about the major axis

$$(EI)_{eff} = E_a I_{ax} + E_s I_{sx} + K_e E_{cm} I_{cx} \quad 2.59E+13$$

about the minor axis

$$(EI)_{eff} = E_a I_{ay} + E_s I_{sy} + K_e E_{cm} I_{cy} \quad 1.88E+13$$

3-Non dimensional slenderness

$$N_{crx} = \frac{(EI)_{eff} \pi^2}{(L)^2} \quad 1.60E+07$$

$$N_{cry} = \frac{(EI)_{eff} \pi^2}{(L)^2} \quad 1.16E+07$$

$$\lambda_x = \sqrt{\frac{N_{pl,Rk}}{N_{cr}}} \quad 0.456241549$$

$$\lambda_x = \sqrt{\frac{N_{pl,Rk}}{N_{cr}}} \quad 0.535331938$$

4-resistance of the composite column under axial compression

$$\frac{N_{ed}}{\chi N_{pl,Rd}} \leq 1.0$$

about the major axis

$$\phi = 0.5[1 + \alpha(\lambda - 0.2) + \lambda^2] \quad 0.647639239$$

$$\chi = \frac{1}{\phi + \sqrt{\phi^2 - \lambda^2}} \quad \chi \leq 1.0 \quad 0.90310453$$

$$N_{ed} = \chi N_{pl,Rd} \quad 2999.893408 \text{ KN}$$

about the minor axis

$$\phi = 0.5[1 + \alpha(\lambda - 0.2) + \lambda^2] \quad 0.725446467$$

$$\chi = \frac{1}{\phi + \sqrt{\phi^2 - \lambda^2}} \quad \chi \leq 1.0 \quad 0.823024769$$

$$N_{ed} = \chi N_{pl,Rd} \quad 2733.887936 \text{ KN}$$

5-Resistance of the composite column under axial compression and uniaxial bending

$$Z_r = \sum_{i=1}^n A_{ri} e_i \quad 37699.08 \quad \text{mm}^3$$

$$Z_s = \quad 6.43E+05 \quad \text{mm}^3$$

$$Z_c = \frac{h_1 h_2}{4} - Z_s - Z_r \quad 6767550.92 \quad \text{mm}^3$$

Check that the position of neutral axis is in the flange

Neutral Axis in flange: $d/2 - t_f \leq h_n \leq d/2$

$$N_{pm} = A_c f_{cd} \quad 1466264$$

$$h_n = \frac{N_{pm} - A_{rn}(2f_{rd} - f_{cd}) + (b_f - t_w)(d - 2t_f)(2f_{yd} - f_{cd})}{2h_1 f_{cd} + 2b_f(2f_{yd} - f_{cd})} \quad 84.25579705 \quad \text{mm}$$

it come between the 85 ≤ 85.10 ≤ 95 so the neutral axis is in the flange

Section modulus about neutral axis

$Z_{rn} = 0$ (As there is no reinforcement with in the region of $2h_n$ from the middle line of the cross section)

$$Z_{sn} = b_f h_n^2 - \frac{(b_f - t_w)(d - 2t_f)^2}{4} \quad 39832.86744 \quad \text{mm}^3$$

$$Z_{cn} = h_1 h_n^2 - Z_{sn} - Z_{rn} \quad 2160869.327 \quad \text{mm}^3$$

Plastic moment resistance of section

$$M_{ed} = (Z_s - Z_{sn}) f_{yd} + 1/2 (Z_c - Z_{cn}) f_{cd} + (Z_r - Z_{rn}) f_{rd} \quad 203807610.3 \quad \text{N.mm}$$

for interaction curve

point A

$$N_A = N_{pi} R_d \quad 3321.756574 \quad \text{KN}$$

$$M_A = 0 \quad 0 \quad \text{KN.m}$$

point B

$$N_B = 0 \quad 0 \quad \text{KN}$$

$$M_B = Z_{sn} f_{yd} + 1/2 Z_{cn} f_{cd} + Z_{rn} f_{rd} \quad 27.96546125 \quad \text{KN.m}$$

point C

$$N_C = A_c f_{cd} \quad 1466.264 \quad \text{KN}$$

$$M_C = Z_{sn} f_{yd} + 1/2 Z_{cn} f_{cd} + Z_{rn} f_{rd} \quad 42.71727517 \quad \text{KN.m}$$

point D

$$N_D = 0.5 A_c f_{cd} \quad 733.132 \quad \text{KN}$$

$$M_D = Z_s f_{yd} + 1/2 Z_c f_{cd} + Z_r f_{rd} \quad 231.7730716 \quad \text{KN.m}$$

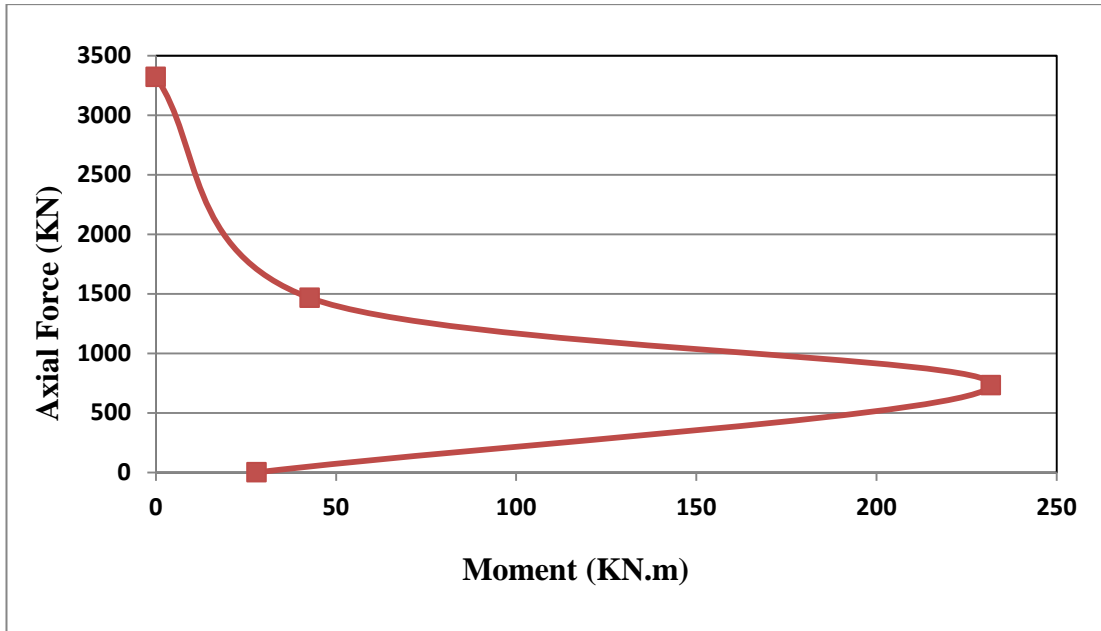


Figure A.2: The Interaction Curve for Composite Column

Steel column design according to Eurocode 3

In order to calculate the plastic resistance of steel columns, the design compression resistance is taken as the design plastic resistance. The plastic resistance equation for Class 1, 2, 3 cross-sections is

$$N_{c,Rd} = \frac{Af_y}{\gamma_{M_0}} \quad (\text{A.1})$$

The plastic resistance of Class 4 cross-section equation is

$$N_{c,Rd} = \frac{A_{eff} f_y}{\gamma_{M_1}} \quad (\text{A.2})$$

where

A Cross-sectional area

A_{eff} The area of the effective cross-section

f_y Yield strength of steel section

γ_{M_2} Resistance of cross-section whatever the class

γ_{M_1} Resistance of members to instability

The design value of the compression force N_{Ed} at every cross-section should satisfy

$$\frac{N_{Ed}}{N_{c,Rd}} \leq 1.0 \quad (\text{A.3})$$

The non-dimensional slenderness λ is given by

$$\lambda = \sqrt{\frac{Af_y}{N_{cr}}} \quad \text{for class 1, 2 or 3 cross-sections} \quad (\text{A.4})$$

$$\lambda = \sqrt{\frac{A_{eff} f_y}{N_{cr}}} \quad \text{for class 4 cross-section} \quad (A.5)$$

where

N_{cr} the elastic critical force for the relevant buckling mode

$$N_{cr} = \frac{\pi^2 EI}{l_{cr}^2} \quad (A.6)$$

l_{cr} The buckling length

E Modulus of elasticity

I Second moment of area

A compression member should be verified against buckling as follows

$$\frac{N_{Ed}}{N_{b,Rd}} \leq 1.0 \quad (A.7)$$

where:

N_{Ed} is the design value of the compression force

$N_{b,Rd}$ is the design buckling resistance of the compression member

The design buckling resistance of a compression member should be taken as

$$N_{b,Rd} = \frac{\chi A f_y}{\gamma_{M_1}} \quad \text{For class 1,2 and 3 cross-section} \quad (A.8)$$

$$N_{b,Rd} = \frac{\chi A_{eff} f_y}{\gamma_{M_1}} \quad \text{For class 4 cross-section} \quad (A.9)$$

where:

χ the reduction factor for the relevant buckling mode

$$\chi = \frac{1}{\phi + \sqrt{\phi^2 - \lambda^2}} \quad \text{But } \chi \leq 1 \quad (\text{A.10})$$

where

$$\phi = 0.5[1 + \alpha(\lambda - 0.2) + \lambda^2] \quad (\text{A.11})$$

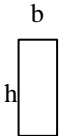
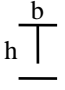


α An imperfection factor, the imperfection factor corresponding to the appropriate buckling curve should be obtained from Table A.1 based on the selection from Table A.2

Table A.1: Imperfection Factors for Flexural Buckling Curves

Buckling curve	a	b	c	d
Imperfection factor α	0.21	0.34	0.49	0.76

The value of, χ , for the appropriate non-dimensional slenderness, λ , may alternatively be determined from Figure 2.1 or Table 2.2

Table A.2: Selection of Buckling Curve for a Cross-Section

Cross section type	Limits	Buckling about axis	Buckling curve	
Rolled open section  	$h/b > 1,2$ $t \leq 40\text{mm}$	y-y	a	
		z-z	b	
	$h/b \leq 1,2$ flange thickness $\leq 100\text{mm}$ flange thickness $> 100\text{mm}$	40mm < flange thickness < 100mm	y-y	b
			z-z	c
			y-y	b
			z-z	c
Hollow sections 	hot rolled cold formed see 5.5.1.4(4) and figure 5.5.2	any	a	
		any	b or c	
	none	any	c	

Steel Beam-Column Design

The behavior of column subjected to axial load and bending moment can be given by interaction curve showing the reduction of ultimate load with increasing moment. An approximation to this curve can be obtained by considering fully plastic sections for different arbitrary positions of the neutral axis.

There are two possible zones to look into position of the neutral axis; neutral axis in the web ($y_n \leq (h - t_f)/2$), and neutral axis in the flange ($y_n > (h - t_f)/2$).

a) Neutral Axis in the web ($y_n \leq (h - t_f)/2$)

$$N_M = 2f_y t_w y_n \tag{A.12}$$

$$M_N = f_y b t_f (h - t_f) + f_y \left[\left(\frac{h - 2t_f}{2} \right)^2 - y_n^2 \right] t_w \quad (\text{A.13})$$

where

y_n The distance from centroid axis to neutral axis

b) Neutral Axis in flange ($y_n > (h - t_f)/2$)

$$N_M = f_y \left[t_w (h - 2t_f) + 2b \left(t_f - \frac{h}{2} + y_n \right) \right] \quad (\text{A.14})$$

$$M_N = f_y b \left(\frac{h}{2} - y_n \right) (h - y_n) t_f \quad (\text{A.15})$$

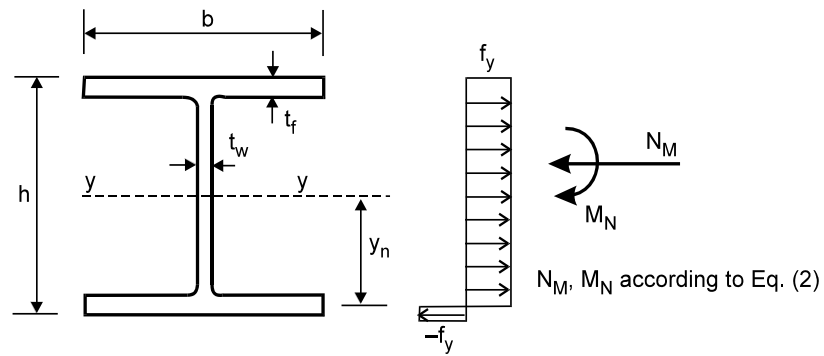
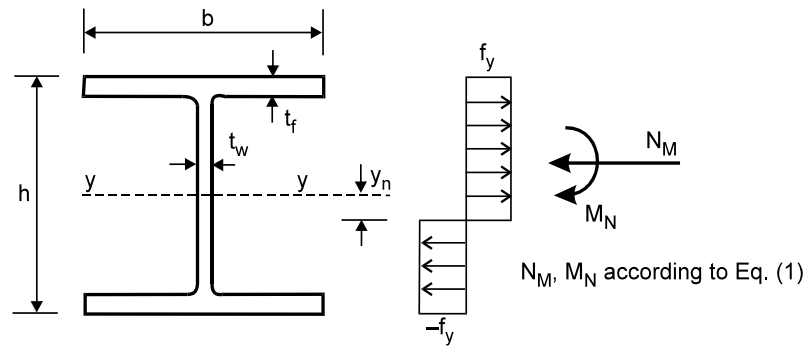
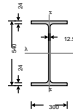


Figure A.3: The Stress Distribution and Neutral Axis Location

Steel column design SHEET (EN 1993-1-1)



Column and loading details

Column details

Column section;

HE 550 A

System length for buckling about y axis;

$L_y = ;4000$; mm

System length for buckling about z axis;

$L_z = ;4000$; mm;

Column loading

Axial load;

$N_{Ed} = 225$ kN; (Compression)

Moment about y axis at end 1;

$M_{y,Ed1} = 0.0$ kNm

Moment about y axis at end 2;

$M_{y,Ed2} = 0.0$ kNm

Moment about z axis at end 1;

$M_{z,Ed1} = 160.5$ kNm

Moment about z axis at end 2;

$M_{z,Ed2} = 69.6$ kNm

Single curvature bending about z axis

Shear force parallel to z axis;

$V_{z,Ed} = 0$ kN

Shear force parallel to y axis;

$V_{y,Ed} = 64$ kN

Material details

Steel grade;

S275

Yield strength;

$f_y = 275$ N/mm²

Ultimate strength;

$f_u = 430$ N/mm²

Modulus of elasticity;

$E = 210$ kN/mm²

Poisson's ratio;

$\nu = 0.3$

Shear modulus;

$G = E / [2 \times (1 + \nu)] = 80.8$ kN/mm²

Buckling length for flexural buckling about y axis

End restraint factor;

$K_y = 2.000$

Buckling length;

$L_{cr,y} = L_y \times K_y = 8000$ mm

Section classification

Web section classification (Table 5.2)

Coefficient depending on f_y ;

$$\varepsilon = \sqrt{(235 \text{ N/mm}^2 / f_y)} = \mathbf{0.924}$$

Depth between fillets;

$$c_w = h - 2 \times (t_f + r) = \mathbf{438.0 \text{ mm}}$$

Ratio of c/t ;

$$\text{ratio}_w = c_w / t_w = \mathbf{35.04}$$

Length of web taken by axial load;

$$l_w = \min(N_{Ed} / (f_y \times t_w), c_w) = \mathbf{65.5 \text{ mm}}$$

For class 1 & 2 proportion in compression;

$$\alpha = (c_w/2 + l_w/2) / c_w = \mathbf{0.575}$$

Limit for class 1 web;

$$\text{Limit}_{1w} = (396 \times \varepsilon) / (13 \times \alpha - 1) = \mathbf{;56.56}$$

The web is class 1

Flange section classification (Table 5.2)

Outstand length;

$$c_f = (b - t_w) / 2 - r = \mathbf{;116.7; \text{ mm}}$$

Ratio of c/t ;

$$\text{ratio}_f = c_f / t_f = \mathbf{4.86}$$

Conservatively assume uniform compression in flange

Limit for class 1 flange;

$$\text{Limit}_{1f} = 9 \times \varepsilon = \mathbf{8.32}$$

Limit for class 2 flange;

$$\text{Limit}_{2f} = 10 \times \varepsilon = \mathbf{9.24}$$

Limit for class 3 flange;

$$\text{Limit}_{3f} = 14 \times \varepsilon = \mathbf{12.94}$$

The flange is class 1

Overall section classification

The section is class 1

Resistance of cross section (cl. 6.2)

Shear parallel to y axis (cl. 6.2.6)

Design shear force;

$$V_{y,Ed} = \mathbf{63.7 \text{ kN}}$$

Shear area;

$$A_{vy} = 2 \times b \times t_f - (t_w + 2 \times r) \times t_f = \mathbf{;12804;}$$

mm^2

Plastic shear resistance;

$$V_{pl,y,Rd} = A_{vy} \times (f_y / \sqrt{3}) / \gamma_{M0} = \mathbf{2032.9 \text{ kN}}$$

PASS - Shear resistance parallel to y axis exceeds the design shear force

$V_{y,Ed} \leq 0.5 \times V_{pl,y,Rd}$ - No reduction in f_y required for bending/axial force

Compression (cl. 6.2.4)

Design force;

$$N_{Ed} = \mathbf{225 \text{ kN}}$$

Design resistance;

$$N_{c,Rd} = N_{pl,Rd} = A \times f_y / \gamma_{M0} = \mathbf{5823 \text{ kN}}$$

PASS - The compression design resistance exceeds the design force

Bending about z axis (cl. 6.2.5)

Design bending moment;

$$M_{z,Ed} = \max(\text{abs}(M_{z,Ed1}), \text{abs}(M_{z,Ed2})) = \mathbf{160.5}$$

kNm

Section modulus about z axis;

$$W_z = W_{pl,z} = \mathbf{;1106.9; \text{ cm}^3}$$

Design resistance;

$$M_{c,z,Rd} = W_z \times f_y / \gamma_{M0} = \mathbf{304.4 \text{ kNm}}$$

PASS - The bending design resistance about the z axis exceeds the design moment

Combined bending and axial force (cl. 6.2.9)

Ratio design axial to design plastic resistance;

$$n = \text{abs}(N_{Ed}) / N_{pl,Rd} = \mathbf{0.039}$$

Ratio web area to gross area;

$$a = \min(0.5, (A - 2 \times b \times t_f) / A) = \mathbf{0.320}$$

Bending about z axis (cl. 6.2.9.1)

Design bending moment;

$$M_{z,Ed} = \max(\text{abs}(M_{z,Ed1}), \text{abs}(M_{z,Ed2})) = \mathbf{160.5}$$

kNm

Plastic design resistance; $M_{pl,z,Rd} = W_{pl,z} \times f_y / \gamma_{M0} = \mathbf{304.4}$ kNm

Modified design resistance; $M_{N,z,Rd} = M_{pl,z,Rd} = \mathbf{,304.4}$; kNm

PASS - Bending resistance about z axis in presence of axial load exceeds design moment

Buckling resistance (cl. 6.3)

Yield strength for buckling resistance; $f_y = \mathbf{275}$ N/mm²

Flexural buckling about y axis

Elastic critical buckling force; $N_{cr,y} = \pi^2 \times E \times I_y / L_{cr,y}^2 = \mathbf{36249}$ kN

Non-dimensional slenderness; $\lambda_y = \sqrt{(A \times f_y / N_{cr,y})} = \mathbf{0.401}$

Buckling curve (Table 6.2); **a**

Imperfection factor (Table 6.1); $\alpha_y = \mathbf{0.21}$

Parameter Φ ; $\Phi_y = 0.5 \times [1 + \alpha_y \times (\lambda_y - 0.2) + \lambda_y^2] = \mathbf{0.601}$

Reduction factor; $\chi_y = \min(1.0, 1 / [\Phi_y + \sqrt{(\Phi_y^2 - \lambda_y^2)}]) = \mathbf{0.953}$

Design buckling resistance; $N_{b,y,Rd} = \chi_y \times A \times f_y / \gamma_{M1} = \mathbf{5547.1}$ kN

PASS - The flexural buckling resistance about the y axis exceeds the design axial load

Flexural buckling about z axis

Elastic critical buckling force; $N_{cr,z} = \pi^2 \times E \times I_z / L_{cr,z}^2 = \mathbf{3504}$ kN

Non-dimensional slenderness; $\lambda_z = \sqrt{(A \times f_y / N_{cr,z})} = \mathbf{1.289}$

Buckling curve (Table 6.2); **b**

Imperfection factor (Table 6.1); $\alpha_z = \mathbf{0.34}$

Parameter Φ ; $\Phi_z = 0.5 \times [1 + \alpha_z \times (\lambda_z - 0.2) + \lambda_z^2] = \mathbf{1.516}$

Reduction factor; $\chi_z = \min(1.0, 1 / [\Phi_z + \sqrt{(\Phi_z^2 - \lambda_z^2)}]) = \mathbf{0.432}$

Design buckling resistance; $N_{b,z,Rd} = \chi_z \times A \times f_y / \gamma_{M1} = \mathbf{2516.4}$ kN

PASS - The flexural buckling resistance about the z axis exceeds the design axial load

Torsional and torsional-flexural buckling (cl. 6.3.1.4)

Torsional buckling length factor; $K_T = \mathbf{1.00}$

Effective buckling length; $L_{cr,T} = K_T \times \max(L_y, L_z) = \mathbf{4000}$ mm

;

;;

Distance from shear ctr to centroid along y axis; $y_0 = \mathbf{,0.0}$; mm

Distance from shear ctr to centroid along z axis; $z_0 = \mathbf{0.0}$ mm

$i_0 = \sqrt{(i_y^2 + i_z^2 + y_0^2 + z_0^2)} = \mathbf{240.8}$ mm

$\beta_T = 1 - (y_0 / i_0)^2 = \mathbf{1.000}$

Elastic critical torsional buckling force; $N_{cr,T} = 1 / i_0^2 \times (G \times I_t + \pi^2 \times E \times I_w / L_{cr,T}^2) = \mathbf{21114}$ kN

Elastic critical torsional-flexural buckling force; $N_{cr,TF} = N_{cr,y} / (2 \times \beta_T) \times [1 + N_{cr,T} / N_{cr,y} - \sqrt{(1 - N_{cr,T} / N_{cr,y})^2 + 4 \times (y_0 / i_0)^2 \times N_{cr,T} / N_{cr,y}}]$

$N_{cr,TF} = \mathbf{21114}$ kN

Non-dimensional slenderness; $\lambda_T = \sqrt{(A \times f_y / \min(N_{cr,T}, N_{cr,TF}))} = \mathbf{0.525}$

Buckling curve (Table 6.2); **b**

Imperfection factor (Table 6.1); $\alpha_T = \mathbf{0.34}$

Parameter Φ ; $\Phi_T = 0.5 \times [1 + \alpha_T \times (\lambda_T - 0.2) + \lambda_T^2] = \mathbf{0.693}$

Reduction factor; $\chi_T = \min(1.0, 1 / [\Phi_T + \sqrt{(\Phi_T^2 - \lambda_T^2)}]) = \mathbf{0.873}$

Design buckling resistance; $N_{b,T,Rd} = \chi_T \times A \times f_y / \gamma_{M1} = \mathbf{5083.2}$ kN

PASS - The torsional/torsional-flexural buckling resistance exceeds the design axial load

Minimum buckling resistance

Minimum buckling resistance;
kN

$$N_{b,Rd} = \min(N_{b,y,Rd}, N_{b,z,Rd}, N_{b,T,Rd}) = \mathbf{2516.4}$$

PASS - The axial load buckling resistance exceeds the design axial load

Combined bending and axial compression (cl. 6.3.3)

Characteristic resistance to normal force;	$N_{Rk} = A \times f_y = \mathbf{5823}$ kN
Characteristic moment resistance about y axis;	$M_{y,Rk} = W_y \times f_y = \mathbf{1271.0}$ kNm
Characteristic moment resistance about z axis;	$M_{z,Rk} = W_z \times f_y = \mathbf{304.4}$ kNm
Moment distribution factor about y axis;	$\Psi_y = M_{y,Ed1} / M_{y,Ed2} = \mathbf{:0.000}$
Moment factor about y axis;	$C_{my} = \max(0.4, 0.6 + 0.4 \times \Psi_y) = \mathbf{0.600}$
Moment distribution factor about z axis;	$\Psi_z = M_{z,Ed2} / M_{z,Ed1} = \mathbf{:0.433}$
Moment factor about z axis;	$C_{mz} = \max(0.4, 0.6 + 0.4 \times \Psi_z) = \mathbf{0.773}$
Moment distribution factor for LTB;	$\Psi_{LT} = M_{y,Ed1} / M_{y,Ed2} = \mathbf{:0.000}$
Moment factor for LTB;	$C_{mLT} = \max(0.4, 0.6 + 0.4 \times \Psi_{LT}) = \mathbf{0.600}$
Interaction factor k_{yy} ; $(N_{Rk} / \gamma_{M1}) = \mathbf{0.605}$	$k_{yy} = C_{my} \times [1 + \min(0.8, \lambda_y - 0.2) \times N_{Ed} / (\chi_y \times$
Interaction factor k_{zy} ; $0.25) \times (\chi_z \times N_{Rk} / \gamma_{M1}) = \mathbf{:0.974}$	$k_{zy} = 1 - \min(0.1, 0.1 \times \lambda_z) \times N_{Ed} / ((C_{mLT} -$
Interaction factor k_{zz} ; $(\chi_z \times N_{Rk} / \gamma_{M1}) = \mathbf{:0.870}$	$k_{zz} = C_{mz} \times [1 + \min(1.4, 2 \times \lambda_z - 0.6) \times N_{Ed} /$
Interaction factor k_{yz} ;	$k_{yz} = 0.6 \times k_{zz} = \mathbf{0.522}$
Section utilisation; $(M_{z,Rk} / \gamma_{M1}) = \mathbf{0.316}$	$UR_{B_1} = N_{Ed} / (\chi_y \times N_{Rk} / \gamma_{M1}) + k_{yz} \times M_{z,Ed} /$
$(M_{z,Rk} / \gamma_{M1}) = \mathbf{0.548}$	$UR_{B_2} = N_{Ed} / (\chi_z \times N_{Rk} / \gamma_{M1}) + k_{zz} \times M_{z,Ed} /$

PASS - The buckling resistance is adequate

Reinforcement concrete column design

In order to calculate the design compressive strength for reinforced concrete column

$$f_{cd} = \alpha_{cc} \times \frac{f_{ck}}{\gamma_c} \quad (\text{A.16})$$

where

γ_c the partial safety factor for concrete

α_{cc} the coefficient taking account of long term effects on the compressive strength

The total amount of longitudinal reinforcement should not be less than $A_{s,min}$

$$A_{s,min} = \frac{0.10N_{Ed}}{f_{yd}} \text{ Or } 0.002A_c \text{ whichever is greater} \quad (\text{A.17})$$

where:

F_{yd} the design yield strength of the reinforcement

N_{Ed} the design axial compression force

The nominal cover shall be specified on the drawings. It is defined as a minimum cover, c_{min} , plus an allowance in design for deviation, ΔC_{dev}

$$C_{nom} = C_{min} + \Delta C_{dev} \quad (\text{A.18})$$

The greater value for, c_{min} , satisfying the requirements for both bond and environmental conditions shall be used

$$C_{min} = \max\{C_{min,b}; C_{min,dur}\} \quad (\text{A.19})$$

where

$c_{min,b}$ minimum cover due to bond requirement

$c_{min,dur}$ minimum cover due to environmental conditions

A rectangular stress distribution may be assumed. The factor, λ , defining the effective height of the compression zone and the factor, η , defining the effective strength, follow from:

$$\lambda = 0.8 \text{ for } f_{ck} \leq 50 \text{ MPa} \quad (\text{A.20})$$

$$\lambda = 0.8 - (f_{ck} - 50)/400 \text{ for } 50 < f_{ck} \leq 90 \text{ MPa} \quad (\text{A.21})$$

And

$$\eta = 1.0 \text{ for } f_{ck} \leq 50 \text{ MPa} \quad (\text{A.22})$$

$$\eta = 1.0 - (f_{ck} - 50)/200 \text{ for } 50 < f_{ck} \leq 90 \text{ MPa} \quad (\text{A.23})$$

Note: If the width of the compression zone decreases in the direction of the extreme compression, fibre, the value, ηf_{cd} , should be reduced by 10%.

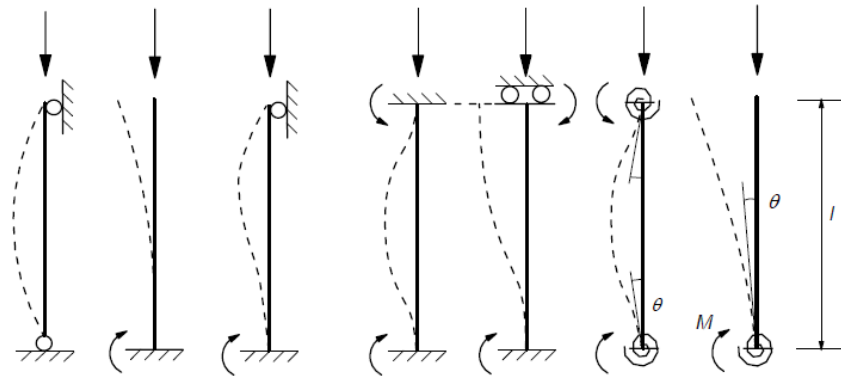
The slenderness ratio is defined as follows:

$$\lambda = l_0 / i \quad (\text{A.24})$$

where:

l_0 The effective length

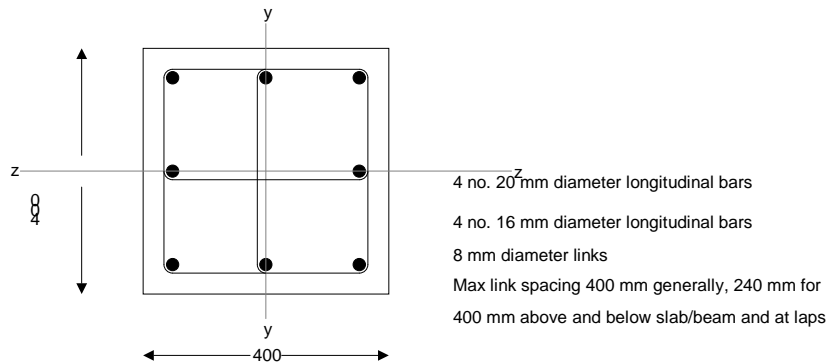
i the radius of gyration of the uncracked concrete section



a) $l_0 = l$ b) $l_0 = 2l$ c) $l_0 = 0,7l$ d) $l_0 = l/2$ e) $l_0 = l$ f) $l/2 < l_0 < l$ g) $l_0 > 2l$

Figure A.4: Examples of different buckling modes and corresponding effective lengths for isolated members

RC column design SHEET (EN1992-1)



Column input details

Column geometry

Overall depth; $h = 400$ mm
 Overall breadth; $b = 400$; mm

Concrete details

Concrete strength class; **C25/30**
 Partial safety factor for concrete (2.4.2.4(1)); $\gamma_C = 1.50$
 Coefficient α_{cc} (3.1.6(1)); $\alpha_{cc} = 0.85$
 Maximum aggregate size; $d_g = 20$ mm

Reinforcement details

Nominal cover to links; $c_{nom} = 30$ mm
 Longitudinal bar diameter; $\phi = 20$ mm and 16 mm
 Link diameter; $\phi_v = 8$ mm
 Total number of longitudinal bars; $N = 8$
 No. of bars per face parallel to z axis; $N_z = 3$
 No. of bars per face parallel to y axis; $N_y = 3$
 Area of longitudinal reinforcement;
 $= 2060.88 \text{ mm}^2$ $A_s = (4 \times \pi \times 20^2 / 4) + (4 \times \pi \times 16^2 / 4)$
 Characteristic yield strength; $f_{yk} = 450 \text{ N/mm}^2$
 Partial safety factor for reinft (2.4.2.4(1)); $\gamma_S = 1.15$
 Modulus of elasticity of reinft (3.2.7(4)); $E_s = 200 \text{ kN/mm}^2$

Fire resistance details

Fire resistance period; $R = 60$ min
 Exposure to fire; **Exposed on more than one side**
 Ratio of fire design axial load to design resistance; $\mu_{fi} = 0.70$

Calculated column properties

Concrete properties

Area of concrete;	$A_c = h \times b = 160000 \text{ mm}^2$
Characteristic compression cylinder strength;	$f_{ck} = 25 \text{ N/mm}^2$
Design compressive strength (3.1.6(1));	$f_{cd} = \alpha_{cc} \times f_{ck} / \gamma_C = 14.2 \text{ N/mm}^2$
Mean value of cylinder strength (Table 3.1);	$f_{cm} = f_{ck} + 8 \text{ MPa} = 33.0 \text{ N/mm}^2$
Secant modulus of elasticity (Table 3.1);	$E_{cm} = 22000 \text{ MPa} \times (f_{cm} / 10 \text{ MPa})^{0.3} = 31.5 \text{ kN/mm}^2$

Rectangular stress block factors

Depth factor (3.1.7(3));	$\lambda_{sb} = 0.8$
Stress factor (3.1.7(3));	$\eta = 1.0$

Strain limits

Compression strain limit (Table 3.1);	$\epsilon_{cu3} = 0.00350$
Pure compression strain limit (Table 3.1);	$\epsilon_{c3} = 0.00175$

Design yield strength of reinforcement

Design yield strength (3.2.7(2));	$f_{yd} = f_{yk} / \gamma_S = 391.3 \text{ N/mm}^2$
-----------------------------------	---

Check nominal cover for fire and bond requirements

Min. cover reqd for bond (to links) (4.4.1.2(3));	$c_{min,b} = \max(\phi_v, \phi - \phi_v) = 12 \text{ mm};$
Min axis distance for fire (EN1992-1-2 T 5.2a);	$a_{fi} = 40 \text{ mm}$
Allowance for deviations from min cover (4.4.1.3);	$\Delta C_{dev} = 10 \text{ mm}$
Min allowable nominal cover;	$C_{nom_min} = \max(a_{fi} - \phi / 2 - \phi_v, c_{min,b} + \Delta C_{dev}) = 22.0 \text{ mm}$

PASS - the nominal cover is greater than the minimum required

Effective depths of bars for bending about z axis

Area of per bar;	$A_{bar1} \text{ of } \phi 20 \text{ mm} = \pi \times \phi^2 / 4 = 314 \text{ mm}^2$
	$A_{bar2} \text{ of } \phi 16 \text{ mm} = \pi \times \phi^2 / 4 = 201.1 \text{ mm}^2$
Spacing of bars in faces parallel to y axis (c/c);	$s_y = (h - 2 \times (c_{nom} + \phi_v) - \phi) / (N_y - 1) = 152 \text{ mm}$
Layer 1 (in tension face);	$d_{z1} = h - c_{nom} - \phi_v - \phi / 2 = 352 \text{ mm}$
Layer 2;	$d_{z2} = d_{z1} - s_y = 200 \text{ mm}$
Layer 3;	$d_{z3} = d_{z2} - s_y = 48 \text{ mm}$
2nd moment of area of reinf about z axis;	$I_{sz} = 2 \times (2 A_{bar1} + A_{bar2}) \times (d_{z1} - h/2)^2 = 3831.1 \text{ cm}^4$
Radius of gyration of reinf about z axis;	$i_{sz} = \sqrt{I_{sz} / A_s} = 136.3 \text{ mm}$
Effective depth about z axis (5.8.8.3(2));	$d_z = h / 2 + i_{sz} = 336.3 \text{ mm}$

Effective depths of bars for bending about y axis

Area per bar;	$A_{bar1} = \pi \times 20^2 / 4 = 314 \text{ mm}^2$
	$A_{bar2} = \pi \times 16^2 / 4 = 201.1 \text{ mm}^2$
Spacing of bars in faces parallel to z axis (c/c);	$s_z = (b - 2 \times (c_{nom} + \phi_v) - \phi) / (N_z - 1) = 152 \text{ mm}$
Layer 1 (in tension face);	$d_{y1} = b - c_{nom} - \phi_v - \phi / 2 = 352 \text{ mm}$
Layer 2;	$d_{y2} = d_{y1} - s_z = 200 \text{ mm}$

Layer 3;
 2nd moment of area of reinf about y axis;
 3831.1 cm⁴
 Radius of gyration of reinf about y axis;
 Effective depth about y axis (5.8.8.3(2));

$$d_{y3} = d_{y2} - s_z = \mathbf{48 \text{ mm}}$$

$$I_{sy} = 2 \times (2 A_{\text{bar}1} + A_{\text{bar}2}) \times (d_{y1} - b/2)^2 =$$

$$i_{sy} = \sqrt{I_{sy} / A_s} = \mathbf{136.3 \text{ mm}}$$

$$d_y = b / 2 + i_{sy} = \mathbf{336.3 \text{ mm}}$$

Axial load capacity with zero moment

Strain with uniform compression (Fig. 6.1);
 Stress in reinforcement;
 Axial load capacity;
 2964.04 kN

$$\epsilon_0 = \epsilon_{c3} = \mathbf{0.00175}$$

$$\sigma_0 = \min(\epsilon_0 \times E_s, f_{yd}) = \mathbf{350.0 \text{ N/mm}^2}$$

$$N_{Rd0} = (A_s \times \sigma_0) + (A_c - A_s) \times \eta \times f_{cd} =$$

Axial and bending capacity with zero strain in tension face reinforcement

(bending about z axis)

Moment of resistance of concrete

Depth to neutral axis;
 Concrete compression force;
 Concrete moment of resistance;
 kNm

$$z_1 = d_{z1} = \mathbf{352.0 \text{ mm}}$$

$$F_{zc1} = (\eta \times f_{cd}) \times (\lambda_{sb} \times z_1) \times b = \mathbf{1599.5 \text{ kN}}$$

$$M_{zc1} = F_{zc1} \times (h / 2 - (\lambda_{sb} \times z_1) / 2) = \mathbf{94.7}$$

Moment of resistance of reinforcement

Strain in layer 1;
 Force in layer 1;
 Moment of resistance of layer 1;
 Strain in layer 2;
 Force in layer 2;
 kN
 Moment of resistance of layer 2;
 Strain in layer 3;
 Force in layer 3;
324.43 kN
 Moment of resistance of layer 3;

$$\epsilon_{z11} = \epsilon_{cu3} \times (1 - d_{z1} / z_1) = \mathbf{0.00000}$$

$$F_{z11} = N_z \times A_{\text{bar}} \times \min(f_{yd}, E_s \times \epsilon_{z11}) = \mathbf{0.0 \text{ kN}}$$

$$M_{Rdz11} = F_{z11} \times (h / 2 - d_{z1}) = \mathbf{0.0 \text{ kNm}}$$

$$\epsilon_{z21} = \epsilon_{cu3} \times (1 - d_{z2} / z_1) = \mathbf{0.00151}$$

$$F_{z21} = 2 \times A_{\text{bar}} \times \min(f_{yd}, E_s \times \epsilon_{z21}) = \mathbf{121.46}$$

$$M_{Rdz21} = F_{z21} \times (h / 2 - d_{z2}) = \mathbf{0.0 \text{ kNm}}$$

$$\epsilon_{z31} = \epsilon_{cu3} \times (1 - d_{z3} / z_1) = \mathbf{0.00302}$$

$$F_{z31} = (2 A_{\text{bar}1} + A_{\text{bar}2}) \times \min(f_{yd}, E_s \times \epsilon_{z31}) =$$

$$M_{Rdz31} = F_{z31} \times (h / 2 - d_{z3}) = \mathbf{49.3 \text{ kNm}}$$

Combined axial load and moment resistance

Axial load capacity;
 Moment of resistance about z axis;

$$N_{Rdz1} = \mathbf{2045.37 \text{ kN}}$$

$$M_{Rdz1} = \mathbf{144 \text{ kNm}}$$

Axial and bending capacity with concrete at ultimate strain and tension steel at

yield (bending about z axis)

This is often referred to as the 'balance failure point'.

Moment of resistance of concrete

Strain in tension reinforcement;
 Depth to neutral axis;

$$\epsilon_{z12} = f_{yd} / E_s = \mathbf{0.00196}$$

$$z_2 = d_{z1} \times (\epsilon_{cu3} / (\epsilon_{cu3} + \epsilon_{z12})) = \mathbf{225.64 \text{ mm}}$$

Concrete compression force(3.1.7(3));
kN

$$F_{zc2} = (\eta \times f_{cd}) \times (\lambda_{sb} \times z_2) \times b = \mathbf{1025.31}$$

Concrete moment of resistance;
kNm

$$M_{zc2} = F_{zc2} \times (h / 2 - (\lambda_{sb} \times z_2) / 2) = \mathbf{112.52}$$

Moment of resistance of reinforcement

Strain in layer 1;

$$\varepsilon_{z12} = \varepsilon_{cu3} \times (1 - d_{z1} / z_2) = \mathbf{-0.00196}$$

Force in layer 1;
325 kN

$$F_{z12} = (2 A_{bar1} + A_{bar2}) \times \min(f_{yd}, E_s \times \varepsilon_{z12}) = -$$

Moment of resistance of layer 1;

$$M_{Rdz12} = F_{z12} \times (h / 2 - d_{z1}) = \mathbf{49.4 \text{ kNm}}$$

Strain in layer 2;

$$\varepsilon_{z22} = \varepsilon_{cu3} \times (1 - d_{z2} / z_2) = \mathbf{0.00040}$$

Force in layer 2;
kN

$$F_{z22} = 2 \times A_{bar} \times \min(f_{yd}, E_s \times \varepsilon_{z22}) = \mathbf{32.18}$$

Moment of resistance of layer 2;

$$M_{Rdz22} = F_{z22} \times (h / 2 - d_{z2}) = \mathbf{0.0 \text{ kNm}}$$

Strain in layer 3;

$$\varepsilon_{z32} = \varepsilon_{cu3} \times (1 - d_{z3} / z_2) = \mathbf{0.00276}$$

Force in layer 3;
324.4 kN

$$F_{z32} = (2 A_{bar1} + A_{bar2}) \times \min(f_{yd}, E_s \times \varepsilon_{z32}) =$$

Moment of resistance of layer 3;

$$M_{Rdz32} = F_{z32} \times (h / 2 - d_{z3}) = \mathbf{49.3 \text{ kNm}}$$

Combined axial load and moment resistance

Axial load capacity;

$$N_{Rdz2} = \mathbf{1056.89 \text{ kN}}$$

Moment of resistance about z axis;

$$M_{Rdz2} = \mathbf{211.22 \text{ kNm}}$$

Moment capacity with zero axial load (about z axis)

Moment of resistance of concrete

By iteration:-

Position of neutral axis;

$$z_3 = \mathbf{78.5 \text{ mm}}$$

Concrete compression force(3.1.7(3));
kN

$$F_{zc3} = \eta \times f_{cd} \times \min(\lambda_{sb} \times z_3, h) \times b = \mathbf{356.7}$$

Moment of resistance;
= 60.1 kNm

$$M_{Rdzc3} = F_{zc3} \times [h / 2 - (\min(\lambda_{sb} \times z_3, h)) / 2]$$

Moment of resistance of reinforcement

Strain in layer 1;

$$\varepsilon_{z13} = \varepsilon_{cu3} \times (1 - d_{z1} / z_3) = \mathbf{-0.01219}$$

Stress in layer 1;

$$\sigma_{z13} = \text{if}(\varepsilon_{z13} < 0, \max(-1 \times f_{yd}, E_s \times \varepsilon_{z13}),$$

$$\min(f_{yd}, E_s \times \varepsilon_{z13})) = \mathbf{-391.3 \text{ N/mm}^2}$$

Force in layer 1;

$$F_{z13} = (2 A_{bar1} + A_{bar2}) \times \sigma_{z13} = \mathbf{-324.43 \text{ kN}}$$

Moment of resistance of layer 1;

$$M_{Rdz13} = F_{z13} \times (h / 2 - d_{z1}) = \mathbf{49.3 \text{ kNm}}$$

Strain in layer 2;

$$\varepsilon_{z23} = \varepsilon_{cu3} \times (1 - d_{z2} / z_3) = \mathbf{-0.00542}$$

Stress in layer 2;

$$\sigma_{z23} = \text{if}(\varepsilon_{z23} < 0, \max(-1 \times f_{yd}, E_s \times \varepsilon_{z23}),$$

$$\min(f_{yd}, E_s \times \varepsilon_{z23})) = \mathbf{-391.3 \text{ N/mm}^2}$$

Force in layer 2;

$$F_{z23} = 2 \times A_{bar2} \times \sigma_{z23} = \mathbf{-157.4 \text{ kN}}$$

Moment of resistance of layer 2;

$$M_{Rdz23} = F_{z23} \times (h / 2 - d_{z2}) = \mathbf{0.0 \text{ kNm}}$$

Strain in layer 3;

$$\varepsilon_{z33} = \varepsilon_{cu3} \times (1 - d_{z3} / z_3) = \mathbf{0.00136}$$

Stress in layer 3;

$$\sigma_{z33} = \text{if}(\varepsilon_{z33} < 0, \max(-1 \times f_{yd}, E_s \times \varepsilon_{z33}),$$

$$\min(f_{yd}, E_s \times \varepsilon_{z33})) = \mathbf{272.0 \text{ N/mm}^2}$$

Force in layer 3; $F_{z33} = (2 A_{\text{bar1}} + A_{\text{bar2}}) \times \sigma_{z33} = \mathbf{225.5 \text{ kN}}$
 Moment of resistance of layer 3; $M_{\text{Rdz33}} = F_{z33} \times (h / 2 - d_{z3}) = \mathbf{34.3 \text{ kNm}}$
 Resultant concrete/steel force; $F_{z3} = 100.4 \text{ kN}$

PASS - This is approximately equal to zero (< 0.1% of N_{Rd0})

Combined moment of resistance

Moment of resistance about z axis; $M_{\text{Rdz3}} = \mathbf{143.7 \text{ kNm}}$

Axial and bending capacity with NA depth 1.25 times that for zero strain in tension face reinf (bending about z axis)

Moment of resistance of concrete

Depth to neutral axis; $z_4 = 1.25 \times d_{z1} = \mathbf{440.0 \text{ mm}}$
 Concrete compression force(3.1.7(3)); $F_{z\text{c}4} = (\eta \times f_{\text{cd}}) \times \min(h, (\lambda_{\text{sb}} \times z_4)) \times b = \mathbf{1999.36 \text{ kN}}$
 Concrete moment of resistance; $M_{z\text{c}4} = F_{z\text{c}4} \times (h / 2 - \min(h, (\lambda_{\text{sb}} \times z_4)) / 2) = \mathbf{48 \text{ kNm}}$

Moment of resistance of reinforcement

Strain in layer 1; $\epsilon_{z14} = \epsilon_{\text{c}3} \times z_4 \times (1 - d_{z1} / z_4) / (z_4 - h/2) = \mathbf{0.00064}$
 Force in layer 1; $F_{z14} = (2 A_{\text{bar1}} + A_{\text{bar2}}) \times \min(f_{\text{yd}}, E_s \times \epsilon_{z14}) = \mathbf{106.46 \text{ kN}}$
 Moment of resistance of layer 1; $M_{\text{Rdz14}} = F_{z14} \times (h / 2 - d_{z1}) = \mathbf{-16.2 \text{ kNm}}$
 Strain in layer 2; $\epsilon_{z24} = \epsilon_{\text{c}3} \times z_4 \times (1 - d_{z2} / z_4) / (z_4 - h/2) = \mathbf{0.00175}$
 Force in layer 2; $F_{z24} = 2 \times A_{\text{bar}} \times \min(f_{\text{yd}}, E_s \times \epsilon_{z24}) = \mathbf{140.77 \text{ kN}}$
 Moment of resistance of layer 2; $M_{\text{Rdz24}} = F_{z24} \times (h / 2 - d_{z2}) = \mathbf{0.0 \text{ kNm}}$
 Strain in layer 3; $\epsilon_{z34} = \epsilon_{\text{c}3} \times z_4 \times (1 - d_{z3} / z_4) / (z_4 - h/2) = \mathbf{0.00286}$
 Force in layer 3; $F_{z34} = N_z \times A_{\text{bar}} \times \min(f_{\text{yd}}, E_s \times \epsilon_{z34}) = \mathbf{324.4 \text{ kN}}$
 Moment of resistance of layer 3; $M_{\text{Rdz34}} = F_{z34} \times (h / 2 - d_{z3}) = \mathbf{49.3 \text{ kNm}}$

Combined axial load and moment resistance

Axial load capacity; $N_{\text{Rdz4}} = \mathbf{2570.99 \text{ kN}}$
 Moment of resistance about z axis; $M_{\text{Rdz4}} = \mathbf{81.1 \text{ kNm}}$

Axial load and bending capacities for bending about y axis

The column is square and is doubly symmetrically reinforced, therefore the interaction diagram for bending about the y axis will be the same as that about the z axis.

Zero strain in tension face reinf; $N_{\text{Rdy1}} = N_{\text{Rdz1}} = \mathbf{2045.37 \text{ kN}}$
 $M_{\text{Rdy1}} = M_{\text{Rdz1}} = \mathbf{144 \text{ kNm}}$
 Concrete and tension steel simultaneously at yield; $N_{\text{Rdz2}} = \mathbf{1056.89 \text{ kN}}$ $N_{\text{Rdy2}} =$
 $M_{\text{Rdy2}} = M_{\text{Rdz2}} = \mathbf{211.22 \text{ kNm}}$
 Zero axial load; $M_{\text{Rdy3}} = M_{\text{Rdz3}} = \mathbf{143.7 \text{ kNm}}$

NA depth 1.25x that for no strain in tension reinf.;

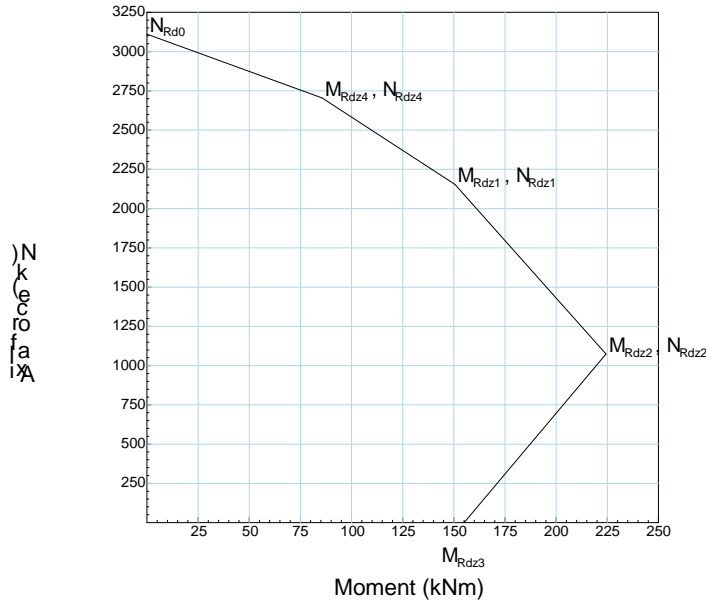
$$N_{Rdz4} = \mathbf{2570.99 \text{ kN}}$$

$N_{Rdy4} =$

$$M_{Rdy4} = M_{Rdz4} = \mathbf{81.1 \text{ kNm}}$$

Interaction diagram for bending about z axis

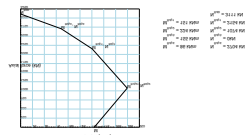
400 mm x 400 mm column, 4 no. 20 mm longitudinal bars and 4 no. 16 mm longitudinal bars



$N_{Rd0} = 2964.04 \text{ kN}$
 $M_{Rdz1} = 144 \text{ kNm}$ $N_{Rdz1} = 2045.37 \text{ kN}$
 $M_{Rdz2} = 211.22 \text{ kNm}$ $N_{Rdz2} = 1056.89 \text{ kN}$
 $M_{Rdz3} = 143.7 \text{ kNm}$ $N_{Rdz3} = 100.4 \text{ kN}$
 $M_{Rdz4} = 81.1 \text{ kNm}$ $N_{Rdz4} = 2570.99 \text{ kN}$

Interaction diagram for bending about y axis

400 mm x 400 mm column, 4 no. 20 mm longitudinal bars and 4 no. 16 mm longitudinal bars



Appendix B: The Calculation of Confined Concrete

For unconfined concrete substituting, $f'_l=0$ and $\varepsilon_{co}=0.002$ for composite, and reinforced concrete columns.

Plain Concrete (Unconfined Concrete)					
$h =$	400	mm	area of core of section	85264	mm ²
$b =$			$f'_o =$	25	MPa
the reinforcement	4 ϕ 20 and 4 ϕ 16		$\varepsilon_{co} =$	0.002	
the link is	ϕ 8		$E_c =$	25000	MPa
$S =$	100	mm			
$dc = bc =$	340	mm			
$s' =$	92	mm			
$f_{yh} =$	450	MPa			

$$\rho_x = \rho_y = \frac{A_{sx}}{Sd_c} \quad \text{or} \quad \frac{A_{sy}}{Sb_c}$$

$$A_{sx} = A_{sy} = 2 \left(\frac{\pi 20^2}{4} \right) + \left(\frac{\pi 16^2}{4} \right) \quad 829.3805 \text{ mm}^2$$

$$\rho_x = \rho_y = \quad 0.024394$$

$$f_{Ly} = f_{Lx} = \rho_x f_{yh} \quad \text{or} \quad \rho_y f_{yh} \quad 10.97709$$

$$A_i = \sum_{i=1}^n \frac{(w_i)^2}{6} \quad 25392$$

$$K_e = \frac{\left(1 - \sum_{i=1}^n \frac{(w_i)^2}{6b_c d_c} \right) \left(1 - \frac{S'}{2b_c} \right) \left(1 - \frac{S'}{2d_c} \right)}{1 - \rho_{cc}} \quad 0.589209$$

ρ_{cc} = ratio of area of longitudinal reinforcement to area of core of section

$$\rho_{cc} = 0.009727$$

$$f'_L = f_L K_e \quad 0 \text{ MPa}$$

$$f'_{cc} = f'_{co} \left(-1.254 + 2.254 \sqrt{1 + \frac{7.94 f'_L}{f'_{co}}} - 2 \frac{f'_L}{f'_{co}} \right) \quad 25$$

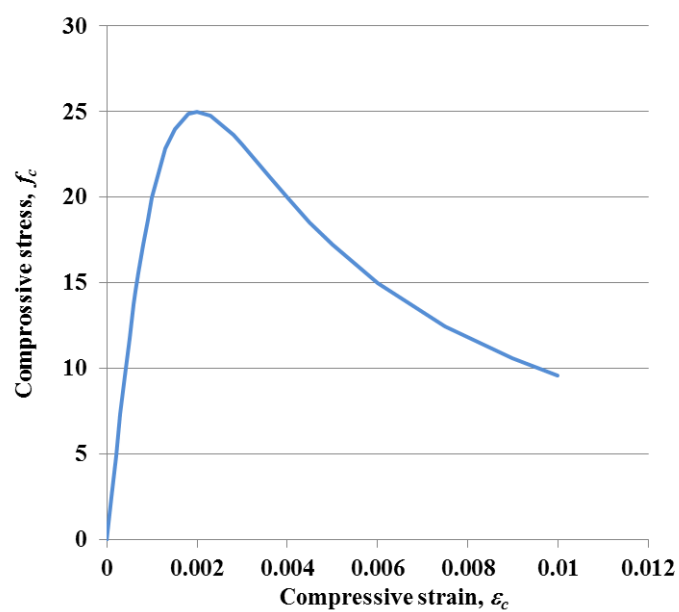
$$\epsilon_{cc} = \epsilon_{co} \left[1 + 5 \left(\frac{f'_{cc}}{f'_{co}} - 1 \right) \right] \quad 0.002$$

$$E_{sec} = \frac{f'_{cc}}{\epsilon_{cc}} \quad 12500$$

$$r = \frac{E_c}{E_c - E_{sec}} \quad 2$$

$$\chi = \frac{\epsilon_c}{\epsilon_{cc}}$$

$$f_c = \frac{f'_{cc} \chi r}{r - 1 + \chi^r}$$



- **Composite Column**

condined for composite column

partially confined concrete

h =	310	mm	$A_s =$	314.15	mm ²
b =	310	mm	area of core of section	48400	mm ²
the reinforcement	4Ø10		$f'_\omega =$	25	MPa
the link is	Ø8		$\epsilon_{co} =$	0.002	
S =	100	mm	$E_c =$	25000	MPa
dc = bc =	258	mm			
s' =	92	mm			
$f_{yh} =$	450	MPa			

$$A_{sx} = A_{sy} = 2 \left(\frac{\pi 10^2}{4} \right) \quad 157.08 \text{ mm}^2$$

$$\rho_x = \rho_y = \frac{A_{sx}}{Sd_c} \quad \text{or} \quad \frac{A_{sy}}{Sb_c} \quad 0.0061$$

$$f_{Ly} = f_{Lx} = \rho_x f_{yh} \quad \text{or} \quad \rho_y f_{yh} \quad 2.7397$$

$$A_i = \sum_{i=1}^n \frac{(w_i)^2}{6} \quad 32267$$

$$K_e = \frac{\left(1 - \sum_{i=1}^n \frac{(w_i)^2}{6b_c d_c} \right) \left(1 - \frac{S'}{2b_c} \right) \left(1 - \frac{S'}{2d_c} \right)}{1 - \rho_{cc}} \quad 0.3502$$

pcc = ratio of area of longitudinal reinforcement to area of core of section

$$\rho_{cc} = 0.0065$$

$$f'_L = f_L K_e = 0.9594 \text{ MPa}$$

$$f'_{cc} = f'_{co} \left(-1.254 + 2.254 \sqrt{1 + \frac{7.94 f'_L}{f'_{co}}} - 2 \frac{f'_L}{f'_{co}} \right) = 31.096$$

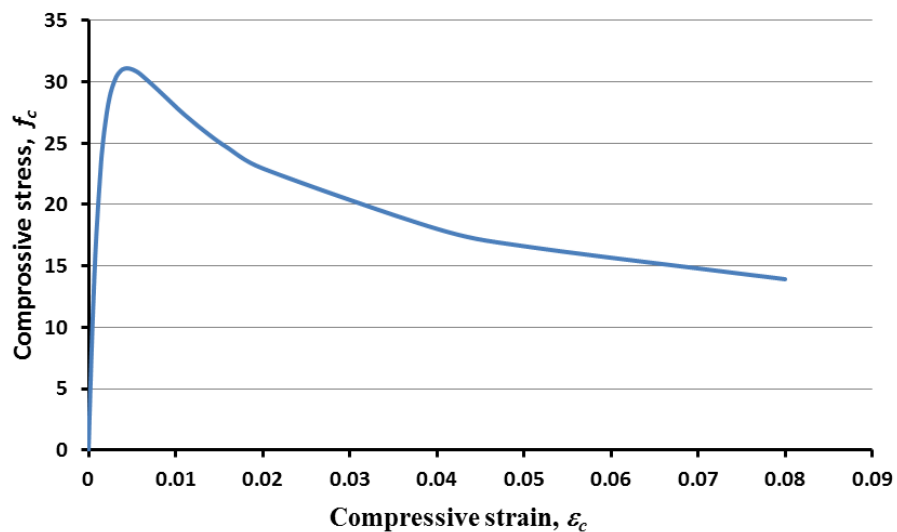
$$\epsilon_{cc} = \epsilon_{co} \left[1 + 5 \left(\frac{f'_{cc}}{f'_{co}} - 1 \right) \right] = 0.0044$$

$$E_{\text{sec}} = \frac{f'_{cc}}{\epsilon_{cc}} = 7006.1$$

$$r = \frac{E_c}{E_c - E_{\text{sec}}} = 1.3894$$

$$\chi = \frac{\epsilon_c}{\epsilon_{cc}}$$

$$f_c = \frac{f'_{cc} \chi^r}{r - 1 + \chi^r}$$



Highly confined concrete

$$f_{Ly} = f_{Lx} = \rho_x f_{yh} \quad \text{or} \quad \rho_y f_{yh} \quad 2.73968$$

$$\text{Area of parabola's (Ae)} = 9633.333$$

$$K_e = \frac{\left(1 - \sum_{i=1}^n \frac{(w_i)^2}{6 \times 170^2}\right) \left(1 - \frac{S'}{2 \times 170}\right) \left(1 - \frac{S'}{2 \times 170}\right) + \left(1 - \sum_{i=1}^n \frac{(w_i)^2}{6 \times 170^2}\right)}{1 - \rho_{cc}} \quad 1.258221$$

$$\rho_{cc} = 0.18825$$

$$f'_L = f_L K_e \quad 3.447124$$

$$f'_{cc} = f'_{co} \left(-1.254 + 2.254 \sqrt{1 + \frac{7.94 f'_L}{f'_{co}}} - 2 \frac{f'_L}{f'_{co}} \right) \quad 43.31362$$

$$\varepsilon_{cc} = \varepsilon_{co} \left[1 + 5 \left(\frac{f'_{cc}}{f'_{co}} - 1 \right) \right] \quad 0.009325$$

$$E_{\text{sec}} = \frac{f'_{cc}}{\varepsilon_{cc}} \quad 4644.669$$

$$r = \frac{E_c}{E_c - E_{\text{sec}}} \quad 1.228179$$

$$\chi = \frac{\varepsilon_c}{\varepsilon_{cc}}$$

$$f_c = \frac{f'_{cc} \chi^r}{r - 1 + \chi^r}$$

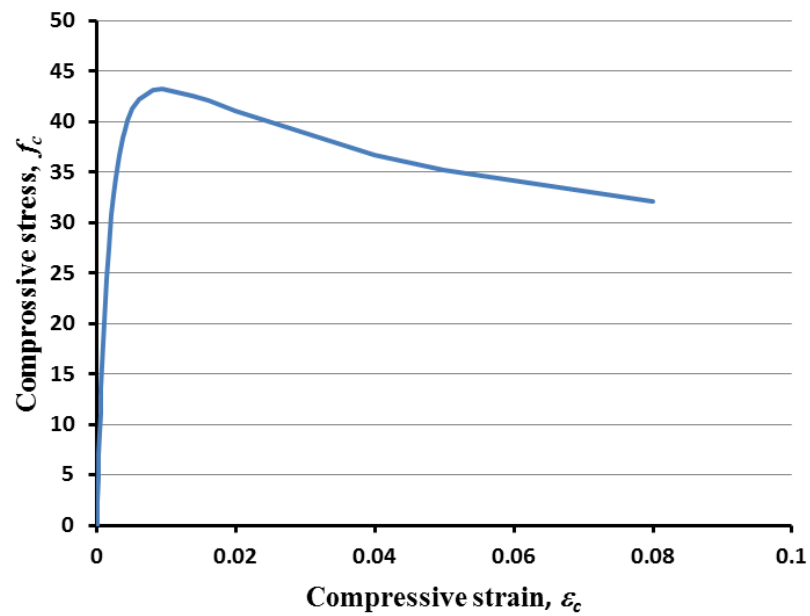
$$\varepsilon_{cc} = \varepsilon_{co} \left[1 + 5 \left(\frac{f'_{cc}}{f'_{co}} - 1 \right) \right] \quad 0.0093$$

$$E_{sec} = \frac{f'_{\alpha}}{\varepsilon_{\alpha}} \quad 4644.7$$

$$r = \frac{E_c}{E_c - E_{sec}} \quad 1.2282$$

$$\chi = \frac{\varepsilon_c}{\varepsilon_{\alpha}}$$

$$f_c = \frac{f'_{\alpha} \chi^r}{r - 1 + \chi^r}$$



• **Reinforced Concrete Column**

h =	400	mm	As =	2060.824	mm ²
b =	400	mm	area of core of section	85264	mm ²
the reinforcement	4Ø20 and 4Ø16		$f_{\omega}' =$	25	MPa
the link is	Ø8				
S =	100	mm	ε _{co} =	0.002	
dc = bc =	340	mm	E _c =	25000	MPa
s' =	92	mm			
f _{yh} =	450	MPa			

$$\rho_x = \rho_y = \frac{A_{sx}}{Sd_c} \text{ or } \frac{A_{sy}}{Sb_c}$$

$$A_{sx} = A_{sy} = 2 \left(\frac{\pi 20^2}{4} \right) + \left(\frac{\pi 16^2}{4} \right) \quad 829.3805 \text{ mm}^2$$

$$\rho_x = \rho_y = \quad 0.024394$$

$$f_{Ly} = f_{Lx} = \rho_x f_{yh} \text{ or } \rho_y f_{yh} \quad 10.97709$$

$$A_i = \sum_{i=1}^n \frac{(w_i)^2}{6} \quad 25392$$

$$K_e = \frac{\left(1 - \sum_{i=1}^n \frac{(w_i)^2}{6b_c d_c} \right) \left(1 - \frac{S'}{2b_c} \right) \left(1 - \frac{S'}{2d_c} \right)}{1 - \rho_{cc}} \quad 0.597929$$

pcc = ratio of area of longitudinal reinforcement to area of core of section

$$pcc = 0.02417$$

$$f'_L = f_L K_e \quad 6.563527 \text{ MPa}$$

$$f'_{cc} = f'_{co} \left(-1.254 + 2.254 \sqrt{1 + \frac{7.94 f'_L}{f'_{co}}} - 2 \frac{f'_L}{f'_{co}} \right) \quad 54.49023$$

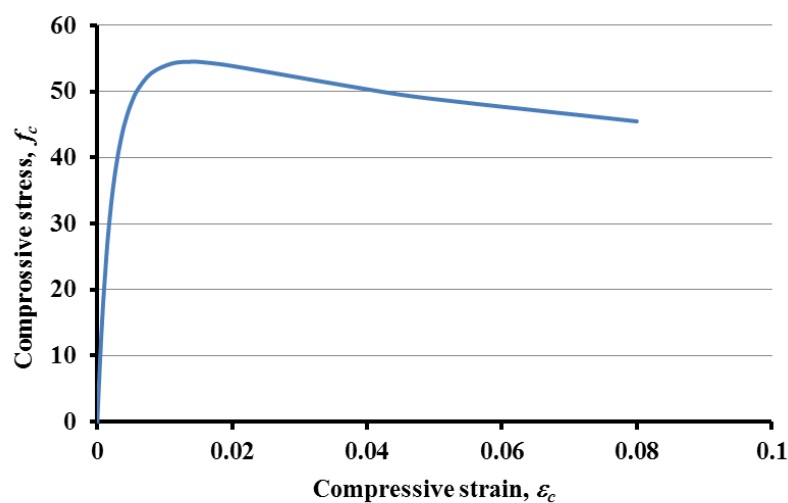
$$\epsilon_{cc} = \epsilon_{co} \left[1 + 5 \left(\frac{f'_{cc}}{f'_{co}} - 1 \right) \right] \quad 0.013796$$

$$E_{sec} = \frac{f'_{cc}}{\epsilon_{cc}} \quad 3949.686$$

$$r = \frac{E_c}{E_c - E_{sec}} \quad 1.187631$$

$$\chi = \frac{\epsilon_c}{\epsilon_{cc}}$$

$$f_c = \frac{f'_{cc} \chi^r}{r - 1 + \chi^r}$$



Appendix C: PEEQ Contour Presentations, Ductility Calculations, and Stress Contour at Failure

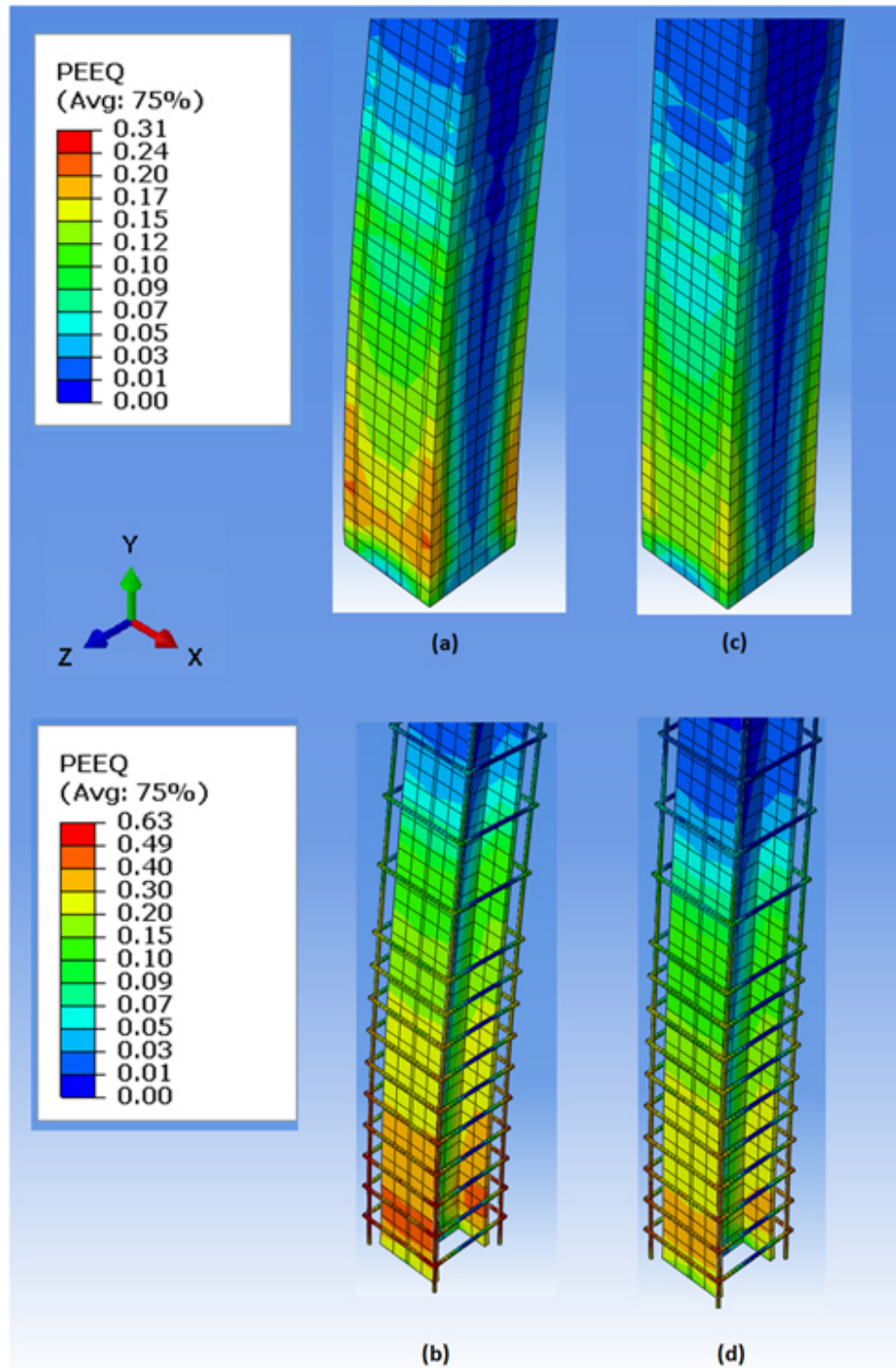


Figure C.1: PEEQ Contour at Maximum Force Level (a, and b) and at Maximum Displacement Level (c, and d) of CC-10P

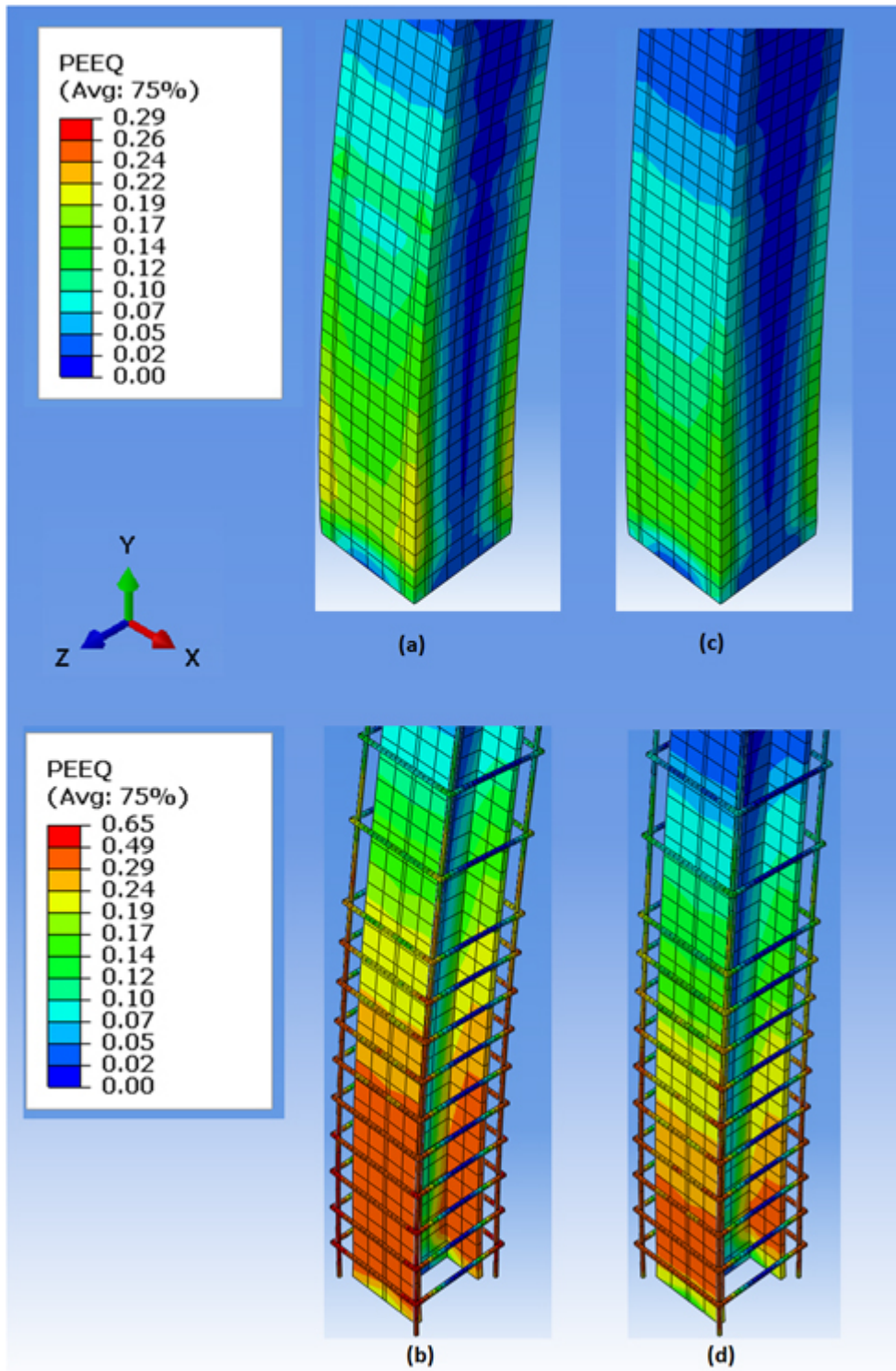


Figure C.2: Stress Contour at Maximum Force Level (a, and b) and at Maximum Displacement Level (c, and d) of CC-15P

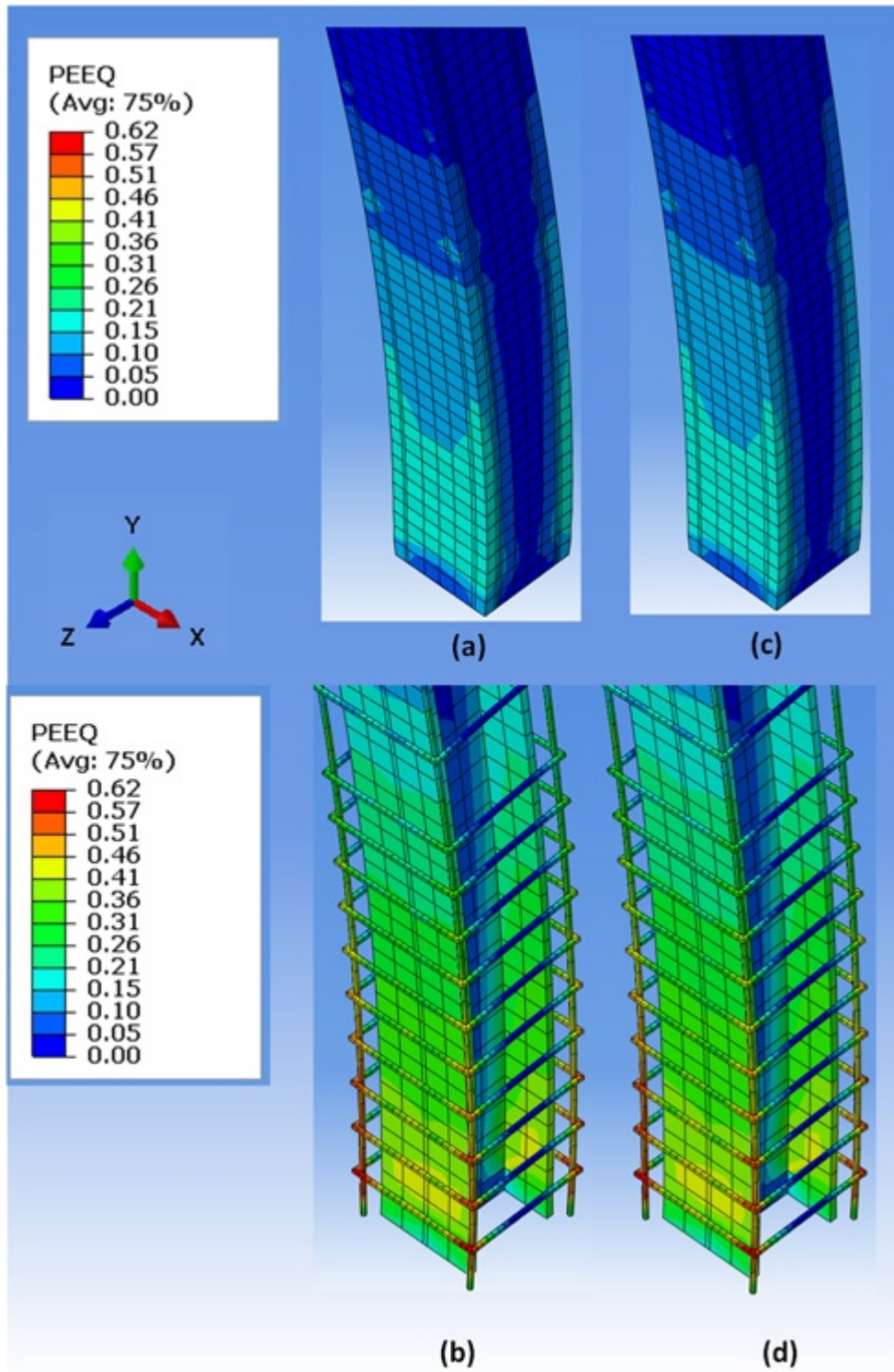


Figure C.3: Stress Contour at Maximum Force Level (a, and b) and at Maximum Displacement Level (c, and d) of CC-20P

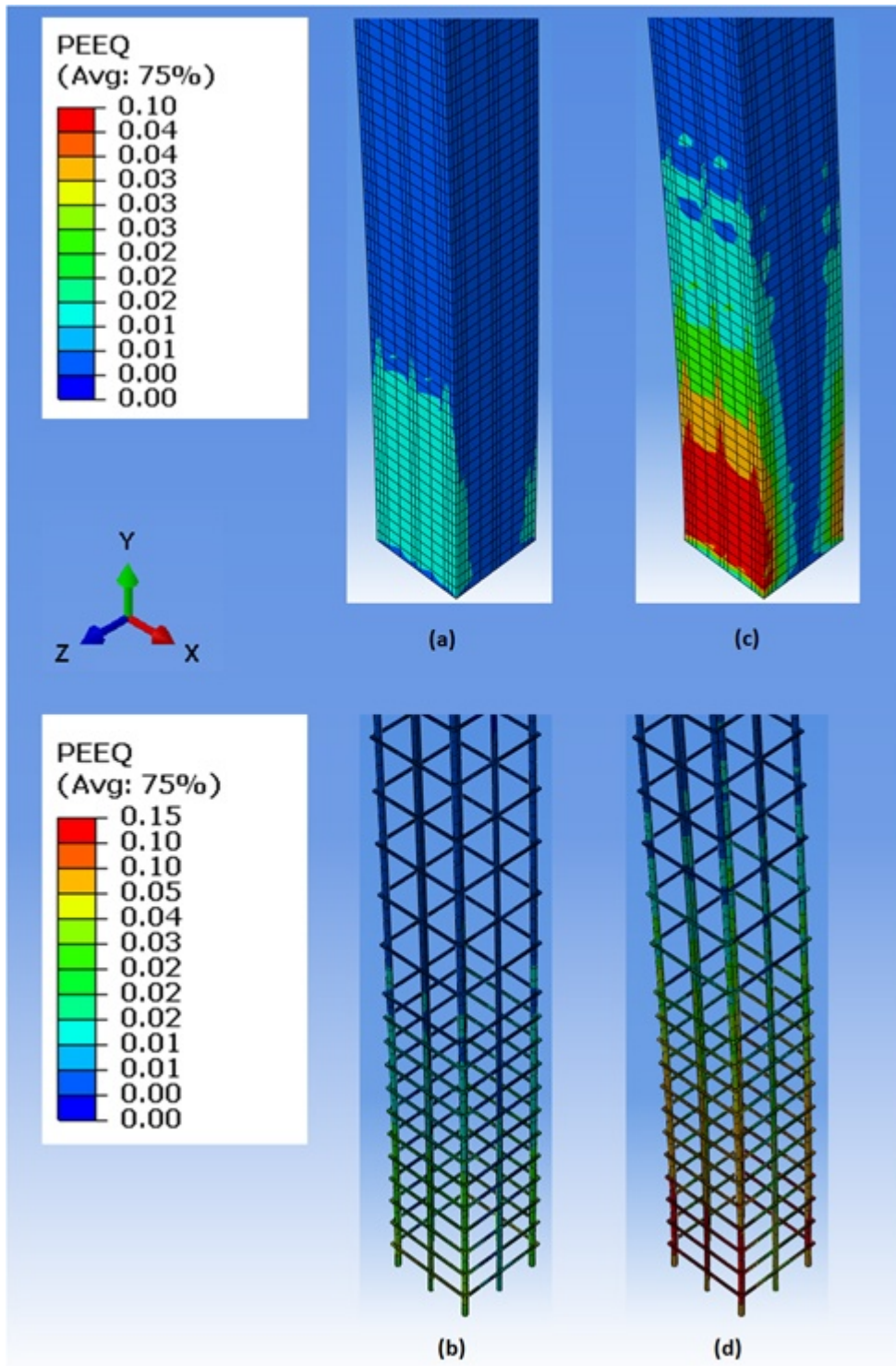


Figure C.4: Stress Contour at Maximum Force Level (a, and b) and at Maximum Displacement Level (c, and d) of RC-10P

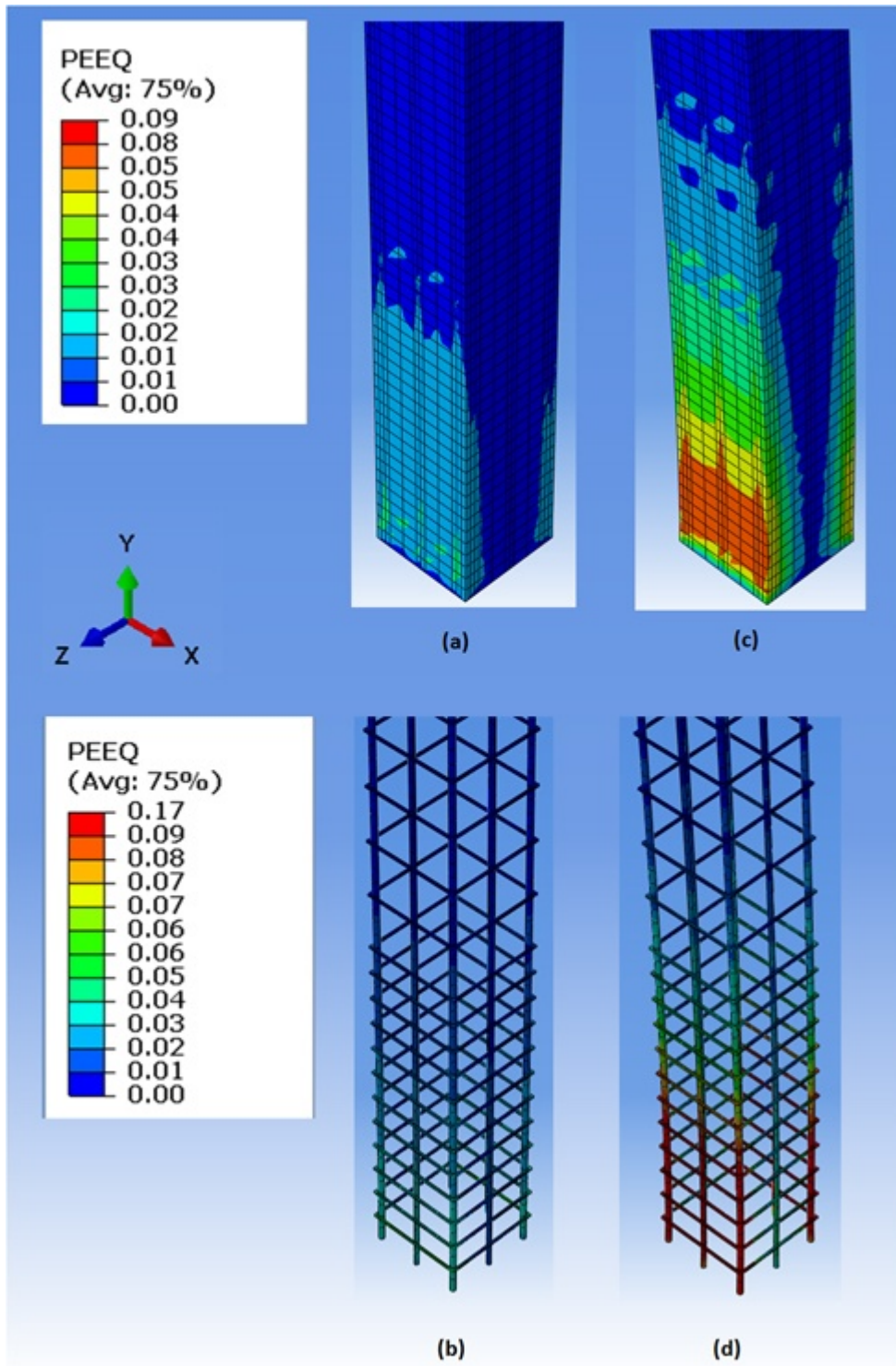


Figure C.5: Stress Contour at Maximum Force Level (a, and b) and at Maximum Displacement Level (c, and d) of RC-15P

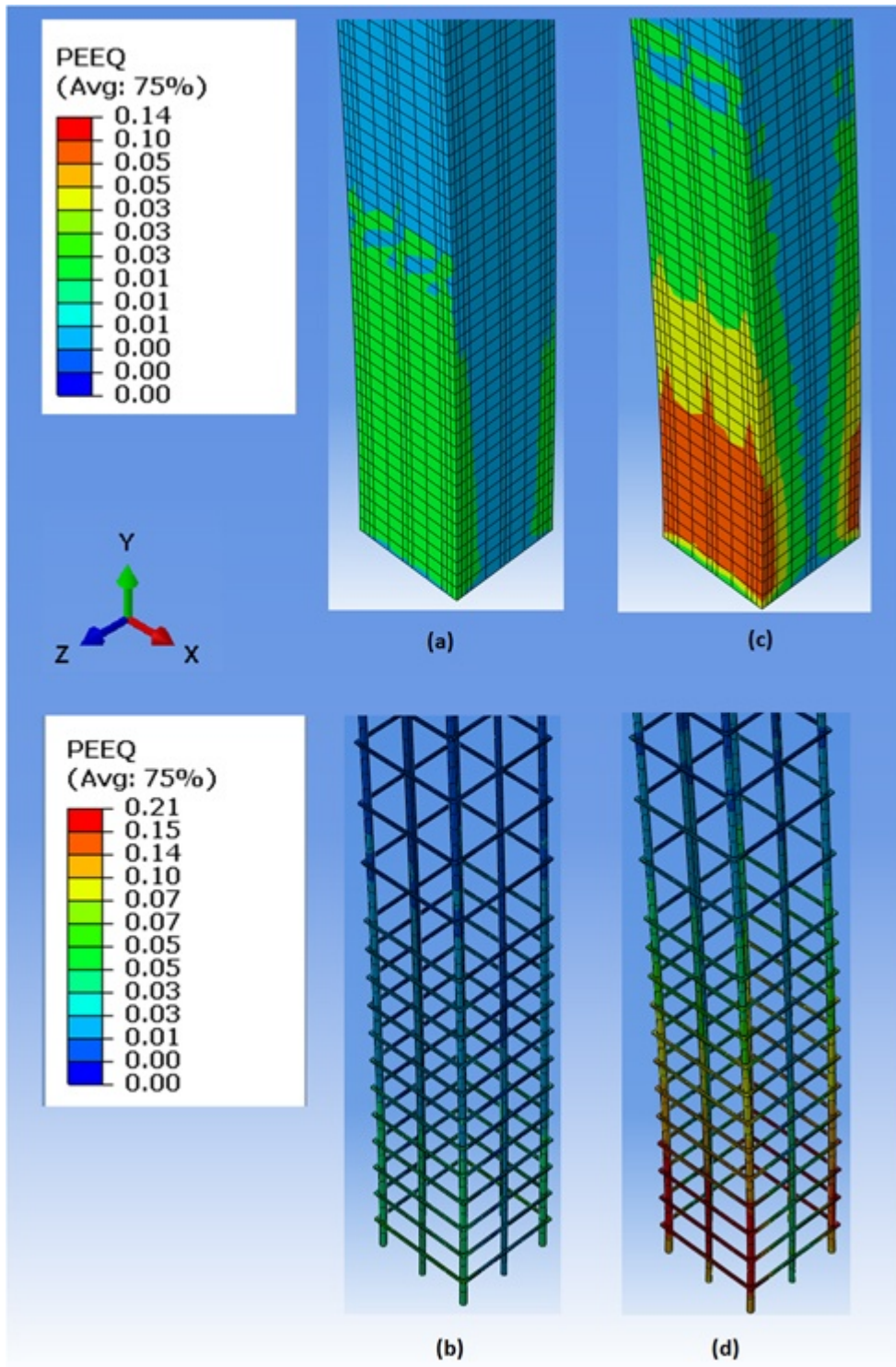


Figure C.6: Stress Contour at Maximum Force Level (a, and b) and at Maximum Displacement Level (c, and d) of RC-20P

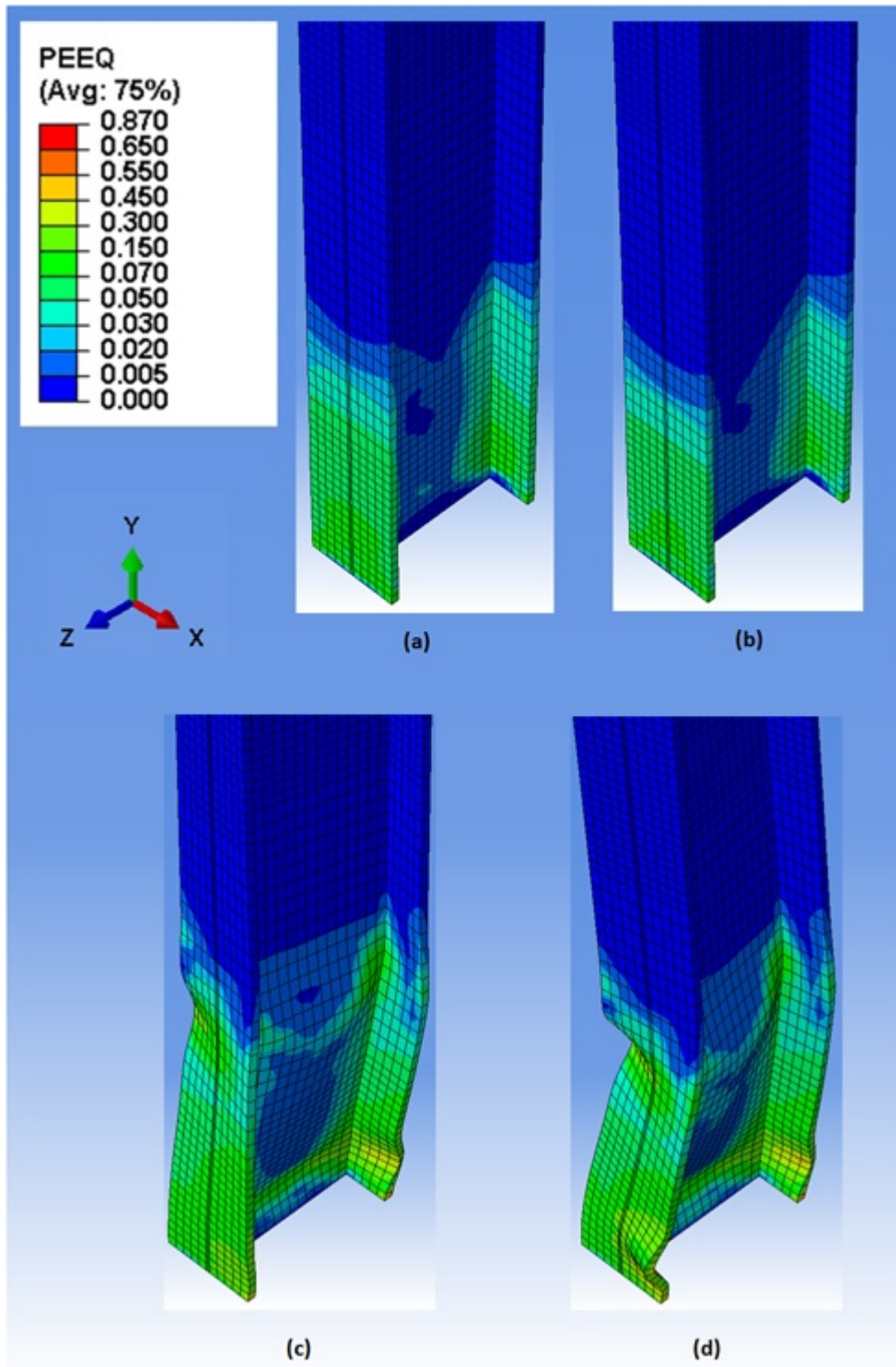


Figure C.7: Stress Contour at Maximum Force Level (a, and b) and at Maximum Displacement Level (c, and d) of SC-10P

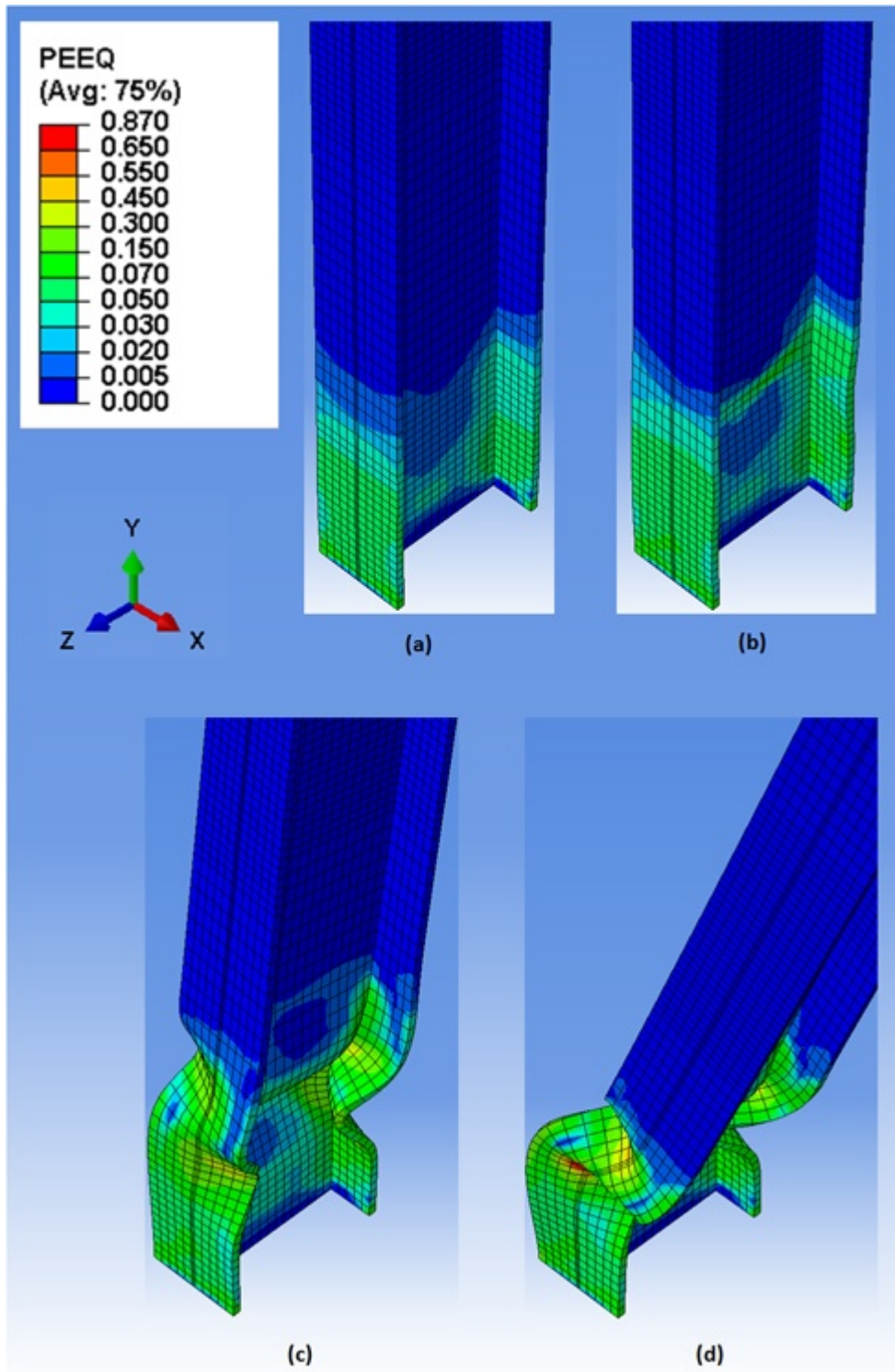


Figure C.8: Stress Contour at Maximum Force Level (a, and b) and at Maximum Displacement Level (c, and d) of SC-15P

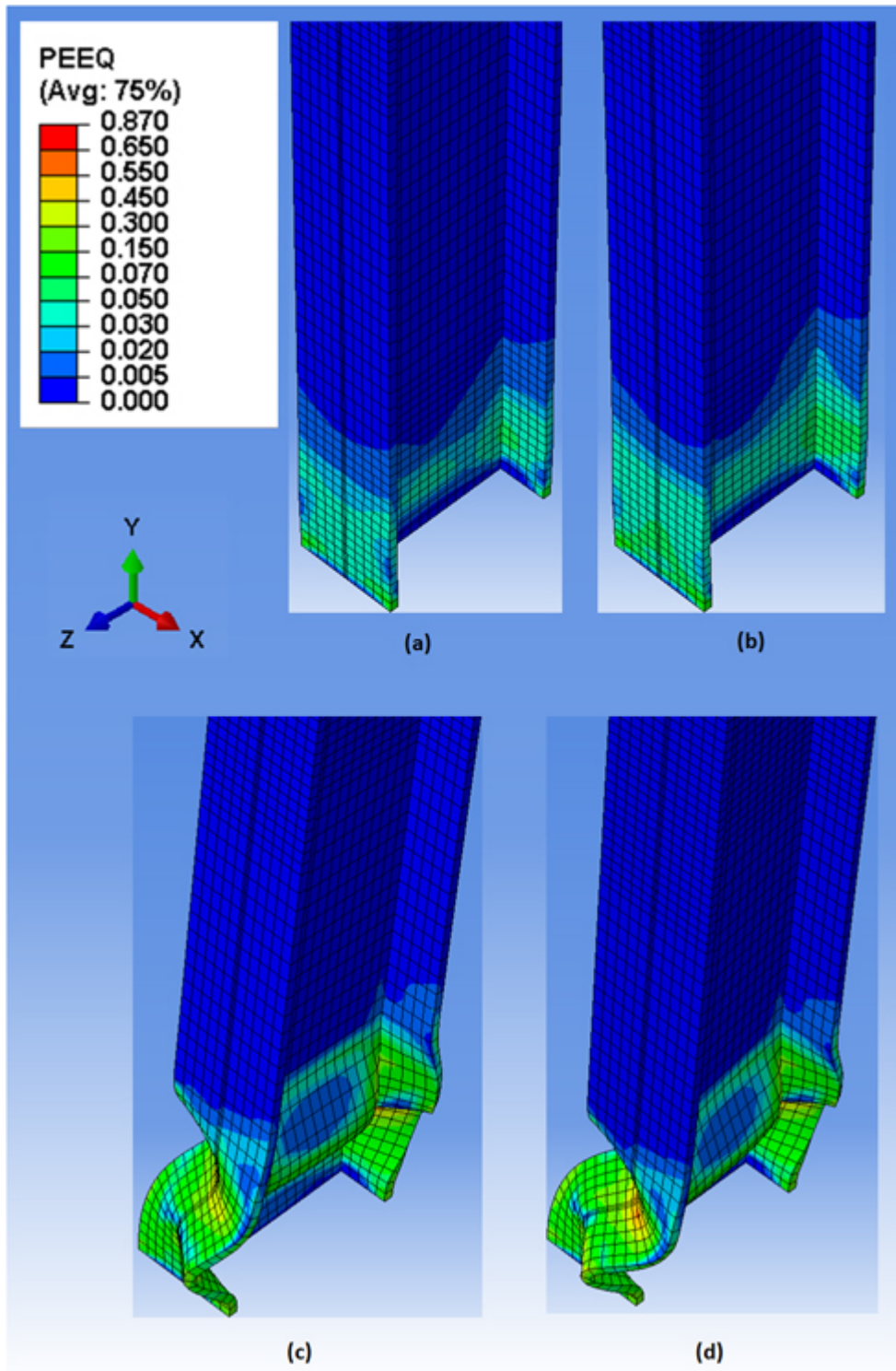


Figure C.9: Stress Contour at Maximum Force Level (a, and b) and at Maximum Displacement Level (c, and d) of CC-20P

Table C.1: The Curvature Ductilites Calculation

Specimen	$K_{0.6-s-c}$ N.mm ²	M_{uc1} kN.m	M_{uc2} kN.m	ϕ_{u1}	ϕ_{u2}	ϕ_{yc}	μ_{ϕ}
SC-10P	1E+11	1507.48 1518883786.52	1530.29	0.032 0.032	-0.032	0.015	2.1
SC-15P	1E+11	1491.79 1507082848.51	1522.37	0.035 0.033	-0.031	0.015	2.2
SC-20P	1E+11	1313.25 1342571780.34	-1371.9	0.024 0.023	-0.023	0.013	1.7
RC-10P	4E+10	653.86 642455127.98	-631.05	0.055 0.055	-0.055	0.016	3.4
RC-15P	4E+10	647.96 628345100.78	-608.73	0.069 0.069	-0.069	0.016	4.4
RC-20P	4E+10	619.42 607738885.49	596.053	0.074 0.066	-0.057	0.015	4.3
CC-10P	2E+10	374.51 373693835.27	372.874	0.197 0.194	-0.192	0.019	10.4
CC-15P	2E+10	339.33 328950511.15	318.567	0.195 0.195	-0.194	0.016	11.8
CC-20P	2E+10	326.46 319903880.38	313.344	0.156 0.148	-0.141	0.016	9.3

Table C.2: The Displacement Ductilites Calculation

Specimen	K_{sec-c} N/mm	H_{u1} kN	H_{u2} kN	Δ_{u-c1} mm	Δ_{u-c2} mm	Δ_{yc} mm	μ_{Δ}
SC-10P	9721.6	469.59 466306	463.022	200.31 200.01	199.71	47.966	4.2
SC-15P	9641.7	447.422 474120	500.818	124.60 123.85	123.10	49.174	2.5
SC-20P	9562	402.293 409171.5	-416.05	128.16 128.16	128.16	42.791	3.0
RC-10P	3289.9	199.613 201328.5	203.044	234.69 234.64	234.58	61.196	3.8
RC-15P	3284	200.43 203108	205.786	252.18 251.78	251.38	61.848	4.1
RC-20P	3258.7	199.548 204005.5	208.463	272.73 272.71	272.68	62.603	4.4
CC-10P	1418.6	115.502 118141.5	120.781	714.54 706.39	698.23	83.280	8.5
CC-15P	1401.9	119.757 121239.5	122.722	750.73 749.19	747.65	86.482	8.7
CC-20P	1343.8	118.811 117166.5	115.522	665.77 627.79	589.81	87.190	7.2

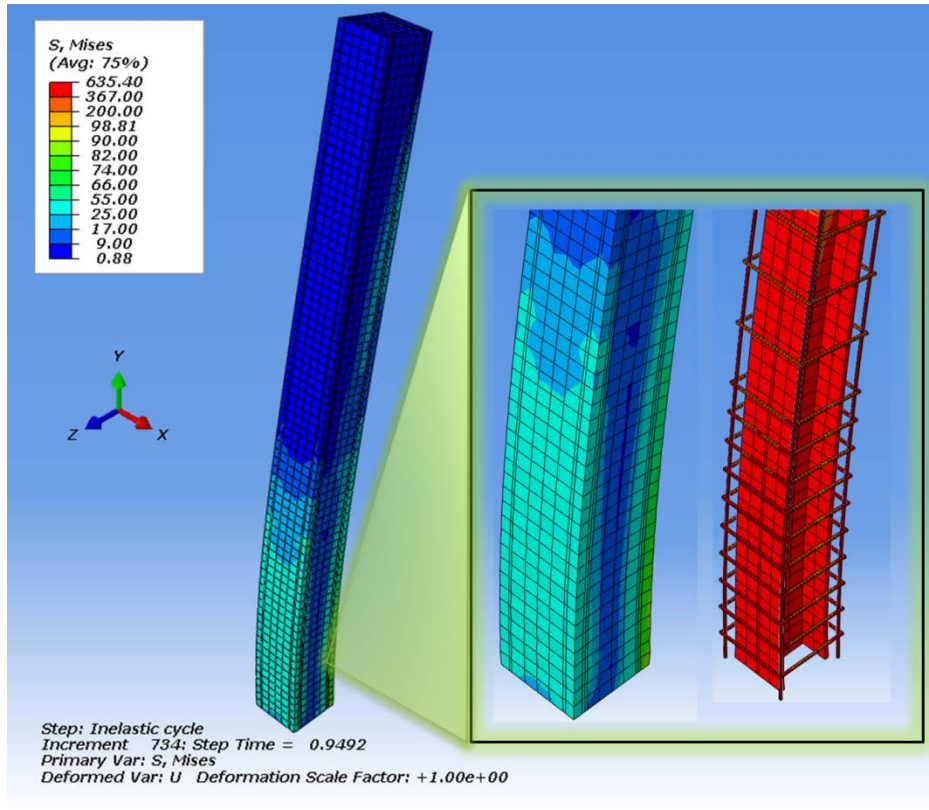


Figure C.10: Stress Contour at Fracture Stage for CC-10P

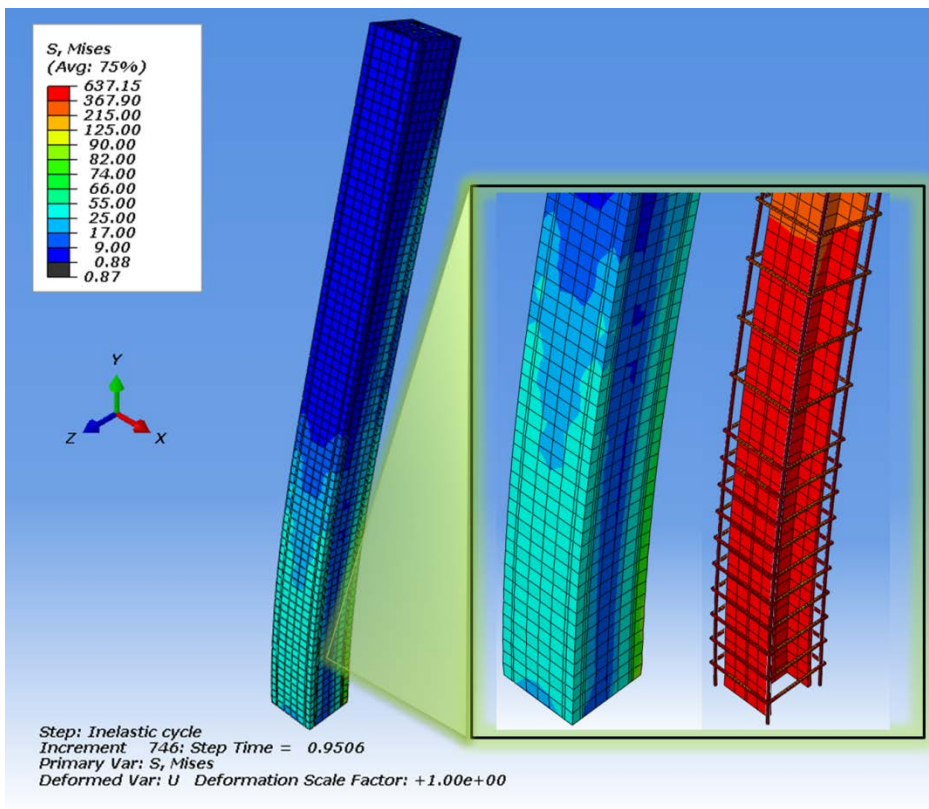


Figure C.11: Stress Contour at Fracture Stage for CC-15P

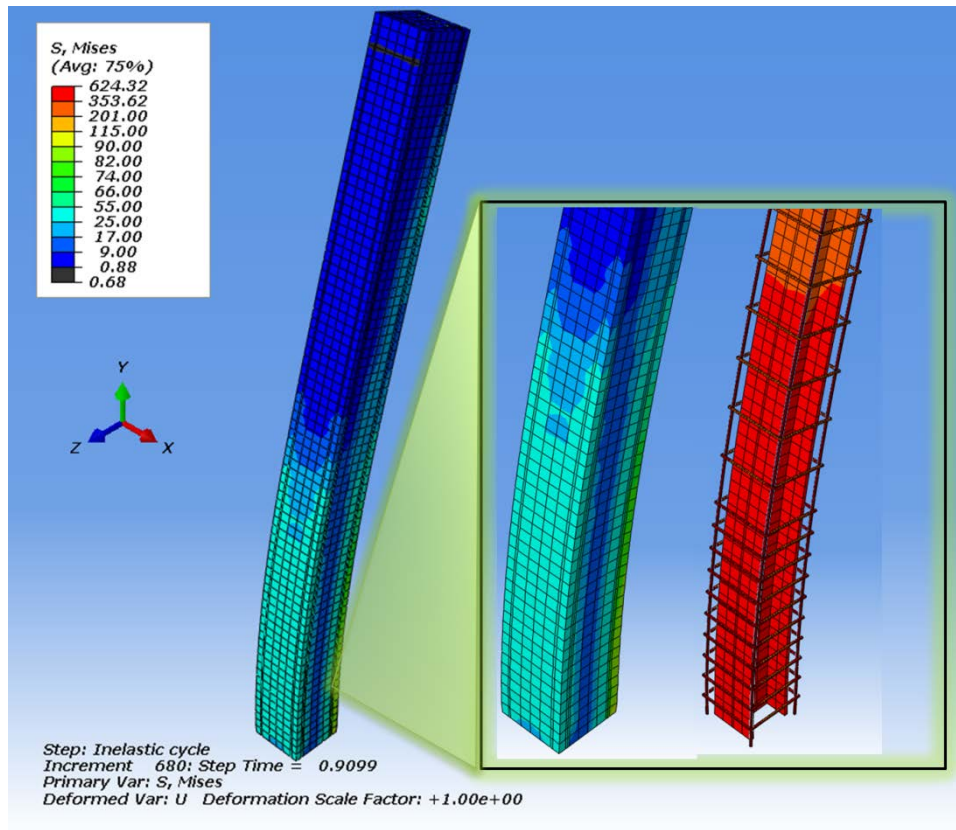


Figure C.12: Stress Contour at Fracture Stage for CC-20P

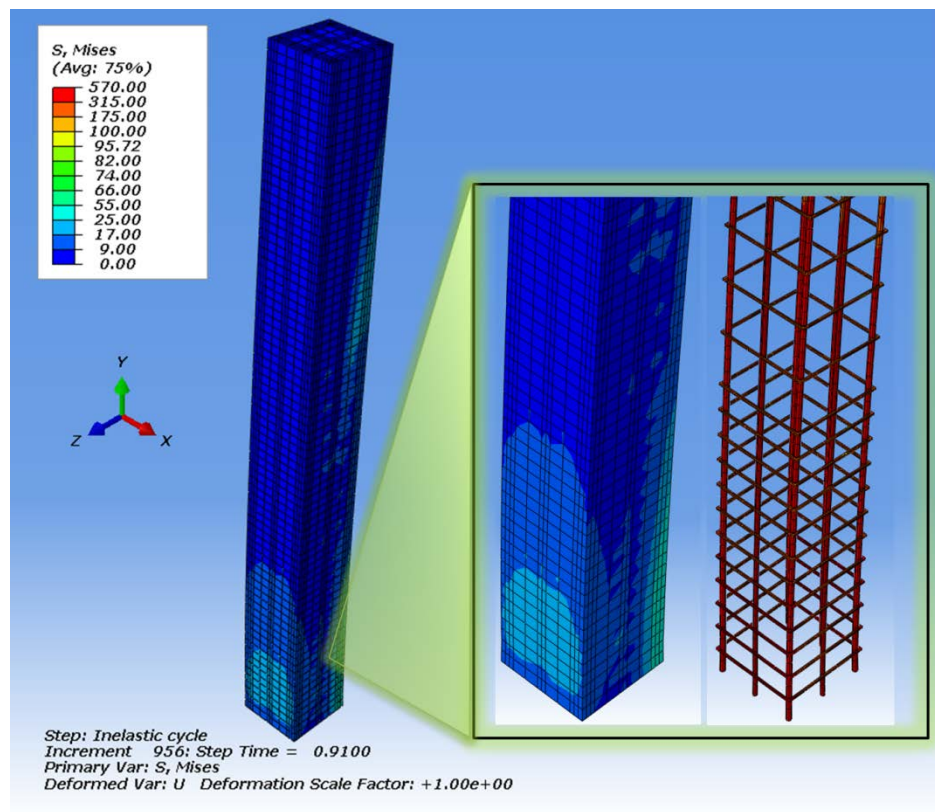


Figure C.13: Stress Contour at Fracture Stage for RC-10P

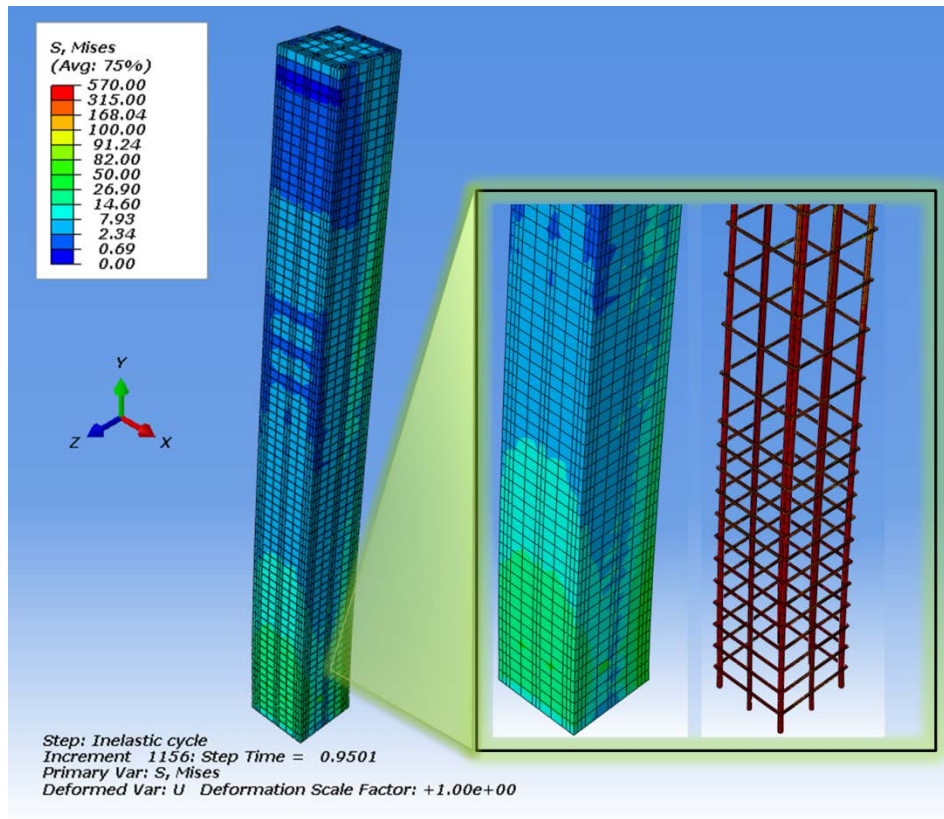


Figure C.14: Stress Contour at Fracture Stage for RC-15P

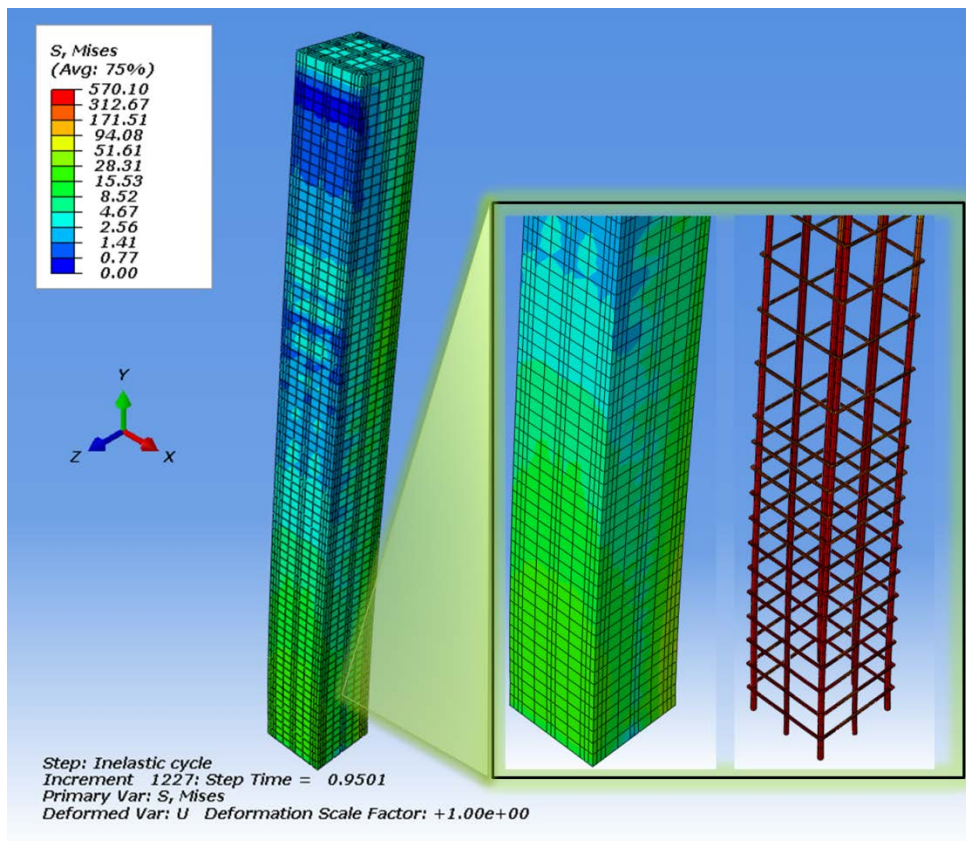


Figure C.15: Stress Contour at Fracture Stage for RC-20P

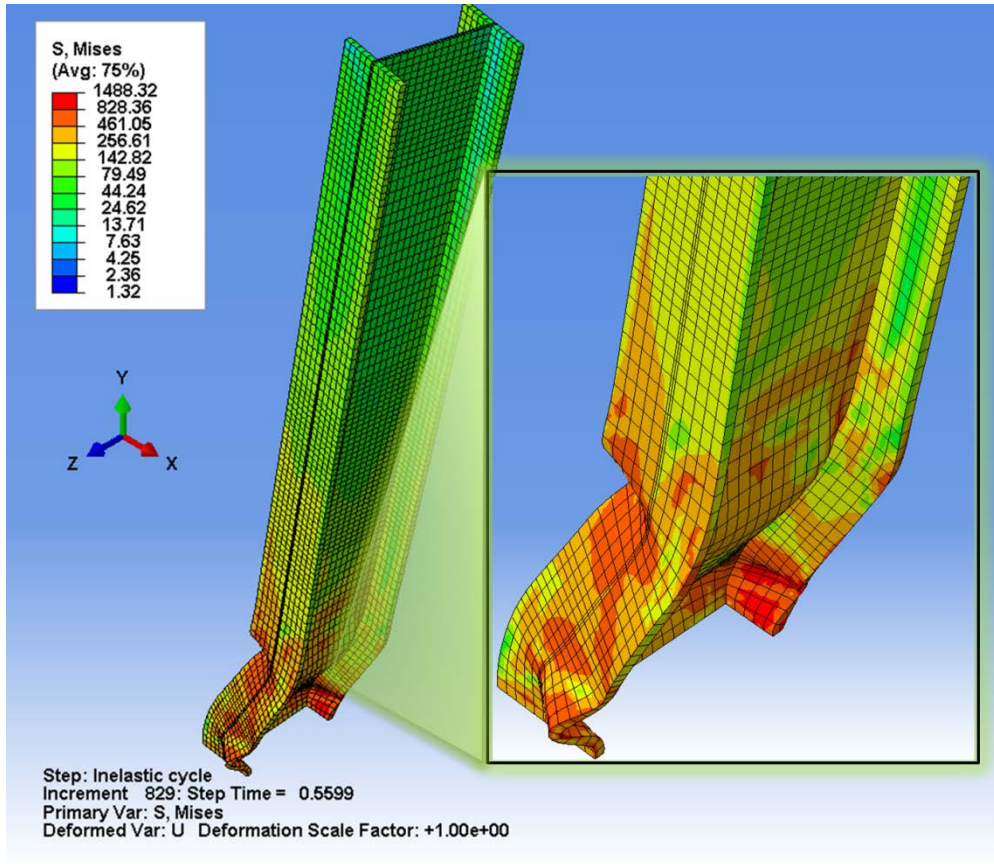


Figure C.16: Stress Contour at Fracture Stage for SC-10P

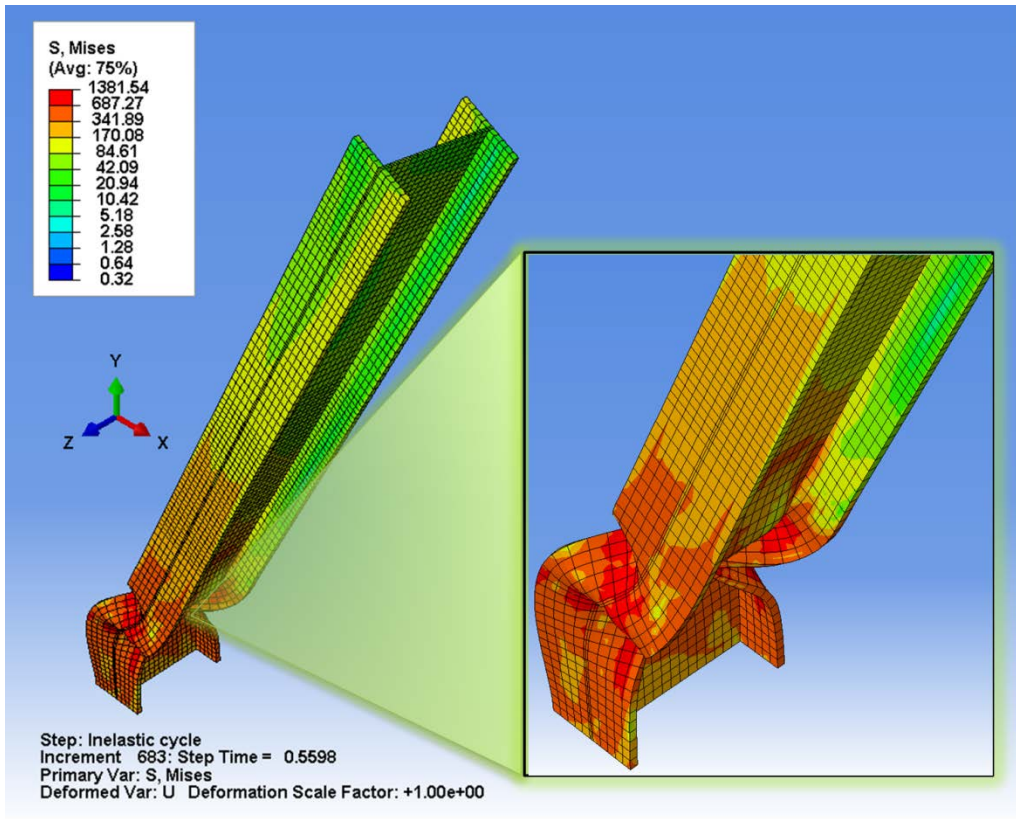


Figure C.17: Stress Contour at Fracture Stage for SC-15P

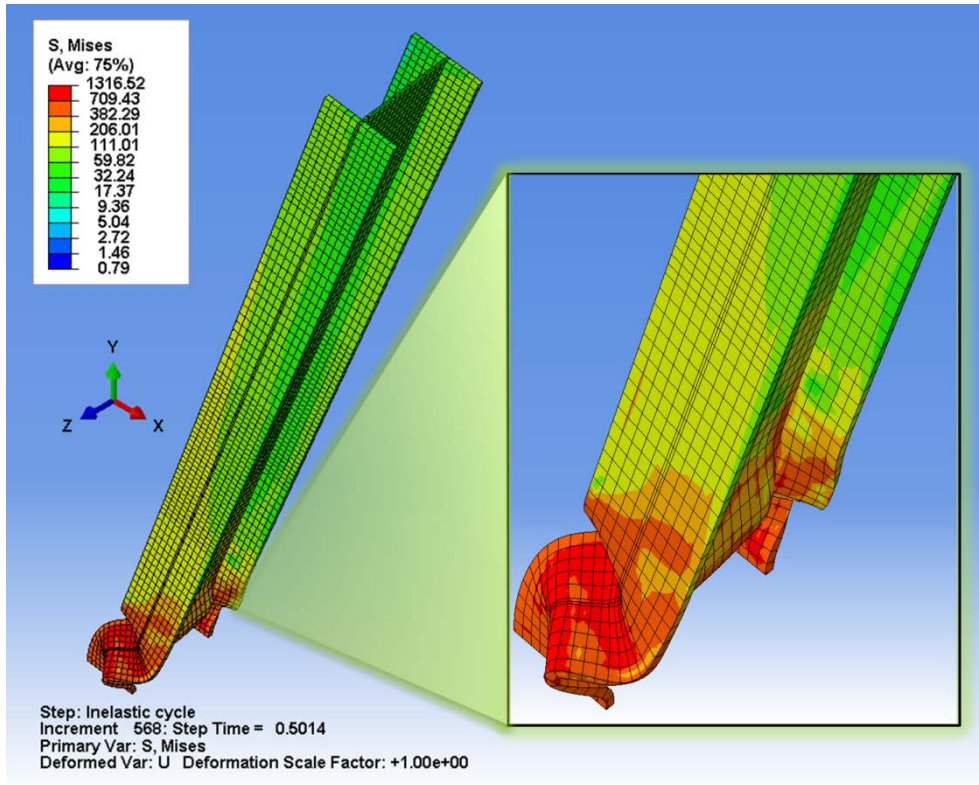


Figure C.18: Stress Contour at Fracture Stage for SC-20P